South Dakota State University
Open PRAIRIE: Open Public Research Access Institutional Repository and Information Exchange

Electronic Theses and Dissertations

2018

Evaluation of the Mechanical Properties of 3D Printed Carbon Fiber Composites

Max James Sauer
South Dakota State University

Follow this and additional works at: https://openprairie.sdstate.edu/etd

Part of the Mechanical Engineering Commons

Recommended Citation
Sauer, Max James, "Evaluation of the Mechanical Properties of 3D Printed Carbon Fiber Composites" (2018). *Electronic Theses and Dissertations*. 2436.
https://openprairie.sdstate.edu/etd/2436

This Thesis - Open Access is brought to you for free and open access by Open PRAIRIE: Open Public Research Access Institutional Repository and Information Exchange. It has been accepted for inclusion in Electronic Theses and Dissertations by an authorized administrator of Open PRAIRIE: Open Public Research Access Institutional Repository and Information Exchange. For more information, please contact michael.biondo@sdstate.edu.

EVALUATION OF THE MECHANICAL PROPERTIES OF 3D PRINTED CARBON FIBER COMPOSITES

BY

MAX JAMES SAUER

A thesis submitted in partial fulfillment of the requirements for the

Master of Science

Major in Mechanical Engineering

South Dakota State University

2018

EVALUATION OF THE MECHANICAL PROPERTIES OF 3D PRINTED CARBON FIBER COMPOSITES

MAX JAMES SAUER

This thesis is approved as a creditable and independent investigation by a candidate for the Master of Mechanical Engineering degree and is acceptable for meeting the thesis requirements for this degree. Acceptance of this thesis does not imply that the conclusions reached by the candidate are necessarily the conclusions of the major department.

Todd Letcher, Ph.D.
Thesis Advisor Date

Kurt Bassett, Ph.D.
Head, Department of Mechanical Engineering Date

Dean, Graduate School Date

I dedicate this work to my entire family for their endless support throughout my studies. I would not be where I am today without the encouragement they have given me.

ACKNOWLEDGEMENTS

I wish to express my sincere appreciation to **Dr. Todd Letcher**, my thesis advisor, for all that he has done for me these throughout my Graduate Studies, as well as during my undergraduate studies. His knowledge, encouragement and support has been paramount to my success. I also wish to thank him for his availability all hours of the day to accommodate my often times hectic schedule.

I would also like to thank **Dr. Zhong Hu**, the graduate coordinator, for his guidance throughout my studies. His advice throughout my coursework as well as his knowledge of Carbon Fiber Composites was much appreciated throughout my research.

I also wish to thank the numerous Faculty members of South Dakota State University who I had the pleasure to work with and learn from throughout my Undergraduate and Graduate Studies. The opportunity to work as a Graduate Teaching assistance was very beneficial for me both in terms of financial assistance during my studies, as well as the knowledge I gained from teaching and engaging with students from a different perspective.

I would like to acknowledge the Materials Evaluation and Testing Lab (METLAB) for their continued support in using the MTS machines for mechanical testing, sample polishing machines for imaging prep, and the Keyence microscopes for image analysis. I also wish to acknowledge the Lab for Engineering of Additive Designs, Education, and Research (LEADER) for any assistance that I needed with 3D printing.

Lastly, I wish to thank my family for their words of encouragement, support, and love throughout my studies. I also wish to thank my wife for her love, support, and understanding during many long nights and weekends.

TABLE OF CONTENTS

ABBREVIATIONS x

LIST OF FIGURES xi

LIST OF TABLES xv

ABSTRACT xvii

CHAPTER 1 - INTRODUCTION 1

1.1 Additive Manufacturing 1

1.2 Literature Review 2

1.2.1 Tensile Properties 2

1.2.2 Impact Properties 4

1.3 Thesis Objectives 5

1.4 Thesis Outline 7

CHAPTER 2 - TENSILE STRENGTH OF SHORT FIBER SPECIMEN 8

2.1 Abstract 8

2.2 Introduction 9

2.3 Experimental Procedure 10

2.3.1 Mechanical Testing 10

2.3.2 Dimensional and Mass Measurement of Samples 15

2.3.3 Testing Parameters 15

2.3.4 Digital Microscopy 16

2.3.5 ImageJ Analysis 19

2.3.6 Micromechanical Modeling 23

2.4 Results and Discussion 26

2.4.1 Dimensional Measurement of Samples 26

2.4.2 Mass Measurement of Samples 31

2.4.3 Mechanical Testing 32

2.4.4 Micromechanical Modeling 43

2.5 Conclusions 44

CHAPTER 3 - TENSILE STRENGTH OF CONTINUOUS FIBER SPECIMEN 46

3.1 Abstract 46

3.2 Introduction 47

3.3 Experimental Procedures 48

3.3.1 Mechanical Testing 48

3.3.2 Dimensional Measurement of Samples 52

3.3.3 Testing Parameters 52

3.3.4 Digital and Laser Microscopy 53

3.3.5 Image J Analysis and Elastic Constants 55

3.3.6 Internal Microstructure 59

3.3.7 Volume Average Stiffness Model 62

3.4 Results and Discussion 65

3.4.1 Fiber Volume Fraction and Void Density Measurement 65

3.4.2 Dimensional Measurement of Samples 65

3.4.3 Mechanical Testing 67

3.4.4 Volume Average Stiffness Modeling 75

3.5 Conclusions 77

CHAPTER 4 - IMPACT STRENGTH OF CARBON FIBER SPECIMEN 79

4.1 Abstract 79

4.2 Introduction 79

4.3 Experimental Procedures 81

4.3.1 Design of Specimen 81

4.3.2 Dimensional Measurement of Samples 91

4.3.3 Mechanical Testing Parameters 91

4.4 Results and Discussion 94

4.4.1 Dimensional Measurement of Samples 94

4.4.2 Mass Measurement of Samples 98

4.4.3 Mechanical Testing of CFF Specimen 99

4.4.4 Mechanical Testing of Control Specimen 100

4.4.5 Mechanical Testing of Off Angle CFF Specimen 101

4.4.6 Mechanical Testing of Carbon CFF with Varying Fiber Layers and Proximities 102

4.4.7 Mechanical Testing of Onyx Specimen 107

4.4.8 Onyx Specimen Results 108

4.5 Conclusions 109

CHAPTER 5 - COMPARISON OF RESULTS WITH MARKFORGED DATA..... 112

CHAPTER 6 - CONCLUSIONS, RECOMMENDATIONS, AND FUTURE WORK. 116

6.1 Conclusions 116

6.2 Short Fiber Composite Tensile Properties 116

6.3 Continuous Fiber Composite Tensile Properties..... 116

6.4 Short and Continuous Fiber Composite Impact Properties..... 117

6.5 Future Work 117

REFERENCES 118

APPENDICES 122

Appendix A: MATLAB Code to Generate Stress-Strain Curves from MTS Data..... 122

Appendix B: MATLAB Code for Generating Subplots of all Data in a given study. 126

Appendix C: MATLAB Code for Short Fiber Modeling 134

Appendix D: MATLAB Code for Volume Average Stiffness Method..... 136

Appendix E: volume_fraction function used in VAS Model..... 142

Appendix F: Experimental Data used in VAS Model 143

Appendix G: Additional Microscope Images of Short Fiber Specimen..... 145

Appendix H: Sample Calculation of the Krenchel Orientation Factor..... 148

Appendix I: Additional Microscope Images of CCF Specimen 151

ABBREVIATIONS

3D	Three Dimensional
ABS	Acrylonitrile Butadiene Styrene
AM	Additive Manufacturing
ASTM	American Society for Testing and Materials
CAD	Computer Aided Design
CF	Carbon Fiber
CFF	Composite Filament Fabrication
CT	Computed Tomography
FDM	Fused Deposition Modeling
FFF	Fused Filament Fabrication
MROM	Modified Rule of Mixtures
PC	Polycarbonate
PEEK	Polyether Ether Ketone
PEI	Polyethylenimine
PETG	Polyethylene Terepthalate Glycol-Modified
PLA	Polylactic Acid
PPSF/PPSU	Polyphenylsulfone
ROM	Rule of Mixtures
SLA	Stereolithography
SLS	Selective Laser Sintering
STL	Standard Tessellation Language
UTS	Ultimate Tensile Strength
VAS	Volume Average Stiffness

LIST OF FIGURES

Figure 2-1: Test specimen dimensions as defined by ASTM D368-10 11

Figure 2-2: Infill types within a single layer of the print from Eiger at an infill density of 25%. 12

Figure 2-3: Infill types within a single layer of the print from Eiger at an infill density of 100%. 13

Figure 2-4: Infill Line Directions within a single layer of the print from Cura at an infill density of 25% 14

Figure 2-5: Mechanical Testing of 3D printed specimen using an MTS Insight Tensile Testing Machine..... 16

Figure 2-6: Keyence Digital Microscope Image with CF Diameter Measurements at 1000x..... 18

Figure 2-7: Keyence Digital Microscope Image with CF Length Measurements at 250x 19

Figure 2-8: Keyence Digital Microscope Image of Representative Cross Section at 250x zoom..... 20

Figure 2-9: ImageJ Threshold image of Representative Cross Section at 250x zoom 21

Figure 2-10: ImageJ Threshold image of cross section used with Directionality at 500x zoom..... 22

Figure 2-11: ImageJ Directionality Histogram of Threshold shown in Figure 10 23

Figure 2-12: Mark Two Tensile Specimen compiled Stress-Strain Curves 33

Figure 2-13: Creator Pro Tensile Specimen compiled Stress-Strain Curves..... 34

Figure 2-14: Effects of Infill Density for Various Infill Types on UTS, Mark Two Specimen..... 35

Figure 2-15: Effects of Infill Density for Various Infill Types on Elastic Modulus, Mark Two Specimen 36

Figure 2-16: Plot of UTS/gram vs Infill Density for Various Infill types, Mark Two Specimen 37

Figure 2-17: Effects of Infill Density for Various Infill Types on UTS, Creator Pro Specimen 38

Figure 2-18: Effects of Infill Density for Various Infill Types on Elastic Modulus, Creator Pro Specimen 39

Figure 2-19: Plot of UTS/gram vs Infill Density for Various Infill types, Creator Pro Specimen 40

Figure 2-20: Comparison of UTS results – Creator Pro vs. Mark Two 41

Figure 2-21: Comparison of Modulus Results – Creator Pro vs. Mark Two 42

Figure 3-1: Test specimen dimensions as defined by ASTM D638-10 49

Figure 3-2: Fill type combinations within a single layer of the print. Types A, D, and E were examined in this study 51

Figure 3-3: Example of Layer Proximities. Each specimen above has 4 total layers of CF Filament. Layer Proximity 1 has 4 groups of fibers each with 1 layer per group, while Layer Proximity 2 has 2 groups of fibers each with 2 layers per group. The amount of fibers per cluster, or group of fibers denotes the Layer Proximity Number. 52

Figure 3-4: Mechanical testing of 3D printed specimen using an MTS 858 universal Testing Machine 53

Figure 3-5: Laser microscope image of 3D printed carbon fiber printed filament cross section at 1000x zoom 56

Figure 3-6: Image J cropped threshold image of 3D printed carbon fiber printed filament cross section at 1000x zoom. The volume fraction of CF yarns in this particular image was found to be 29.552%. 57

Figure 3-7: Laser microscope image of 3D printed Nylon at 200x zoom 58

Figure 3-8: Schematic of the internal structure of a typical carbon fiber reinforced 3D printed specimen used in this study. Left: Top view of the printed specimen. Right: Cross section of the specimen. Solid Nylon regions are white, shell regions are gray, and carbon fiber regions are black 60

Figure 3-9: Stress Strain Curves of Various CF loaded specimen. Note that the control specimen subplot is on a different scale than the rest of the subplots, as the control specimen sustained strain values far greater than the carbon fiber loaded specimen. 68

Figure 3-10: Stress Strain Curves of Various CF loaded specimen, shown on one plot. Control specimen are shown across the bottom of the plot, showing their high strain, low UTS properties. 68

Figure 3-11: Control and Off Angle Fiber Stress Strain Curve 70

Figure 3-12: Effects of Layer Proximity on UTS 71

Figure 3-13: Effects of Layer Proximity on Elastic Modulus 72

Figure 3-14: Plot of Carbon Fiber Volume Fraction vs. UTS and Elastic Modulus for All Specimen 74

Figure 3-15: Plot of $ Value per Sample vs. UTS and Elastic Modulus for All Specimen 75

Figure 3-16: Results of Volume Average Stiffness Model with Experimental Data 76

Figure 4-1: Test specimen dimensions as defined by ASTM D256-10 82

Figure 4-2: Brim Support Representation. Top: View of specimen with Brim attached. Bottom: View of specimen after removal of Brim support 84

Figure 4-3: Isotropic Fiber Infill within a single layer of a CFF Specimen, 0°. Other fiber directions used were 45°, 45° alternating, and 90°. 85

Figure 4-4: Example of Part Orientations. CFF parts were printed in U and S orientations while Nylon control parts were printed in all four orientations. 86

Figure 4-5: Example of Layer Proximities. Each specimen in this figure has 16 carbon fiber layers distributed in different groupings. 87

Figure 4-6: Demonstration of Carbon Fiber layer placement in Notch Up vs. Notch Side specimen. Blue is floor/ceiling layers, black is CF layers, white is nylon infill layers, and red is layers completely bisected by the notch in the part. 89

Figure 4-7: Izod Pendulum Impact Apparatus 92

Figure 4-8: Diagram of Impact Apparatus with Pendulum angles shown. Note: Not to scale. Diagram for angle demonstration only. 93

Figure 4-9: Representation of All data gathered for CFF Study, sorted by number of Fiber Layers. Red X's show specimen which did not break upon impact. 100

Figure 4-10: Subplot of various Fiber Layer Proximities for Notch up and Notch Side CFF Specimen 103

Figure 4-11: Comparison of fiber layers relative to notch for Notch Up and Notch Side CFF Specimen 104

Figure 4-12: Comparison of Different Fiber Proximities for Notch Up CFF Specimen 106

Figure 4-13: Common failure mode of CFF Specimen 107

Figure 4-14: Graphical Representation of Onyx Specimen Results 109

LIST OF TABLES

Table 2-1: Print Parameters for Test Specimen printed on the Mark Two 12

Table 2-2: Print Parameters for Test Specimen printed on the Creator Pro 14

Table 2-3: Sample Prep Polishing Procedure 17

Table 2-4: Mark Two Specimen Width Measurements 27

Table 2-5: Mark Two Specimen Thickness Measurements 28

Table 2-6: Creator Pro Specimen Width Measurements 29

Table 2-7: Creator Pro Specimen Thickness Measurements 30

Table 2-8: Mark Two Part Mass vs. Eiger Estimate 31

Table 2-9: Creator Pro Part Mass vs. Cura Estimate 32

Table 2-10: Table of variable group Average Tensile Data, Mark Two Specimen..... 37

Table 2-11: Table of variable group average Tensile Data, Creator Pro 40

Table 2-12: Micromechanical Structure Properties 43

Table 3-1: Print Parameters for Test Specimen 50

Table 3-2: Molded specimen polishing procedure..... 54

Table 3-3: Assumed material properties of Nylon filament [32]..... 59

Table 3-4: Assumed material properties of carbon fiber yarn in filament..... 59

Table 3-5: Internal microstructure dimensions 61

Table 3-6: Comparison of specimen width vs. nominal width of CAD part 66

Table 3-7: Comparison of specimen thickness vs. nominal thickness of CAD part..... 66

Table 3-8: Control and Off Angle CF Specimen Results 70

Table 3-9: Results of VAS Model Compared to Experimental Data..... 77

Table 4-1: Print Parameters for CFF Specimen 83

Table 4-2: Print Parameters for Onyx Specimen 90

Table 4-3: Width Data for CFF Specimen 95

Table 4-4: Thickness Data for CFF Specimen 96

Table 4-5: Onyx Width Analysis 97

Table 4-6: Onyx Thickness Analysis 97

Table 4-7: CFF Mass Analysis 98

Table 4-8: Onyx Mass Analysis 99

Table 4-9: CFF Control Specimen Impact Resistance Data 101

Table 4-10: Comparison of Off Angle Fiber Specimen with 0° Fiber Fill Specimen 102

Table 4-11: Comparison of Notch Up vs. Notch Side CFF Specimen Results 105

Table 4-12: Comparison of Onyx Specimen Results 109

Table 5-1: Comparison of Thesis Results with Markforged Data: Carbon CFF 113

Table 5-2: Comparison of Thesis Results with Markforged Data: Nylon and Onyx Specimen 114

ABSTRACT

EVALUATION OF THE MECHANICAL PROPERTIES OF 3D PRINTED CARBON FIBER COMPOSITES

MAX JAMES SAUER

2018

Studies have been done involving the use of carbon fiber as a reinforcement for three dimensional (3D) printed parts. The Markforged Mark Two is a commercial grade 3D printer capable of printing parts reinforced with continuous fibers such as carbon fiber, Kevlar, and fiberglass.

Short Carbon Fiber Composite tensile specimen were printed on both a Markforged Mark Two and Flashforge Creator Pro using Markforged Onyx filament. The results of these parts were compared for their tensile properties, dimensional accuracy, and mass estimates. The Creator Pro was capable of producing stronger parts on average, while the Mark Two produced more dimensionally accurate parts. Parts printed with the Creator Pro achieved higher Ultimate Tensile Strengths and Elastic Moduli than their respective Mark Two counterparts on average. Various analytical models were employed to estimate the Elastic Modulus of these parts printed at 100% infill. The Modified Rule of Mixtures Model was found to be the most accurate estimate of these short fiber composites.

Continuous Carbon Fiber Composite tensile specimen were printed with a Markforged Mark Two. Various Carbon Fiber orientations and layer proximities were tested and their effects on Tensile Strength and Modulus of Elasticity were examined. A Volume Average Stiffness (VAS) model was also used to predict the elastic properties of

these 3d-printed specimen. Tensile Testing of the 3d-printed specimen showed that material properties were directly related to the number of carbon fiber strands loaded in tension within the part, and that the increase in these material properties was linear.

Impact specimen were printed with a Markforged Mark Two. Both short/discontinuous and long continuous carbon fiber specimen were printed. For the Continuous fiber specimen, effects of part orientation, number of carbon fiber layers, and carbon fiber layer proximity were studied. For short fiber specimen, layer height and material infill raster angles were studied.

CHAPTER 1 - INTRODUCTION

1.1 Additive Manufacturing

Additive Manufacturing (AM), also referred to as 3D printing, is a manufacturing process that produces three dimensional (3D) parts from computer-aided design (CAD) software. From the CAD software, a file is generated in Standard Tessellation Language (STL), which is then imported into a software called a Slicer, which slices, or discretizes the model into layers and generates the instructions used by the 3D printer. These instructions, sometimes called G-code, are loaded onto the 3D printer to fabricate the desired part. Additive Manufacturing can be divided into many different categories. The most common categories include: Fused Deposition Modeling (FDM), Selective Laser Sintering (SLS), and Stereolithography (SLA) [1]. FDM will be the focus of this thesis.

Many different materials exist which can be used for FDM printing. The most common materials used in desktop equipment are Acrylonitrile Butadiene Styrene (ABS) and Polylactic Acid (PLA). Polyethylene Terepthalate Glycol-Modified (PETG) and Polyamide (Nylon) are also sometimes used in desktop equipment, however, these usually require slight modifications to the extruders of standard desktop 3D printing equipment. Industrial grade FDM 3D printers will typically expand the list of available materials to include Polyether Ether Ketone (PEEK), Polyethylenimine (PEI) [2], Polycarbonate (PC), Polyphenylsulfone (PPSF/PPSU), ASA, and ULTEM [3]. In this thesis, the main focus will be on Nylon polymers with and without reinforcement.

1.2 Literature Review

1.2.1 Tensile Properties

The tensile properties of 3D printed parts vary greatly depending on the material(s) used to produce the part. Several authors have evaluated the tensile properties of standard 3D printed parts with a large variance in material properties. Rodriguez et al reported an Ultimate Tensile Strength (UTS) of 24 MPa for ABS parts [4], and Sood et al reported a UTS of 16.1 MPa for ABS parts [5]. Letcher and Waytashek reported a UTS of 64 MPa and a Tensile Modulus of 3.6 GPa for PLA parts [6], and Melenka et al reported a UTS of 34 MPa and a Tensile Modulus of 1.1 GPa for PLA parts with 80% infill density [7].

There are a few ways to increase the tensile strength of these 3D printed parts by utilizing Carbon Fiber (CF) which include the use of short or chopped carbon fibers or the use of continuous carbon fibers for reinforcement. Several authors have evaluated the effects of these carbon fiber arrangements in 3D printed parts with some success in strength increases. Ivey et al studied a PLA+CF filament from 3DXMax and observed a UTS of 60 MPa for all parts and a Tensile Modulus of 6 GPa for CF reinforced parts as opposed to a Tensile Modulus of 3 GPa for non-reinforced parts [8]. Ferreira et al studied a PLA+CF filament from Proto-Pasta and compared it to a standard PLA filament. They observed a drop in Tensile strength for CF reinforced filaments from 54.7 MPa non-reinforced down to 53.4 MPa for PLA+CF. The Tensile Modulus for PLA was found to be 3.3 GPa, while PLA+CF increased the Tensile Modulus to 7.5 GPa [2]. Tekinalp et al compared a custom made ABS+CF filament to that of a compression molded specimen of the same material. It was shown that the 3D printed parts using the ABS+CF filament performed nearly

equally to the compression molded specimen. A Tensile Strength of 65 MPa was observed for the ABS+CF printed parts, with a Tensile Modulus of 13 GPa [9].

When comparing the results of the standard FDM printed parts with the short fiber reinforced parts, it is apparent that the addition of short fibers provides an increase in the Tensile Modulus of the parts, while providing little to no benefit to the UTS of the parts. This leads to the next method of reinforcement which is with the use of continuous carbon fibers within the print. Li et al treated a bundle of CF in PLA to improve its bonding characteristics to the PLA filament, and fed the CF bundle into the extrusion head of the printer simultaneously with the PLA filament to produce a continuous carbon fiber reinforced part. The UTS of these specimen was found to be 91 MPa [10]. Yang et al developed a custom extruder where the CF bundle was fed into the nozzle of the extruder while ABS filament was extruded normally through the entire extruder, which was shown to prevent the tearing of carbon fibers through the extrusion process. A UTS of 147 MPa was observed, as well as a Tensile Modulus of 4.185 GPa [11]. Nakagawa et al hand laid layers of continuous fibers onto the printed part in the middle of the 3D printing process, and studied the effects of different heat treatments on the fibers. This study showed that Heat treatment of the produced part yielded UTS results 1.5 times with the use of thermal bonding [12].

With the addition of Continuous Carbon fibers into the printed part, it is apparent that both the Ultimate Tensile Strength and the Tensile Modulus of the part can be significantly increased when compared to standard FDM Parts. In this thesis, it will be shown that in some cases, these Continuous Carbon Fiber composites can meet or exceed

the tensile properties of 6061 Aluminum, which has an Ultimate Tensile Strength of 310 MPa, and a Modulus of Elasticity of 68.9 GPa [13].

1.2.2 Impact Properties

Impact testing subjects material to a quick blow by a swinging pendulum. This impact measures the energy absorption of the material, which is an indicator of material toughness [14]. Specimen conforming to ASTM D256-10 contain a v-shaped notch, which provides a stress concentrator on the material. The notch tests the materials resistance to crack propagation.

A study done by Roberson et al [15] sought to study the effects of 3D printed impact specimen which had v-notches either printed with the part or machined after printing. This study also studied the effects of printing the specimen in different orientations on the build plate. For the case of ABS, it was found that part orientation made a significant difference in Impact Resistance, while printed vs. milled v-notch specimen showed statistically insignificant differences in Impact Resistance. Further studies have been performed to analyze the impact resistance of various materials 3D printed with FDM printing methods [14, 16, 17] and these studies all concluded that part orientation of the specimen during printing was an important factor due to the inherent anisotropic nature of FDM printed specimen. The studies concluded that specimen printed with 0° raster angles yielded higher impact resistances than parts printed with other infill directions. The anisotropy of FDM parts may be due to polymer molecules aligning themselves with the direction of flow while being extruding in the fused deposition modelling process [18]. Another source of anisotropy may be due to the formation of pores within the print, and weak interlayer bonding of the material [19].

Composite materials suffer a serious limitation due to the negative effects from localized impact loadings [20]. Failure modes due to impact loading include splitting, delamination, intralaminar matrix cracking, longitudinal matrix splitting, fiber/matrix debonding, fiber pull-out, and fiber fracture [21-25]. Interlaminar shear deformations and flexure are the main energy absorbing mechanisms in composite materials subject to impact loading [26].

Carbon fibers are commonly used as a mechanical reinforcement of materials in composites manufacturing due to their high specific modulus, strength, stiffness, and low density [27]. Strength properties of carbon fiber composites largely rely on the mechanical properties of the carbon fiber, as well as fiber/matrix adhesion.

Further studies have been done to analyze the impact resistance of carbon fiber composites. A study performed by Ozkan et al studied the effects of carbon fiber sizing on impact resistance of carbon fiber composites [27]. It was concluded that the sizing material type used had no effect on impact resistance, but impact resistance was found to decrease with an increase in Carbon Fibers within the composite. It is generally said that the addition of fibers into a ductile polymer matrix makes the material brittle which decreases impact resistance [28-31].

1.3 Thesis Objectives

Markforged has developed a commercially available semi-industrial grade 3D printer with the capability to automatically and repeatably reinforce Nylon FDM printed parts with a variety of continuous fibers, including glass, Kevlar fibers, and carbon fiber. The first iteration of this printer, the Mark One, was capable of printing these Nylon FDM

parts with concentric rings of fibers for reinforcement [32]. The objective of this printer is to produce parts that are stronger than standard FDM parts, reliably with consistent results.

The second iteration of this printer, The Mark Two by MarkForged is similar to the Mark One 3D printer in that it reinforces FDM printed components with continuous glass, Kevlar, and carbon fibers. Both printers have two extruders and utilize the Composite Filament Fabrication (CFF) technology. While the Mark One is only capable of embedding concentric rings of carbon fiber along the outside geometry of the component, the Mark Two allows for concentric placement of fibers as well as isotropic placement of fibers. Both Concentric and Isotropic Fiber fill patterns can be used simultaneously or independent of each other, yielding much more flexibility for the designed.

While Markforged has released Mechanical Properties of parts printed with the Mark Two [33], few studies have been done to examine these mechanical properties in detail, and little is known about how physical part parameters such as placement of carbon fibers affect mechanical properties. In the case of Impact properties, the author was not able to find any literature regarding impact testing of specimen printed with the Mark Two.

The main objective of this thesis is to analyze the Tensile and Impact Properties of short/discontinuous carbon fiber composites as well as long continuous carbon fiber composites which have been 3D printed. The effects of different printing parameters on these mechanical properties will also be studied. Various Micromechanical models will also be developed to approximate the tensile properties of these short fiber and continuous fiber composites.

1.4 Thesis Outline

Tensile properties of short fiber composites are examined in Chapter 2. Three micromechanical models are also presented to approximate the tensile properties of these composites. Micromechanical properties used in these models were determined via microscope imaging and image analysis software.

Tensile properties of continuous carbon fiber composites are examined in Chapter 3. In this chapter, the Volume Average Stiffness Model is also presented to approximate the tensile properties of continuous fiber composites. Micromechanical properties used in this model were determined with microscope imaging and image analysis software.

Chapter 4 is focused on Impact Resistance of Carbon Fiber Composites. This chapter is broken into two parts; Impact Resistance of short fiber composites and Impact Resistance of Continuous Carbon Fiber Composites.

Chapter 5 compiles the results of Chapters 2 – 4 and compares them with the Mechanical Properties presented by Markforged.

CHAPTER 2 - TENSILE STRENGTH OF SHORT FIBER SPECIMEN

2.1 Abstract

Short Carbon Fiber Composite tensile specimen were printed on both a MarkForged Mark Two and Flashforge Creator Pro using MarkForged Onyx filament. The results of these parts were compared for their tensile properties, dimensional accuracy, and mass estimates. The Creator Pro was capable of producing stronger parts on average, while the Mark Two produced more dimensionally accurate parts. Parts printed with the Creator Pro achieved higher Ultimate Tensile Strengths and Elastic Moduli than their respective Mark Two counterparts on average, with a maximum Tensile Strength of 49.4 MPa and a maximum Elastic Modulus of 3.5 GPa from the Creator Pro, as opposed to maximums of 45 MPa and 2.3 GPa for Tensile Strength and Elastic Modulus, respectively, from the Mark Two. The overall average Elastic Modulus for all specimen printed at 100% infill was found to be 2.6 GPa. Dimensions of the Mark Two specimen had standard deviations of 0.07 mm and 0.05 mm for width and thickness, respectively, while the Creator Pro specimen had standard deviations of 0.14 mm and 0.19 mm, respectively, while both printers seemed to achieve similar width and thickness averages. Eiger mass estimate percent errors ranged from -7% to -12%, while Cura mass estimates ranged anywhere from -39% to 113%. Various analytical models were employed to estimate the Elastic Modulus of these parts printed at 100% infill. A standard Rule of Mixtures model approximated the Elastic Modulus at 22.0 GPa. The Halpin-Tsai model approximated the Elastic Modulus at 3.5 GPa, and the Modified Rule of Mixtures model approximated the Elastic Modulus to be 2.7 GPa. The Modified Rule of Mixtures Model was found to be the most accurate estimate of these short fiber composites.

2.2 Introduction

MarkForged has developed a semi-industrial commercially available 3D printer, the Mark Two by MarkForged, which has the capability of printing parts reinforced with short and continuous carbon fibers, among other continuous fiber types. While the main selling point of the Mark Two is its ability to print continuous fiber composites, MarkForged also sells a material called Onyx which contains short carbon fibers within a nylon polymer matrix, all in one filament.

Finite element analysis models were developed by Tucker III and Liang to understand the effects of different fiber aspect ratios (l/d) on the tensile properties of composites [34]. They then presented several numerical models to approximate the tensile properties of these composites, including the Halpin-Tsai Model and the Mori-Tanaka Model among others. For aspect ratios greater than 8, all models correlated well with Finite Element Analysis results, while these models began to scatter for aspect ratios below 4. It was observed that the Halpin-Tsai model correlated best with short fibers (aspect ratio below 4) while the Mori-Tanaka model did better over the whole range of aspect ratios.

Parandoush and Lin suggested that the Modified Rule of Mixtures model was the easiest model to employ for short fiber composites [35]. Further work with these models was performed by Patanwala et al to compare them to experimental data [36]. In this study, the Rule of Mixtures, Halpin-Tsai, and Modified Rule of Mixtures Models were compared against experimental data for carbon nanotube composites of various carbon fiber volume fractions, and it was shown that the Modified Rule of Mixtures model correlated the best with the experimental data.

Further analysis has been done with the use of CT scans to analyze carbon fiber orientations throughout the test specimen. Various image analysis software was then used to develop fiber orientation histograms to better understand how fibers are oriented within these composites. These results were then used to develop numerical models of the tensile properties [37, 38].

In this study, MarkForged Onyx will be utilized to produce short fiber reinforced composites which will be analyzed for their tensile properties. The micromechanical details of these printed parts will also be observed to develop numerical models to approximate the elastic modulus of these specimen. These parts will be printed with the MarkForged Mark Two as well as a consumer level 3D printer, the Flashforge Creator Pro, which has been modified to print this material.

2.3 Experimental Procedure

2.3.1 Mechanical Testing

The specimen analyzed in this study were modeled with SolidWorks Computer Aided Design (CAD) software (SolidWorks 2016, Dassault Systemes, Waltham, MA USA). The geometry of the specimen was defined by ASTM D638-10 (ASTM D638-10, Standard Test Method for Tensile Properties of Plastics) as a Type I geometry [39]. This geometry and its dimensions are shown in Figure 2-1. The modeled specimen was exported from SolidWorks as a Standard Tessellation Language (STL) file and imported into the appropriate slicer. Two printers were used to print the specimen.

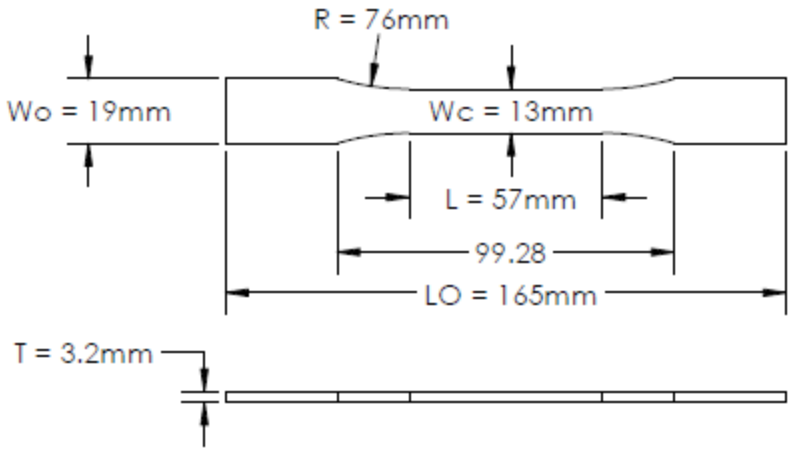

Figure 2-1: Test specimen dimensions as defined by ASTM D368-10

The first printer, the Mark Two by MarkForged (Mark Two, MarkForged, Somerville, MA) was used in conjunction with its custom slicer software, Eiger (Eiger 1.2, MarkForged, Somerville, MA USA). Eiger is the required proprietary slicing software to be used with the Mark Two. The second printer, the Flashforge Creator Pro (Creator Pro, Flashforge, City of Industry, CA USA) was used to compare against the results of the specimen printed with the Mark Two. The Creator Pro was modified to print at elevated temperatures with the addition of an E3D HotEnd upgrade (V6 Gold HotEnd, E3D, Oxfordshire UK). Gcode for parts printed on the Creator Pro was generated with Cura (Cura 3.1.0, David Braam, Ultimaker, Free Software License LGPLv3). All specimen in this study were printed with MarkForged Onyx filament (Onyx, MarkForged, Somerville, MA USA).

The print parameters that were tested and printed on the Mark Two were Layer Height, Infill Density, and Infill Pattern. These parameters are shown in Table 2-1. The infill patterns that were chosen in Eiger are shown in Figure 2-2.

Table 2-1: Print Parameters for Test Specimen printed on the Mark Two

Mark Two Print Parameters	
Layer Height (mm)	0.1 0.2
Infill Pattern	Rectangular (R) Hexagonal (H) Triangular (T)
Infill Percentage(%)	25 50 75 100
Number of Walls	2
Number of Floor Layers	4
Number of Roof Layers	4

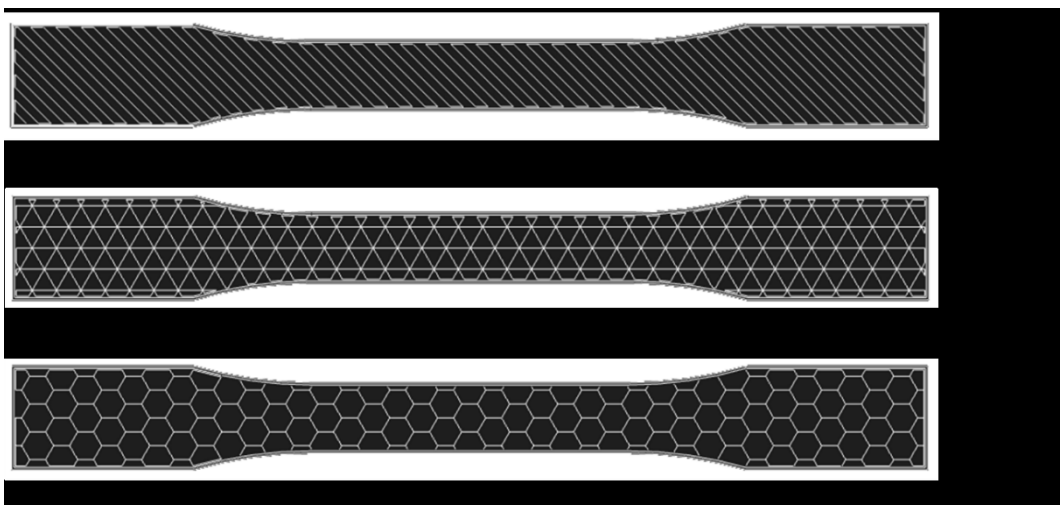

Figure 2-2: Infill types within a single layer of the print from Eiger at an infill density of 25%.

Type R is rectangular infill, which consists of layers of linear tool paths which rotate 90 degrees after each layer. Type T is triangular infill, which consists of layers of triangular tool paths which stack directly on top of one another. Type H is Hexagonal infill, which consists of layers of hexagonal tool paths which stack directly on top of one another. Triangular and Hexagonal infill layers overlap themselves exactly on each layer, that is,

any given layer of a Triangular infill part will look exactly like any other layer, and the same can be said for Hexagonal infill parts. Note that all infill types shown in Figure 2-2 have an infill density of 25%, which is a defined value in Eiger. An infill density of 100% doesn't necessarily imply that the part is 100% solid. Rectangular infill of 100% does fill the entirety of the part, but Triangular and Hexagonal infills of 100% are not entirely full. Figure 2-3 shows infill patterns for an infill density of 100%.

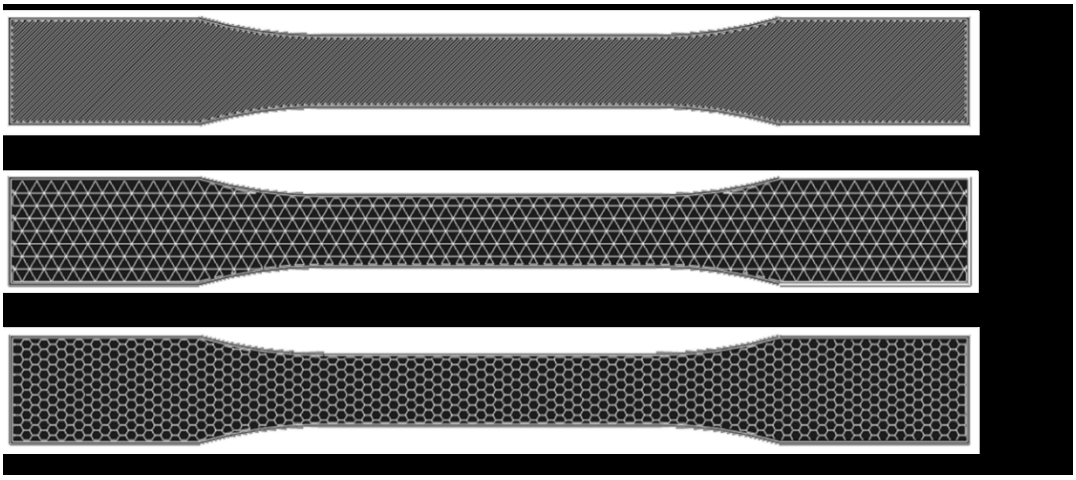

Figure 2-3: Infill types within a single layer of the print from Eiger at an infill density of 100%.

The print parameters that were altered for parts printed on the Creator Pro were Layer Height, Infill Density, and Infill Line direction, with all specimen using the Zig Zag infill pattern as defined by Cura. These parameters are shown in Table 2-2. The infill line directions that were chosen are shown in Figure 2-4. "Alt. 45" is alternating layers of 45 and -45 degree infill line directions, while "0 and 90" are parts with only 0 or 90 degree infill line directions. Note that the infill line directions shown in Figure 2-4 are represented with an infill density of 25%. For parts printed with the Zig Zag infill pattern, 100% infill density is a truly solid part.

Table 2-2: Print Parameters for Test Specimen printed on the Creator Pro

Creator Pro Print Parameters	
Layer Height (mm)	0.1 0.2
Infill Pattern	Zig Zag
Infill Line Directions	45, -45 (R) 0 (Lon) 90 (Tran)
Infill Percentage(%)	25 50 75 100
Number of Walls	2
Number of Floor Layers	4
Number of Roof Layers	4

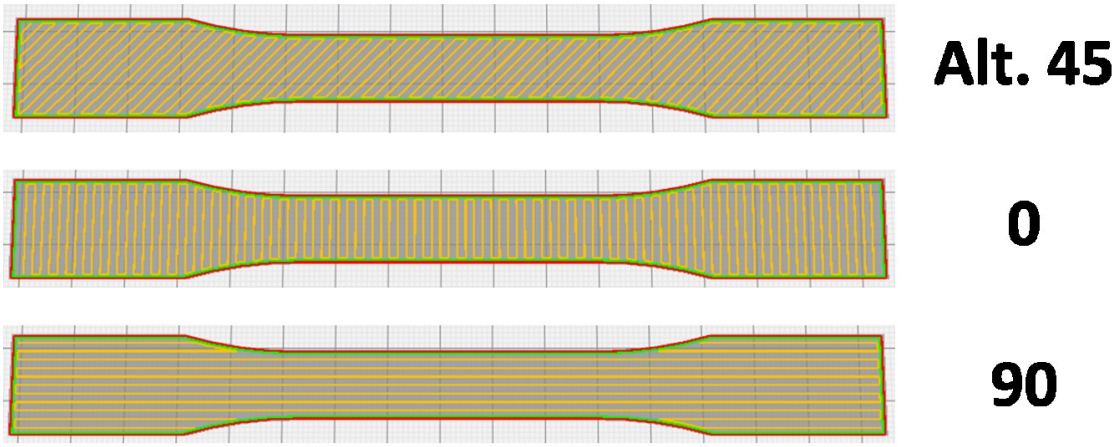

Figure 2-4: Infill Line Directions within a single layer of the print from Cura at an infill density of 25%

When printing with the Creator Pro, the following printer control variables were used:

- Nozzle Temperature – 275 °C
- Build Plate Temperature – 100 °C
- Print Speed – 60 mm/s
- 3 samples printed at a time

- Print Sequence – All at Once

Note that at 0.1mm layer height, the Creator Pro was not capable of printing a quality part at 25% fill density. Thus, this specific specimen grouping was omitted.

2.3.2 Dimensional and Mass Measurement of Samples

All test specimen were measured and weighed before tensile testing. Dimensional measurements were performed with a Mitutoyo Caliper (Mitutoyo 500-196-30). The measurements recorded were the width (Wc) of the tensile section and the thickness (T) of the part, as shown in Figure 2-1. These dimensions were used to calculate the cross section of the tensile region to determine tensile stress. The dimensions and mass of each sample will also be analyzed to compare the dimensional accuracy of the Mark Two with the Creator Pro.

Weight measurements were taken with an US Solid Lab Scale (USS-DBS5, US Solid). These measurements were taken to analyze the accuracy of the mass estimates given by Eiger and Cura.

2.3.3 Testing Parameters

The specimen were evaluated for their tensile properties on an MTS machine (MTS Insight, MTS, Eden Prairie, MN USA) as shown in Figure 2-5. Strain was recorded during the tests using a 20 mm gauge length extensometer (MTS 634.31F-24, Eden Prairie, MN USA). Strain and load data was recorded at 25 Hz and the samples were loaded in tension at a rate of 5 mm/min according to ASTM D638-10 [39]. The data recorded by the MTS Machine was saved as a csv file and analyzed with MATLAB (MATLAB 2017a, The MathWorks, Inc., Natick, MA USA). A sample of the MATLAB script used to analyze the stress-strain data is shown in Appendix A.

Figure 2-5: Mechanical Testing of 3D printed specimen using an MTS Insight Tensile Testing Machine

2.3.4 Digital Microscopy

In order to understand how fibers are oriented within printed a specimen, sample parts were examined with optical microscopy. Sample specimen were printed with the same parameters as all test specimen at 100% infill. Various parts with both 0.1mm and 0.2mm layer height were printed as microscope samples. These samples were then cut to size and cross sectioned with a Digiprep Specimen Mover (DIGIPREP 250, Qualitest North America, Ft. Lauderdale, FL USA) using a 7 step polishing process. First, the cut samples were sanded with 240 grit SiC sandpaper until plane, followed by another step with 320 grit SiC sandpaper until plane. Then, 600 grit SiC sandpaper was used in 1 minute increments, repeating this step as needed. Next, 1200 grit SiC sandpaper was used in 1

minute increments. Following the sandpaper steps were 3 steps with various polishing pads. The first polishing pad step included a TEXPAN polishing pad with 6 µm DIAMAT Diamond polishing compound. The second polishing pad step included an ATLANTIS polishing pad with 1 µm DIAMAT Diamond polishing compound. Finally, a NAPPAD polishing pad was used with 0.05 µm Nanometer Alumina polishing compound. Full details for the polishing procedure can be seen in Table 2-3.

Table 2-3: Sample Prep Polishing Procedure

Step	Abrasive/Surface	Table Speed (RPM)	Spindle Speed (RPM)	Time
1	240 grit SiC paper	100 CCW	100 CCW	Until Plane
2	320 grit SiC paper	100 CW	100 CW	Until Plane
3	600 grit SiC paper	150 CCW	150 CCW	1 min
4	1200 grit SiC paper	150 CW	150 CW	1 min
5	6 µm DIAMAT diamond on TEXPAN polishing pad	150 CCW	150 CCW	3 min
6	1 µm DIAMAT diamond on ATLANTIS polishing pad	200 CW	200 CW	2 min
7	0.05 µm Nanometer Alumina on NAPPAD polishing pad	200 CCW	200 CCW	1 min

After the samples were polished, a microscope (VHX-6000, Keyence Corporation, Elmwood Park, NJ USA) was used to observe various parameters of the carbon fibers within the print, such as carbon fiber length, diameter, volume fraction, and direction. Fiber length and diameter were directly measured with the Keyence Microscope software. Figure 2-6 shows a representative image including diameter measurements, and Figure 2-7 shows a representative image with length measurements. Additional microscope images of short fiber specimen can be seen in Appendix G. For both diameter and length measurements, best judgement was used to choose carbon fibers that were representative of the global

average, and shown in full view of the cross section plane. From the measurements taken with the Keyence Microscope software, averages were obtained for carbon fiber length and diameter. An average length of 108.2 μm was determined from 19 length measurements, and an average diameter of 7.36 μm was determined from 13 diameter measurements. Carbon fiber volume fraction and fiber direction images were taken with the microscope, but were analyzed with image analysis software, ImageJ.

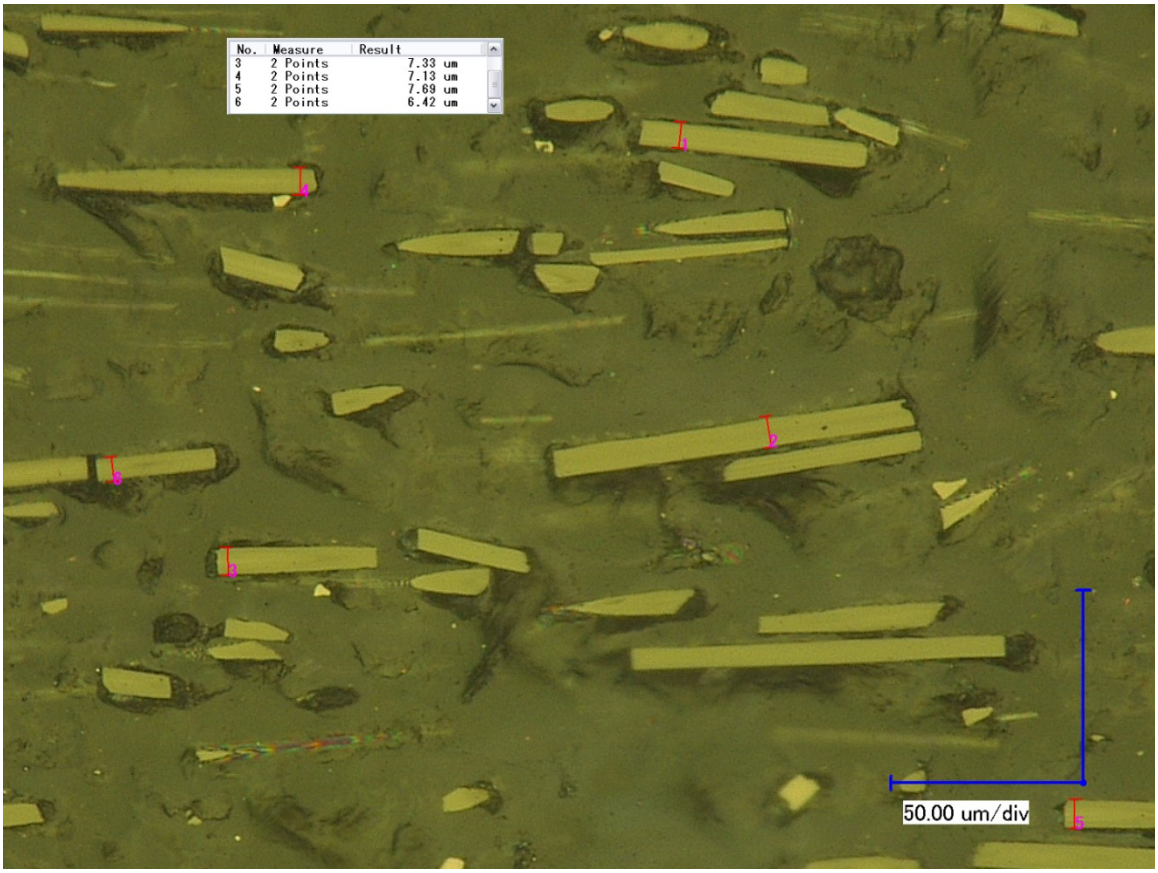

Figure 2-6: Keyence Digital Microscope Image with CF Diameter Measurements at 1000x

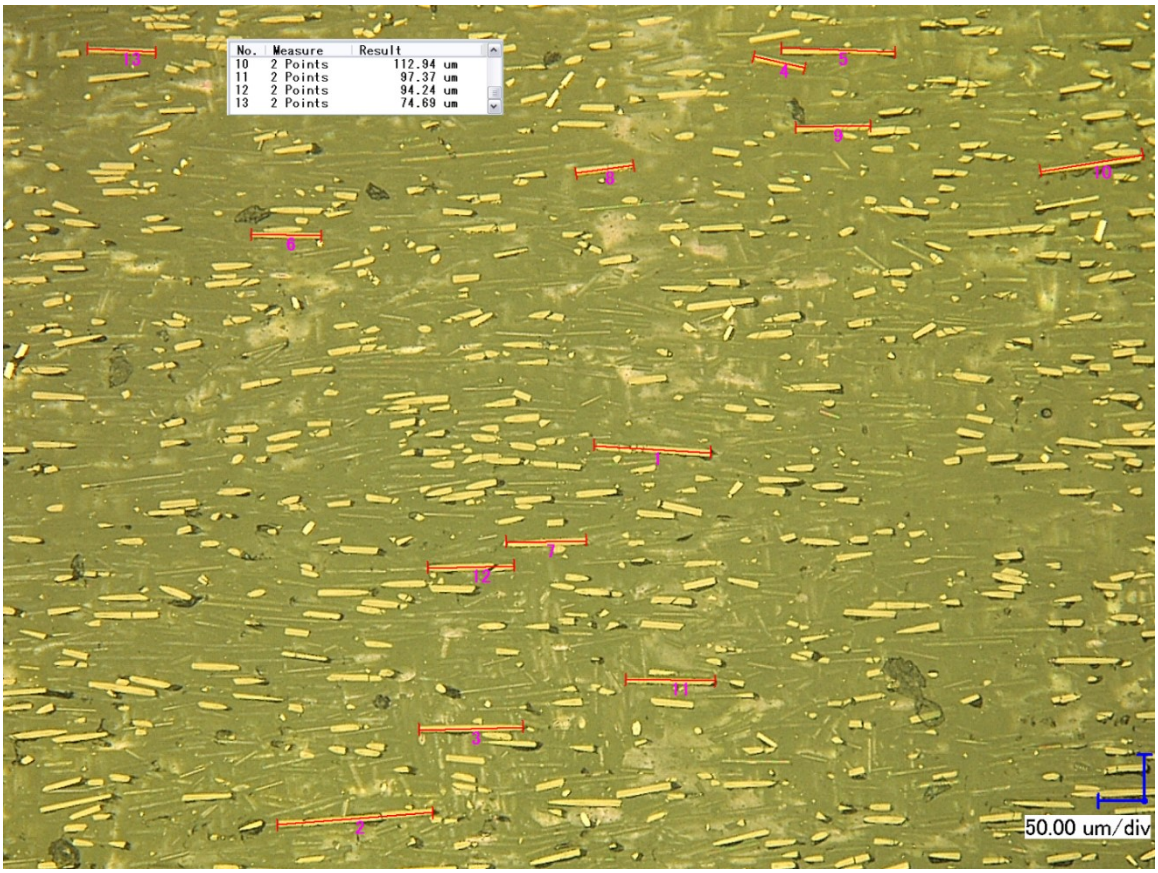

Figure 2-7: Keyence Digital Microscope Image with CF Length Measurements at 250x

2.3.5 ImageJ Analysis

Fiji, a distribution of ImageJ2 [40, 41], is an open-source image analysis software that was used to analyze the microscope images and determine various microstructure parameters of the 3d printed specimen; namely the carbon fiber volume fraction and carbon fiber infill direction histogram. To obtain this information from ImageJ, image thresholding was first performed to generate a black and white image with the regions of interest (individual carbon fibers) in black, with everything else in white. Figures 2-8 and 2-9 show a particular cross section image before and after thresholding.

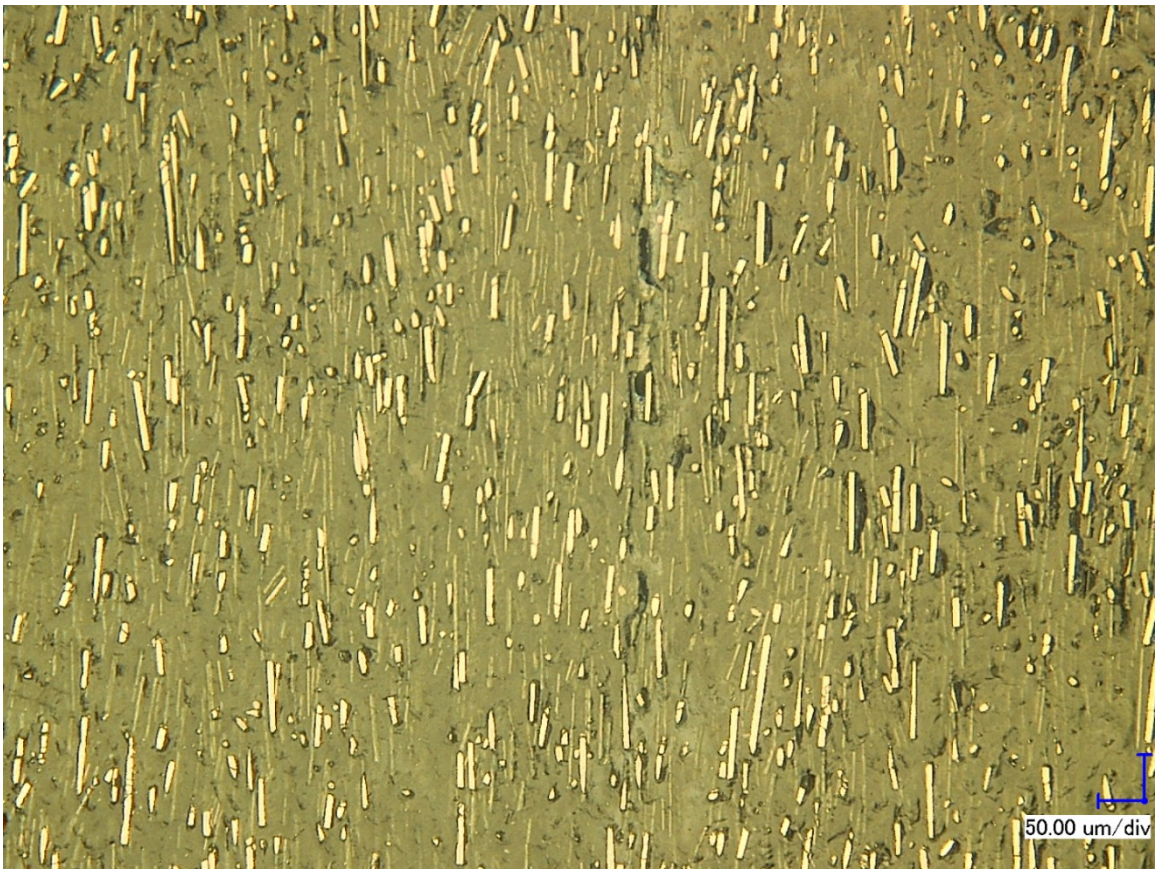

Figure 2-8: Keyence Digital Microscope Image of Representative Cross Section at 250x zoom

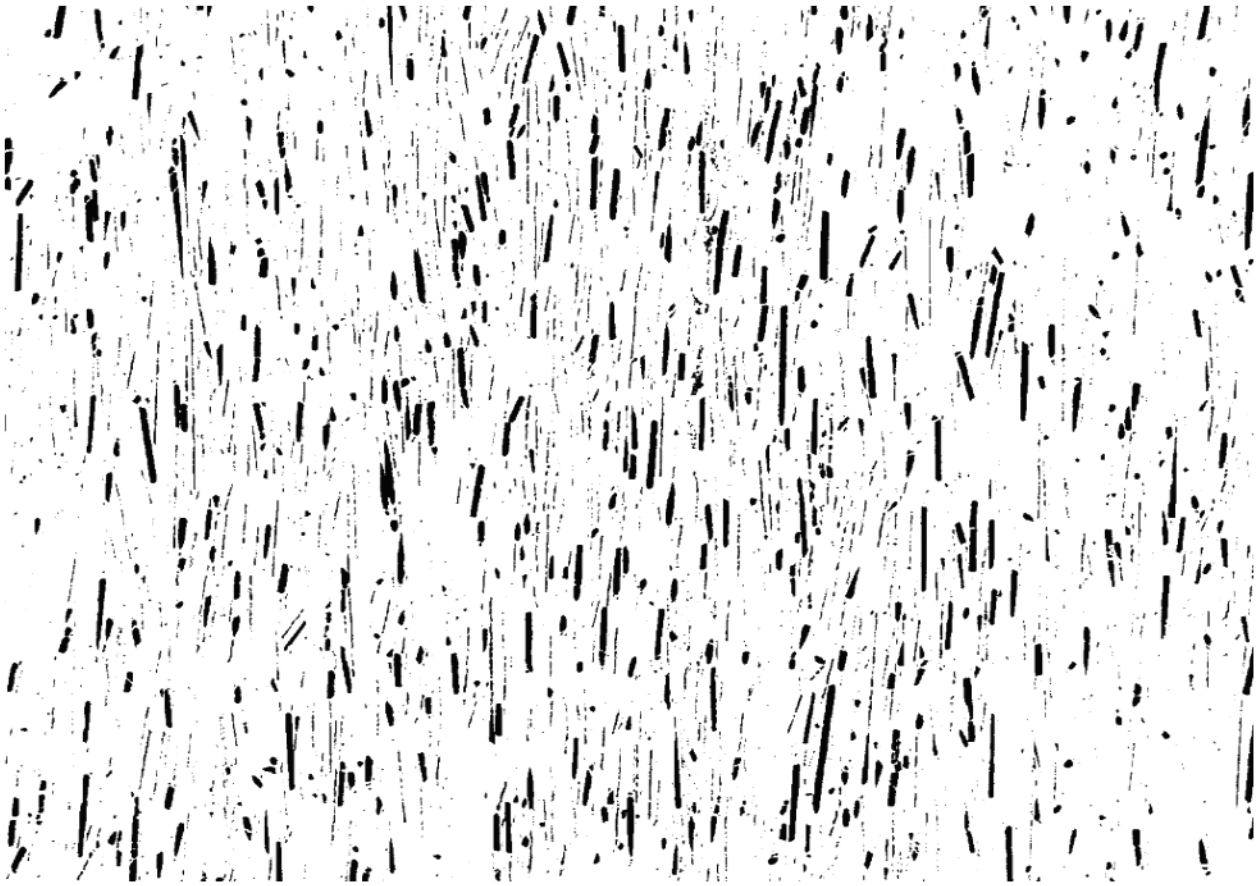

Figure 2-9: ImageJ Threshold image of Representative Cross Section at 250x zoom

To obtain the carbon fiber volume fraction, several microscope cross section images of various zoom levels were chosen as a representative sample of the fiber infill. A total of 10 images similar to Figure 2-8 were analyzed using the analyze particles feature in ImageJ to obtain a volume fraction. This volume fraction from the 10 threshold images had an average of 9.129% carbon fibers.

To gather carbon fiber direction histogram data, directionality was used. Directionality is a plugin that is included with the Fiji distribution of ImageJ2. The same 10 threshold images that were used for carbon fiber volume fraction were also analyzed with directionality to generate carbon fiber direction histograms. A sample image threshold

at 500x zoom and its corresponding Directionality Histogram are shown in Figures 2-10 and 2-11. Angles on the histogram correspond with Cartesian plane angles applied to the original image. These Directionality Histograms will be used further in this study for micromechanical modeling.

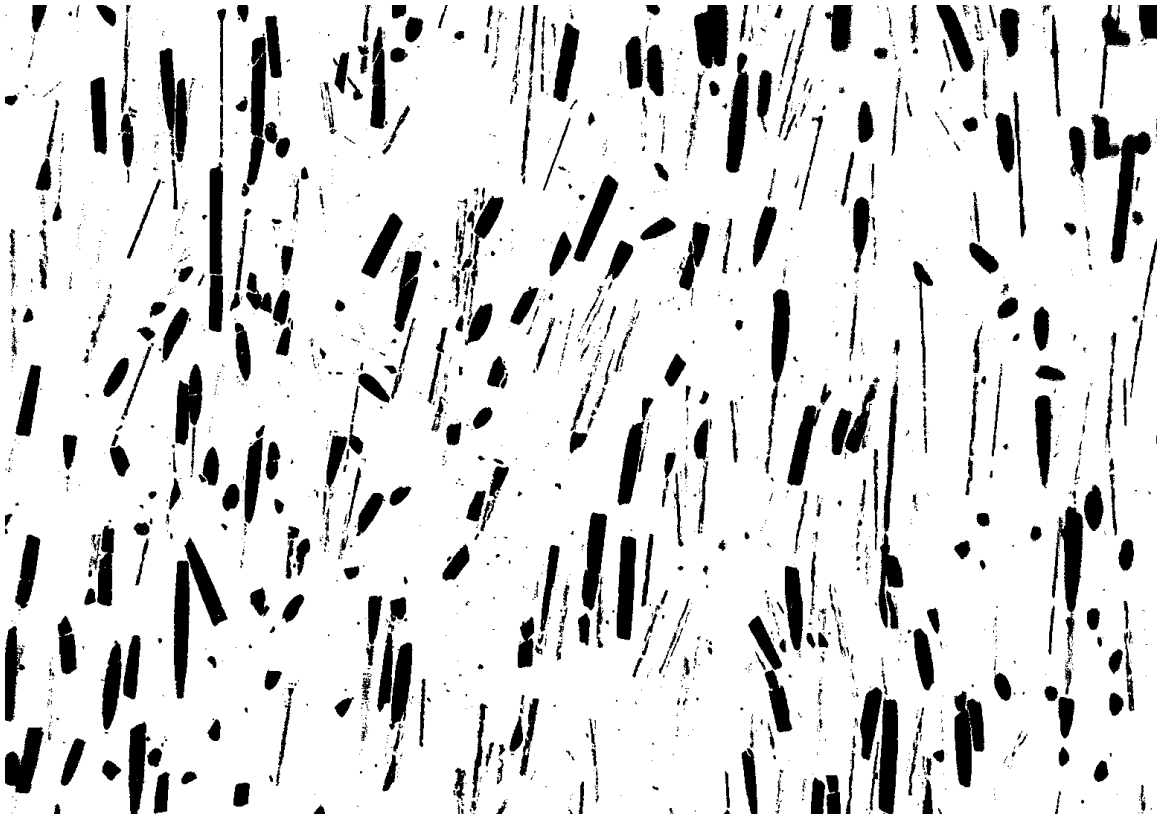

Figure 2-10: ImageJ Threshold image of cross section used with Directionality at 500x zoom

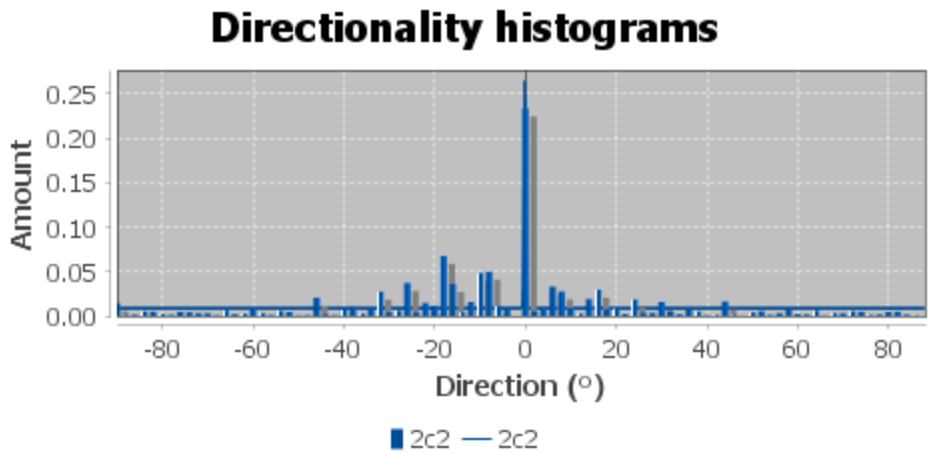

Figure 2-11: ImageJ Directionality Histogram of Threshold shown in Figure 10

The directionality plugin also reports the median direction of the histogram, dispersion, amount, and goodness. Dispersion is defined as the standard deviation of the histogram in degrees. Amount is defined as the percentage of the histogram values within 1 standard deviation to the left or right of center. Goodness is a measure of the fit applied to the histogram as a value from 0 to 1. 0 implies no fit, while 1 implies a good fit. The average direction of all 10 histograms was 0.226 degrees, and the average goodness was 0.855.

2.3.6 Micromechanical Modeling

Three different micromechanical models will be presented here which attempt to model the Elastic Modulus of short-fiber composites. These models are the Rule of Mixtures, the Halpin-Tsai Model, and the Modified Rule of Mixtures.

The first model, the Rule of Mixtures, is presented by Alger in the book *Polymer Science Dictionary* [42]. This model simply defines the elastic modulus in the direction parallel to the fibers to be a function of the moduli of the polymer matrix and fibers

multiplied by their respective volume fractions, and is considered to be an upper bound. This model is shown in Equation 1.

$$E_c = E_f V_f + (1 - V_f) E_m \tag{1}$$

In the rule of mixtures equation above, E_c is the Elastic Modulus of the composite, E_f is the Elastic Modulus of the fibers, E_m is the Elastic Modulus of the polymer matrix, and V_f is the volume fraction of fibers used in the composite.

While the rule of mixtures defines the upper-bound modulus of the composite, the inverse rule of mixtures defines the composite modulus in a direction perpendicular to the fiber direction. This inverse rule of mixtures is considered the lower-bound modulus, and is shown in Equation 2.

$$E_c = \left(\frac{V_f}{E_f} + \frac{1-V_f}{E_m}\right)^{-1} \tag{2}$$

According to Patanwala et al, the Rule of Mixtures model makes several assumptions which causes it to be a poor fit for short fibers composites [36]. These assumptions are: (i) fibers bond perfectly to the polymer matrix that surrounds them, (ii) fibers and the polymer matrix both experience an equal strain when exposed to a longitudinal load, and (iii) the fibers are continuous in length and are perfectly parallel within the polymer matrix. Since these conditions are not met with short fiber composites, the Rule of Mixtures model tends to overestimate the strength of short fiber composites.

The second model, the Halpin-Tsai model, is presented by O'Regan et al [43]. This model includes an efficiency factor based on the fiber length/diameter ratio. It is shown in Equations 3 and 4.

$$E_{\parallel} = E_m \left[\frac{1+2\frac{l}{d}\eta_{\parallel} V_f}{1-\eta_{\parallel} V_f}\right] \tag{3}$$

where the longitudinal efficiency factor, $\eta_{\parallel}$ is defined as

$$\eta_{\parallel} = \left[\frac{\left(\frac{E_f}{E_m}\right)-1}{\left(\frac{E_f}{E_m}\right)+2\left(\frac{l}{d}\right)}\right] \tag{4}$$

In Equations 3 and 4 above, $E_{\parallel}$ is the elastic modulus of the composite in the direction parallel to the fibers, l is the average length of the fibers in the composite, and d is the average diameter of fibers in the composite.

This model assumes that stress and strain are uniform in the longitudinal direction, which is a good assumption for continuous fibers, but doesn't hold true for short fibers. Short fibers experience peak shear stresses and strains at the fiber ends. Short fibers carry loads less effectively than continuous fibers do, which the Halpin-Tsai model does not account for.

Last, the Modified Rule of Mixtures Model is presented by O'Regan et al [43] and refined by Coleman et al [44]. This model includes the Rule of Mixtures model with various correction factors to capture the inefficiencies of short fiber composites. These correction factors include a length correction factor (η_L) which is based on the shear lag theory developed by Cox [45] as well as the Krenchel orientation efficiency factor (η_o) developed by Krenchel [46]. The Modified Rule of Mixtures model is shown below in Equations 5-8.

$$E_c = E_m\left(1 - V_f\right) + \eta_L \eta_o E_f V_f \tag{5}$$

Where the length correction factor (η_L) is given as

$$\eta_L = \left(1 - \frac{\tanh\left(\frac{\beta l}{d}\right)}{\left(\frac{\beta l}{d}\right)}\right) \tag{6}$$

And (β) attempts to quantify the rate of stress buildup in the fiber ends

$$\beta = \sqrt{-\frac{3E_m}{2E_f \ln(V_f)}} \tag{7}$$

The Krenchel orientation factor is an efficiency factor to quantify how well aligned the fibers are within the composite. Perfectly aligned fibers have an orientation factor of 1. The Krenchel orientation factor, which is applied to bin data of a fiber orientation histogram from ImageJ Directionality, is given as

$$\eta_o = \frac{\sum_n V_{f,n} \cos^4 \theta_n}{\sum_n V_{f,n}} \tag{8}$$

where θ_n is the bin angle in degrees, and $V_{f,n}$ is the volume fraction of fibers that are included in that specific bin. A sample calculation of the Krenchel orientation factor is shown in Appendix H.

All three models discussed in this section will be evaluated using a script written with MATLAB (MATLAB 2017a, The MathWorks, Inc., Natick, MA USA). This MATLAB Script can be seen in Appendix C.

2.4 Results and Discussion

2.4.1 Dimensional Measurement of Samples

Specimen were measured in the tensile region to calculate the cross sectional area for use during the analysis of the mechanical testing results. These measurements were also compared to the nominal dimensions of the ASTM Type I specimen as designed. These nominal dimensions are shown in Figure 2-. The measured dimensions were the width of the testing region (Wc) and the thickness of the part (T), which are nominally 13 mm and 3.2 mm, respectively.

Tables 2-4 and 2-5 show the results of the width and thickness measurements for the Mark Two printed specimen, respectively. As an example, the specimen name "**0.1R-**

25” signifies a 0.1 mm layer height specimen printed with Rectangular infill at 25% infill density. The letterings in the specimen names from Tables 2-4 and 2-5 are referenced in the infill pattern row of Table 2-1.

Table 2-4: Mark Two Specimen Width Measurements

	Width (WC): 13 mm nominal		
Specimen Name	Average (mm)	Standard Deviation	% Error
0.1R-25	12.99	0.02	-0.08
0.1R-50	13.00	0.04	-0.03
0.1R-75	12.98	0.02	-0.18
0.1R-100	13.06	0.04	0.44
0.2R-25	13.08	0.01	0.62
0.2R-50	13.07	0.03	0.51
0.2R-75	13.12	0.04	0.92
0.2R-100	13.21	0.10	1.59
0.1H-25	12.98	0.02	-0.15
0.1H-100	13.03	0.03	0.26
0.1T-25	12.97	0.02	-0.23
0.1T-100	13.01	0.03	0.10
0.2H-25	13.08	0.04	0.59
0.2H-100	13.08	0.03	0.64
0.2T-25	13.03	0.01	0.26
0.2T-100	13.06	0.06	0.49
Mark Two Average	13.05	0.07	0.38

Table 2-5: Mark Two Specimen Thickness Measurements

	Thickness (T): 3.2 mm nominal		
Specimen Name	Average (mm)	Standard Deviation	% Error
0.1R-25	3.31	0.04	3.44
0.1R-50	3.32	0.07	3.65
0.1R-75	3.35	0.05	4.79
0.1R-100	3.32	0.07	3.75
0.2R-25	3.35	0.07	4.69
0.2R-50	3.38	0.06	5.52
0.2R-75	3.37	0.06	5.42
0.2R-100	3.35	0.05	4.69
0.1H-25	3.33	0.06	4.06
0.1H-100	3.33	0.08	4.06
0.1T-25	3.34	0.06	4.48
0.1T-100	3.31	0.06	3.33
0.2H-25	3.32	0.06	3.85
0.2H-100	3.33	0.06	3.96
0.2T-25	3.32	0.06	3.75
0.2T-100	3.31	0.06	3.54
Mark Two Average	3.33	0.05	4.06

When looking at the widths of the Mark Two specimen, it is observed that the 100% infill density parts for any infill type generally had the widest measurements. This is most likely due to expansion of the 100% infill density parts, which have no room to expand inward, and must expand only in an outward direction. Overall, the Mark Two specimen had an average width of 13.05 mm, a standard deviation of 0.07 mm, and a 0.38% error from nominal.

The thickness of these Mark Two specimen seemed to be more consistent among the various infill patterns and densities. The average thickness of these specimen was 3.33 mm, with a standard deviation of 0.05 mm, and a 4.06% error from nominal.

Tables 2-6 and 2-7 show the results of the width and thickness measurements for the Creator Pro specimen, respectively. As an example, the specimen name "**0.1Tran-100"** signifies a 0.1 mm layer height specimen printed with Transverse Infill at 100% infill density. The infill direction names from Tables 2-6 and 2-7 are referenced in the infill line directions row of Table 2-2.

Table 2-6: Creator Pro Specimen Width Measurements

	Width (WC): 13 mm nominal		
Specimen Name	Average (mm)	Standard Deviation	% Error
0.1R-50	12.99	0.06	-0.08
0.1R-75	13.15	0.13	1.17
0.1R-100	13.08	0.09	0.59
0.2R-25	13.03	0.04	0.26
0.2R-50	13.06	0.07	0.44
0.2R-75	13.13	0.14	0.97
0.2R-100	13.13	0.17	0.97
0.1Lon-100	12.98	0.15	-0.13
0.2Lon-100	12.91	0.13	-0.69
0.1Tran-100	13.19	0.21	1.47
0.2Tran-100	13.07	0.23	0.56
Creator Pro Average	13.07	0.14	0.56

Table 2-7: Creator Pro Specimen Thickness Measurements

	Thickness (T): 3.2 mm nominal		
Specimen Name	Average (mm)	Standard Deviation	% Error
0.1R-50	3.10	0.06	-3.02
0.1R-75	2.90	0.04	-9.42
0.1R-100	3.24	0.06	1.35
0.2R-25	3.29	0.03	2.71
0.2R-50	3.36	0.05	4.90
0.2R-75	3.36	0.07	5.10
0.2R-100	3.34	0.07	4.48
0.1Lon-100	2.88	0.02	-10.00
0.2Lon-100	2.95	0.03	-7.92
0.1Tran-100	3.02	0.04	-5.54
0.2Tran-100	3.17	0.05	-1.05
Creator Pro Average	3.13	0.19	-2.19

It is observed that the longitudinal parts printed on the Creator Pro were smaller in both width and thickness when compared to the rest of the specimen printed on the Creator Pro. The overall average width for parts on the Creator Pro was 13.07 mm, with a standard deviation of 0.14 mm and an error of 0.56% from nominal. The overall average thickness for these parts was 3.13 mm, with a standard deviation of 0.19 mm and an error of -2.19% from nominal.

When comparing the overall results of the Mark Two specimen with those from the Creator Pro, it is clear that the Mark Two printer came closer to printing dimensionally accurate parts. The Creator Pro had standard deviations twice as high as the Mark Two for width, and nearly four times as high for thickness.

2.4.2 Mass Measurement of Samples

Specimen were weighed before tensile testing in order to compare the actual weight of the specimen with the estimate given by Eiger or Cura. Table 2-8 shows the measurements for the parts printed with the Mark Two and Table 2-9 shows the measurements for the parts printed with the Creator Pro.

Table 2-8: Mark Two Part Mass vs. Eiger Estimate

Specimen Name	Eiger Estimate (g)	Average Mass (g)	Std. Dev.	% Error
0.1R-25	5.58	5.0321	0.0687	-9.82
0.1R-50	7.18	6.5571	0.0488	-8.68
0.1R-75	8.81	8.1827	0.0252	-7.12
0.1R-100	10.44	9.6118	0.0559	-7.93
0.2R-25	7.47	6.5187	0.0329	-12.73
0.2R-50	8.50	7.4756	0.0179	-12.05
0.2R-75	9.58	8.5375	0.0209	-10.88
0.2R-100	10.67	9.5455	0.0390	-10.54
0.1H-25	5.28	4.7189	0.0193	-10.63
0.1H-100	7.82	7.1579	0.0331	-8.47
0.1T-25	6.04	5.3701	0.0200	-11.09
0.1T-100	7.44	6.8560	0.0381	-7.85
0.2H-25	7.28	6.4229	0.0290	-11.77
0.2H-100	8.92	7.8378	0.0208	-12.13
0.2T-25	7.78	6.8198	0.0382	-12.34
0.2T-100	8.67	7.6691	0.0233	-11.54

Table 2-9: Creator Pro Part Mass vs. Cura Estimate

Specimen Name	Cura Estimate (g)	Average Mass (g)	Std. Dev.	% Error
0.1R-50	5	6.3979	0.0712	27.96
0.1R-75	8	6.6972	0.1114	-16.29
0.1R-100	10	9.1337	0.0399	-8.66
0.2R-25	3	6.4120	0.0540	113.73
0.2R-50	6	7.4233	0.0104	23.72
0.2R-75	8	8.3810	0.0453	4.76
0.2R-100	10	9.3084	0.0703	-6.92
0.1Lon-100	10	8.0766	0.1553	-19.23
0.2Lon-100	10	7.5117	0.1859	-24.88
0.1Tran-100	10	6.9704	0.2678	-30.30
0.2Tran-100	10	6.0704	0.0949	-39.30

Eiger mass estimates were given in grams with 0.01g precision. These estimates were fairly consistent across all infill types and densities, with errors between -7% and -12% for all specimen groups. Cura mass estimates were given in grams with 1 gram precision. These estimates were approximate and not very consistent. Errors ranged anywhere from -39% to 113%.

When comparing the mass results between Eiger and Cura, it is clear that Eiger mass estimates are much more accurate than Cura estimates. Parts printed with the Mark Two printer were consistently lighter than the Eiger mass estimate by about 10%.

2.4.3 Mechanical Testing

Tensile specimen were printed with both a MarkForged Mark Two and a Flashforge Creator Pro, and many variables were studied from each printer, including infill type, layer height, and infill density. The results of these tensile specimen will be divided into two sections based on the printer they were manufactured on, and will be discussed independently of each other, before the results from each printer will be compared.

The Ultimate Tensile Strength, Elastic Modulus, and % Strain at break were all determined from the stress-strain curves as tested by a MTS Universal Testing Machine. Figure 2-12 shows the stress-strain curves for all specimen printed on the Mark Two separated into subplots based on their layer height and infill type. Note that all infill densities for a given layer height/infill type specimen are shown on the same subplot, so a range of Ultimate Tensile Strengths can be observed on a single plot.

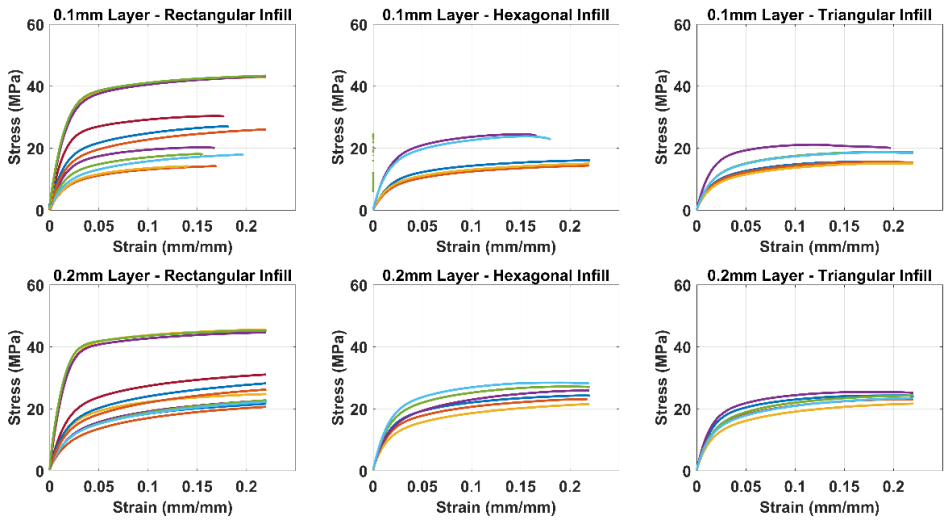

Figure 2-12: Mark Two Tensile Specimen compiled Stress-Strain Curves

Figure 2-13 shows the stress-strain curves for all specimen printed on the Creator Pro separated into subplots based on their layer height and infill line direction. Note that all infill densities for a given layer height/infill line direction specimen are shown on the same subplot, so a range of Ultimate Tensile Strengths can be observed on a single plot.

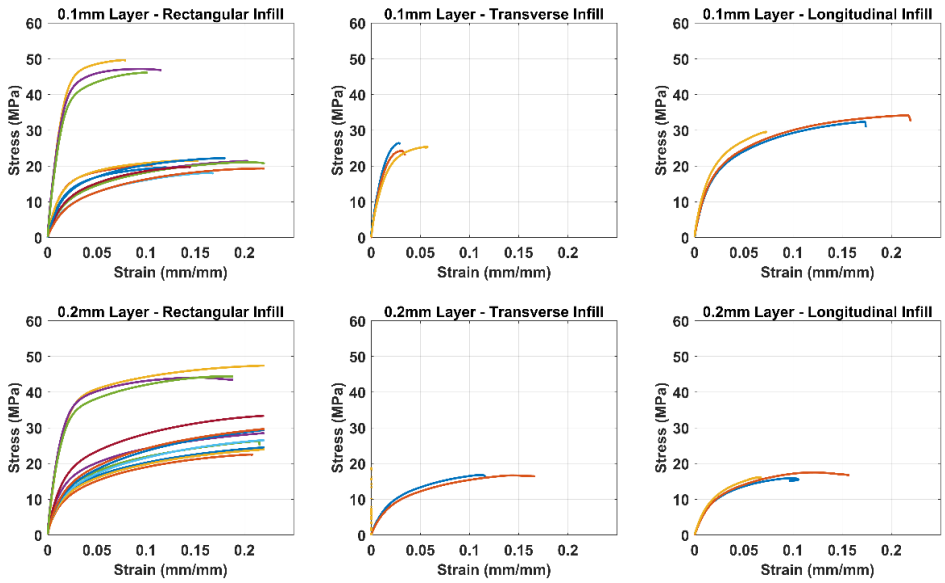

Figure 2-13: Creator Pro Tensile Specimen compiled Stress-Strain Curves

2.4.3.1 Mark Two Specimen Results

Figure 2-14 shows a plot of Ultimate Tensile Strength vs. Infill Density for all test specimen printed with the Mark Two. From the figure, it can be seen that Rectangular infills demonstrate an increase in Ultimate Strength as infill density increases, while the other infill types do not experience the same increase in Ultimate Strength. It is also observed that at lower infill densities, 0.2 mm layer height specimen were stronger than 0.1 mm layer height specimen, regardless of infill type. This trend was less apparent at 100% infill, and for rectangular infill at 100%, there was only a slight difference.

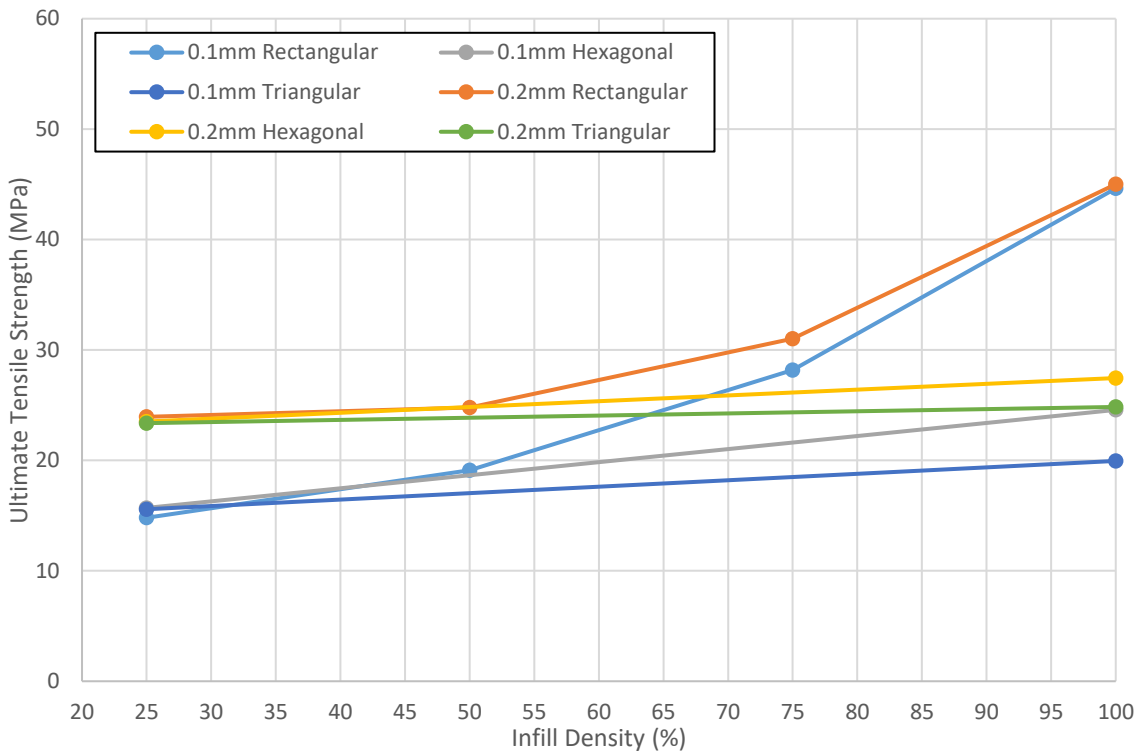

Figure 2-14: Effects of Infill Density for Various Infill Types on UTS, Mark Two Specimen

Figure 2-15 depicts the same groups of specimen and plots Elastic Modulus vs. infill density. Like the Ultimate Strength results, rectangular infill specimen saw increases in Elastic Modulus with an increase in infill density, while the other infill types saw little increase.

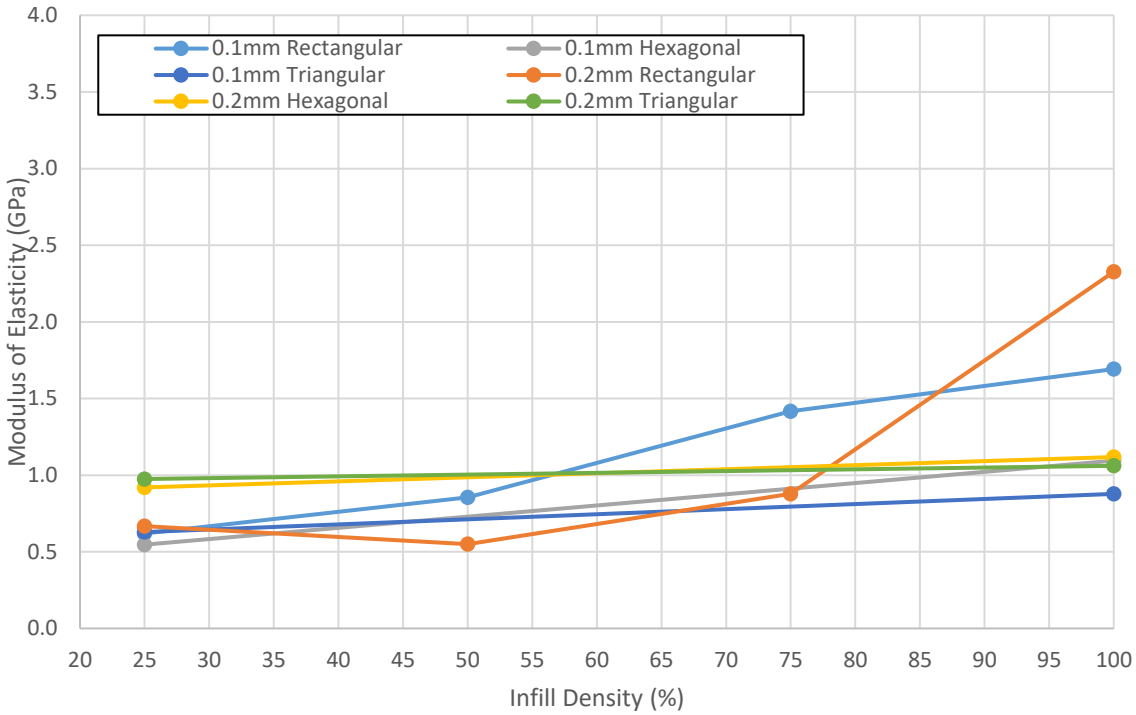

Figure 2-15: Effects of Infill Density for Various Infill Types on Elastic Modulus, Mark Two Specimen

Figure 16 shows Tensile Strength per unit mass vs. infill density. UTS per unit mass can be used as an indicator of material effectiveness towards strength. Like the last two figures, there is an upward trend for the rectangular infill specimen as infill density increases. This shows that an increase in material does result in an increase in strength. However, for the other infill types, there is a downward trend as infill density increases, which implies that the added material did not provide additional strength, only additional mass. With this info, it is apparent that higher infill densities of Hexagonal and Triangular infill are not providing a strength increase that makes the best of the mass of material used. All data discussed in this section can be seen in Table 2-10.

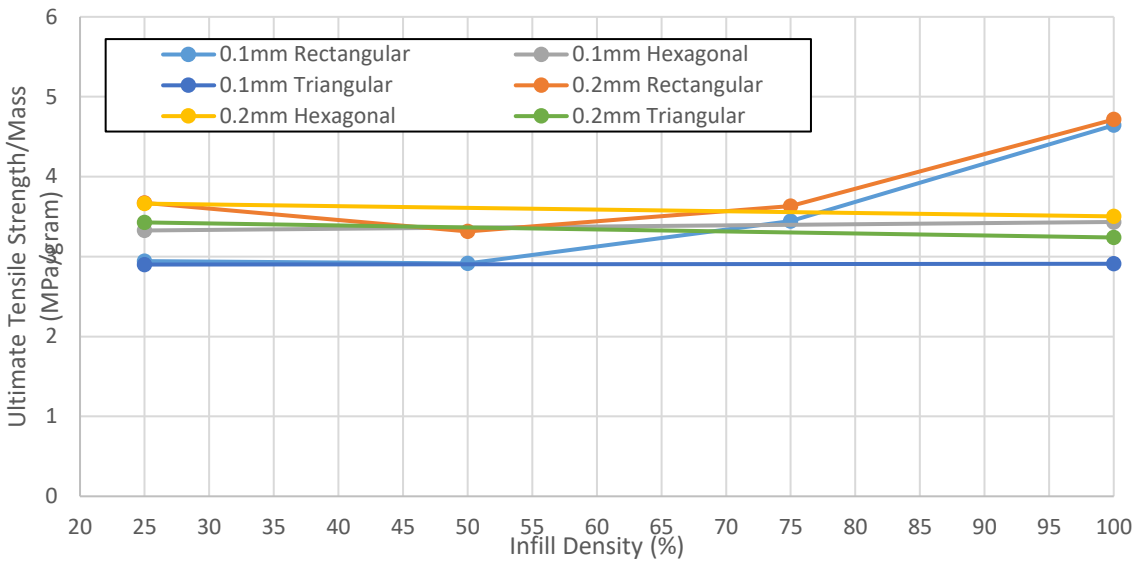

Figure 2-16: Plot of UTS/gram vs Infill Density for Various Infill types, Mark Two Specimen

Table 2-10: Table of variable group Average Tensile Data, Mark Two Specimen

Specimen Names	Infill Type	Fill Density (%)	Layer Height (mm)	Average UTS (MPa)	Std. Dev.	Average Modulus (GPa)	Std. Dev.
0.1R-25	Rectangular	25	0.1	14.8062	0.3954	0.6197	0.0461
0.1R-50	Rectangular	50	0.1	19.1089	1.7037	0.8557	0.2106
0.1R-75	Rectangular	75	0.1	28.1653	2.6813	1.4177	0.3824
0.1R-100	Rectangular	100	0.1	44.6290	0.2940	1.6919	0.2533
0.2R-25	Rectangular	25	0.2	23.9466	1.7912	0.6663	0.2591
0.2R-50	Rectangular	50	0.2	24.7775	0.8335	0.5498	0.0050
0.2R-75	Rectangular	75	0.2	31.0141	2.0575	0.8784	0.2600
0.2R-100	Rectangular	100	0.2	45.0094	1.2267	2.3265	0.1535
0.1H-25	Hexagonal	25	0.1	15.6985	0.8759	0.5465	0.0485
0.1H-100	Hexagonal	100	0.1	24.5742	0.8902	1.0946	0.0751
0.1T-25	Triangular	25	0.1	15.5750	0.1210	0.6289	0.0456
0.1T-100	Triangular	100	0.1	19.9506	1.8245	0.8778	0.2649
0.2H-25	Hexagonal	25	0.2	23.5242	1.4400	0.9198	0.0873
0.2H-100	Hexagonal	100	0.2	27.4568	1.7956	1.1181	0.1298
0.2T-25	Triangular	25	0.2	23.3747	1.6902	0.9748	0.1540
0.2T-100	Triangular	100	0.2	24.8398	1.5582	1.0610	0.1603

2.4.3.2 Creator Pro Results

Figure 2-17 shows a plot of Ultimate Tensile Strength vs. Infill Density for all test specimen printed with the Creator Pro. From the figure, it is shown that increasing infill density results in an increase in Ultimate Strength for Rectangular infill. Note that a 25% infill 0.1 mm layer height specimen group was not tested due to printer limitations as discussed above. Transverse and Longitudinal Specimen were only printed at 100% infill density, but it is shown that they did not achieve the same Ultimate Strength that the Rectangular infill specimen did. For these transverse and longitudinal specimen, the layer height seemed to be more of a factor in Ultimate Strength than the direction of infill, as both 0.1 mm layer height groups achieved higher Ultimate Strengths than the 0.2 mm layer height groups.

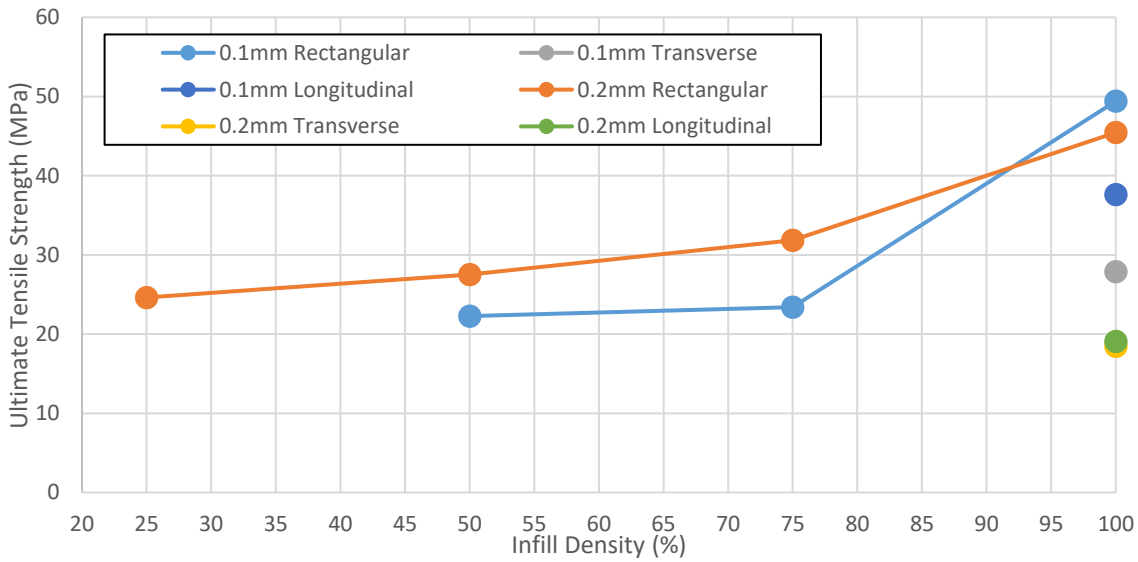

Figure 2-17: Effects of Infill Density for Various Infill Types on UTS, Creator Pro Specimen

Figure 2-18 depicts the same groups of specimen and plots Elastic Modulus vs. infill density. A similar trend was observed where higher infill densities resulted in increased Elastic Moduli. For the Longitudinal and Transverse specimen, 0.1 mm layer

height groups performed better than 0.2 mm layer height groups, similarly to the tensile results from Figure 2-17.

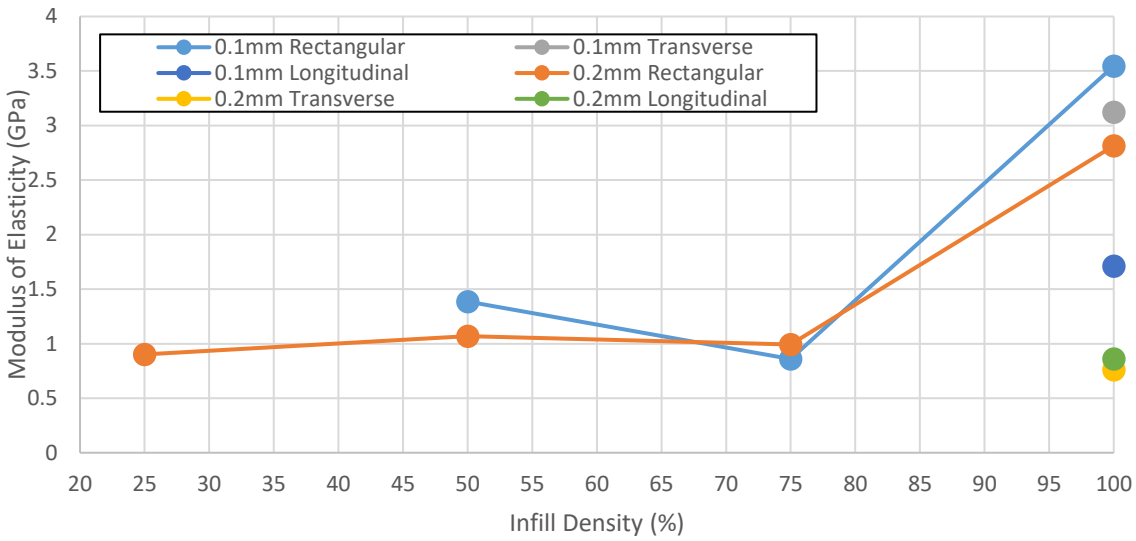

Figure 2-18: Effects of Infill Density for Various Infill Types on Elastic Modulus, Creator Pro Specimen

Figure 2-19 shows the results of Ultimate Tensile Strength per unit mass vs. infill density. UTS per unit mass can be used as an indicator of material effectiveness towards strength. There is a slight increase in the rectangular groupings at 100% infill density, with the rest of the rectangular groupings holding fairly consistent. Overall, the Rectangular groupings and the 0.1mm Longitudinal group have the best UTS per unit mass while the other groupings seemed to be less effective. This implies that Rectangular infill as well as 0.1mm longitudinal specimen would be good choices for the best use of materials to create a given strength of part.

All data discussed in this section can be seen in Table 2-11.

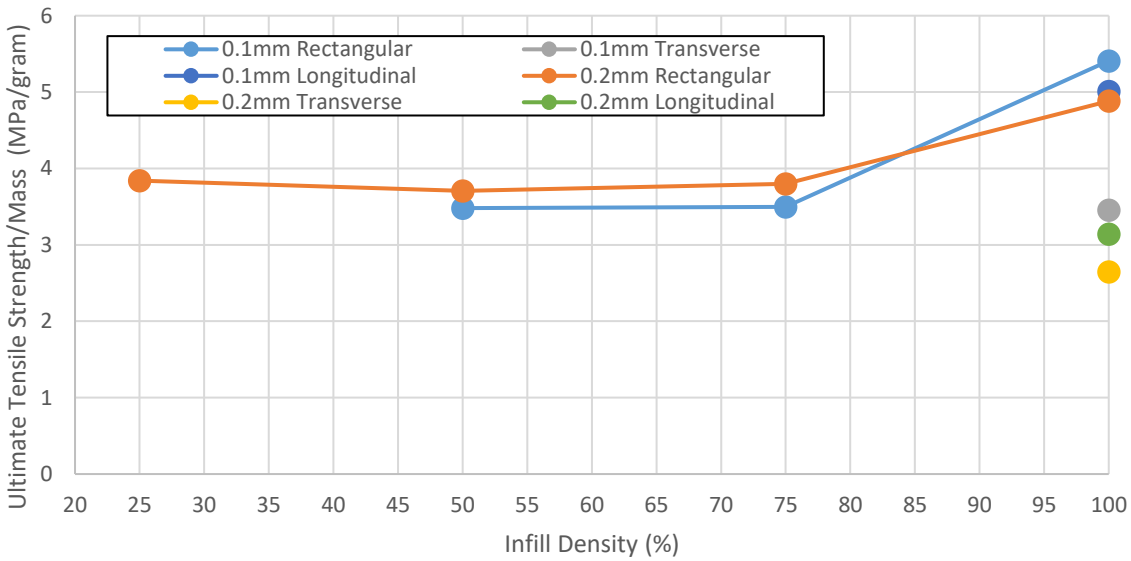

Figure 2-19: Plot of UTS/gram vs Infill Density for Various Infill types, Creator Pro Specimen

Table 2-11: Table of variable group average Tensile Data, Creator Pro

Specimen Names	Infill Type	Fill Density (%)	Layer Height (mm)	Average UTS (MPa)	Std. Dev.	Average Modulus (GPa)	Std. Dev.
0.1R-50	Rectangular	50	0.1	22.2746	0.5476	1.3848	0.1601
0.1R-75	Rectangular	75	0.1	23.4241	1.9787	0.8597	0.2178
0.1R-100	Rectangular	100	0.1	49.4101	3.0661	3.5457	0.6091
0.2R-25	Rectangular	25	0.2	24.6265	1.4696	0.9015	0.0416
0.2R-50	Rectangular	50	0.2	27.5176	1.8513	1.0698	0.1190
0.2R-75	Rectangular	75	0.2	31.8303	2.3989	0.9924	0.1948
0.2R-100	Rectangular	100	0.2	45.4479	3.1530	2.8143	0.1780
0.1Lon-100	Longitudinal	100	0.1	37.6418	2.9211	1.7120	0.4345
0.2Lon-100	Longitudinal	100	0.2	19.0777	0.9986	0.8611	0.0735
0.1Tran-100	Transverse	100	0.1	27.9047	1.6730	3.1237	0.7975
0.2Tran-100	Transverse	100	0.2	18.4571	0.6052	0.7598	0.0692

2.4.3.3 Comparison of Results.

Figures 2-20 and 2-21 show a comparison of UTS and Elastic Modulus results for the Creator Pro and Mark Two printed specimen. Standard deviations of each specimen grouping are shown on their respective bars in each bar chart. From Figure 2-21, it can be seen that overall, 0.2mm layer height parts were stronger than their 0.1mm layer height counterparts, except in the case of the Creator Pro parts printed at 100% infill density, where the 0.1mm layer height parts turned out to be the strongest overall. The Creator Pro also produced parts with a higher UTS than the Mark Two in each infill density category, while maintaining similar standard deviations among the sample group.

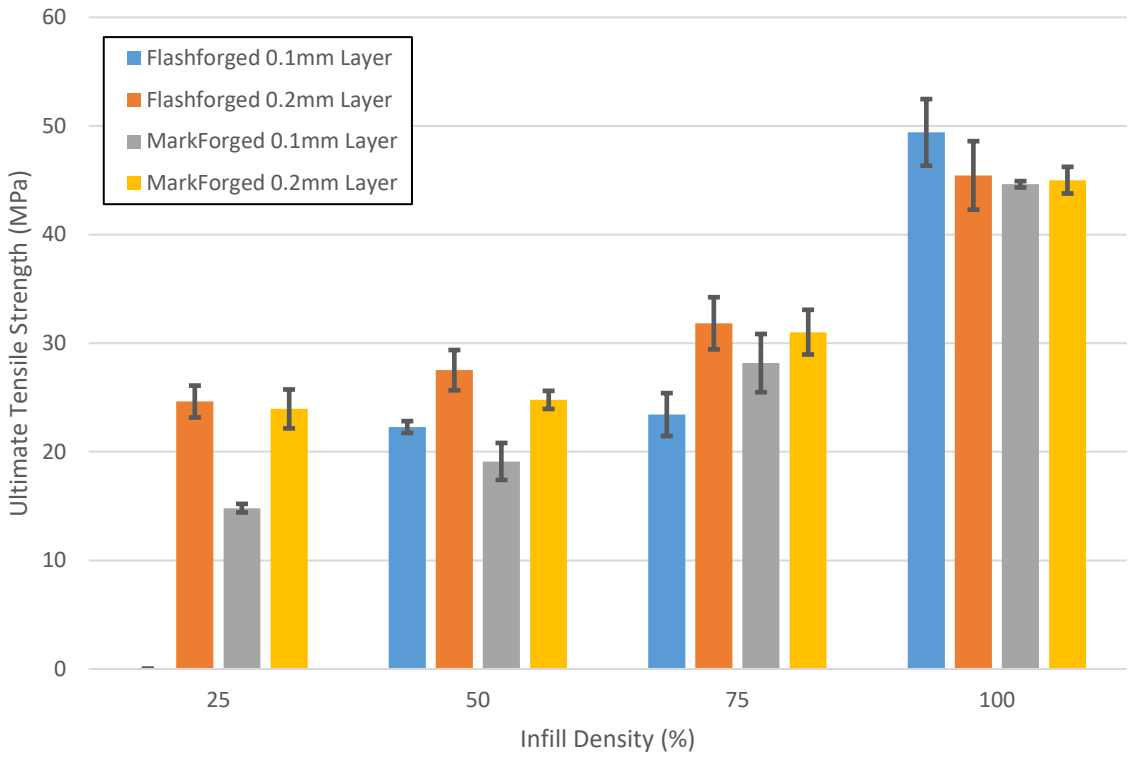

Figure 2-20: Comparison of UTS results – Creator Pro vs. Mark Two

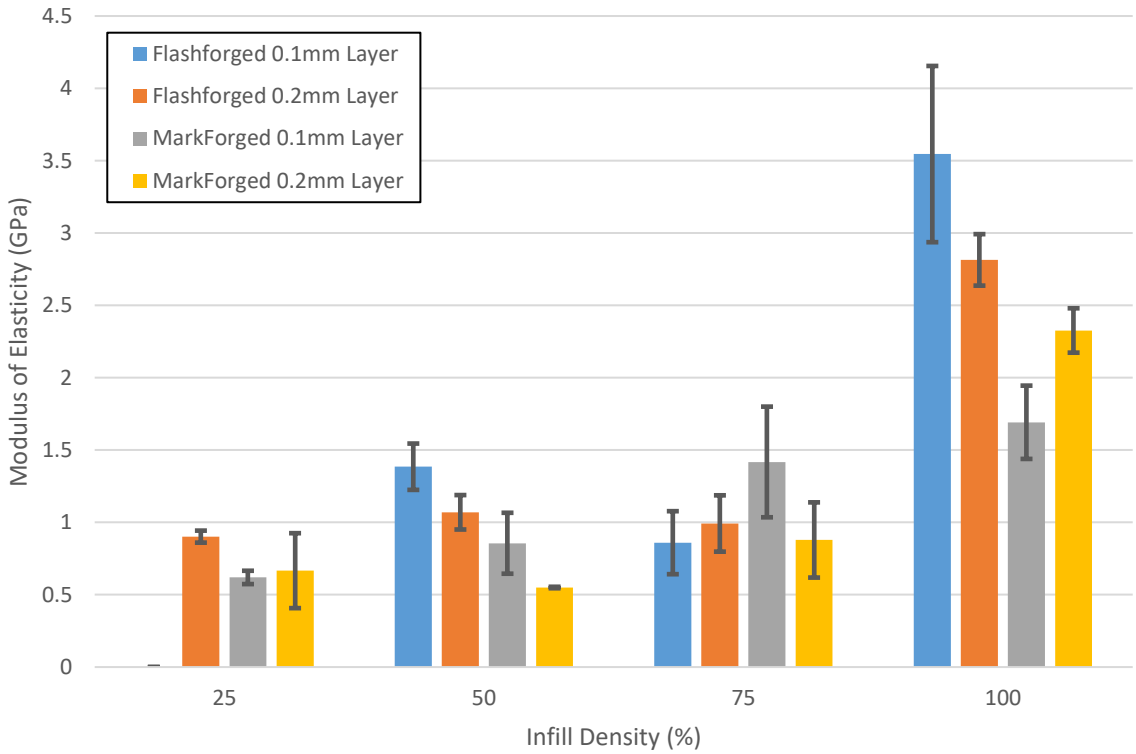

Figure 2-21: Comparison of Modulus Results – Creator Pro vs. Mark Two

From Figure 2-21, it is seen that Elastic Modulus experienced much more variability within the specimen groupings than UTS. The Creator Pro produced parts with a higher Elastic Modulus on average, similar to the UTS data. The Mark Two did achieve the highest Elastic Modulus for the 75% infill density grouping, but the Creator Pro achieved the highest Elastic Modulus in the 100% infill density grouping by a large margin, even when taking the standard deviation into consideration. The average elastic modulus for all 100% infill specimen printed was found to be 2.5946 GPa with a standard deviation of 0.7831 GPa.

2.4.4 Micromechanical Modeling

From the analysis done with the Keyence Microscope and ImageJ, as discussed in the experimental procedure section, properties were obtained for the Onyx micromechanical structure as shown in Table 2-12. The elastic modulus of Nylon was obtained from the Markforged Website and the elastic modulus of the fibers was obtained from Meddad et al [47]. These properties were used in each of the three micromechanical models presented above to estimate the elastic modulus of Onyx parts printed at 100% infill density.

Table 2-12: Micromechanical Structure Properties

Micromechanical Structure	
Average Fiber Diameter (µm)	7.36
Average Fiber Length (µm)	108.2
Average Fiber Fraction (%)	9.129
Orientation Factor - η_o	0.5575
Fiber Modulus (GPa)	232
Nylon Modulus (GPa)	0.94

The Rule of Mixtures model evaluated with the properties listed in Table 2-12 resulted in an Elastic Modulus of 22.03 GPa. As discussed above, the Rule of Mixtures model overestimates the strength of short fiber composites because it assumes that the fibers are continuous and perfectly parallel with the tensile axis. It is clear that this model has overestimated the elastic modulus of these parts, which can be seen in Figure 2-21 in the 100% infill grouping. The Halpin-Tsai model did a much better job at approximating the elastic modulus of these parts with 100% infill, and resulted in an estimate of 3.467 GPa, which is just on the upper end of the range observed from the experimental data. The Modified Rule of Mixtures Model was the best fit with the experimental data overall, and

resulted in an estimate of 2.744 GPa, which is nearest to the middle of the experimental data grouping for 100% infill. The overall average Elastic Modulus for all experimental data at 100% infill is 2.5946 GPa.

Based on these results, it is observed that the Modified Rule of Mixtures Model predicted the Elastic Modulus of these parts most closely. Patanwala et al also made this observation when looking at these three micromechanical models for a variety of specimen of different fiber volume fractions [36]. It is to be expected that the Modified Rule of Mixtures Model would produce the best results of the three models for a wide variety of Micromechanical properties.

2.5 Conclusions

The tensile properties of short carbon fiber composites printed with Onyx on a Mark Two and Creator Pro 3D printer were analyzed and compared with one another. These parts were printed at a variety of infill densities and infill types, as well as varying layer heights. As expected, parts with higher infill densities yielded higher Ultimate Tensile Strengths and Elastic Moduli. Parts printed with the Creator Pro achieved higher Ultimate Tensile Strengths and Elastic Moduli than their respective Mark Two counterparts on average, with a maximum Tensile Strength of 49.4 MPa and a maximum Elastic Modulus of 3.5 GPa from the creator pro, as opposed to maximums of 45 MPa and 2.3 GPa for Tensile Strength and Elastic Modulus, respectively, from the Mark Two.

The dimensional accuracy of both printers and the mass estimates of their respective slicers were also analyzed. The Mark Two yielded more dimensionally accurate parts than the Creator Pro. Dimensions of the Mark Two specimen had standard deviations of 0.07 mm and 0.05 mm for width and thickness, respectively, while the Creator Pro specimen

had standard deviations of 0.14 mm and 0.19 mm, respectively, while both printers seemed to achieve similar width and thickness averages. This implies that the Mark Two was able to print its specimen closer to nominal as a whole. Furthermore, Eiger produced more accurate mass estimates than Cura. Eiger mass estimate percent errors ranged from -7% to -12%.Cura mass estimates ranged anywhere from -39% to 113%. Eiger mass estimates were consistently higher than actual specimen masses by about 10%.

A variety of analytical models for short fiber composites were also used to estimate the Elastic Modulus of parts printed with 100% infill. The Modified Rule of Mixtures Model produced the most accurate results when compared with Experimental Data, resulting in an estimated Elastic Modulus of 2.744 GPa for 100% infill specimen, compared to the overall experimental data average of 2.5946 GPa for all 100% infill specimen.

CHAPTER 3 - TENSILE STRENGTH OF CONTINUOUS FIBER SPECIMEN

3.1 Abstract

Studies have been done involving the use of carbon fiber as a reinforcement for three dimensional (3D) printed parts. The Markforged Mark Two is a commercial grade 3D printer capable of printing parts reinforced with continuous fibers such as carbon fiber, Kevlar, and fiberglass. The previous model, the MarkForged Mark One, was capable of printing continuous fibers only in a concentric nature within the part. The Mark Two printer now has the capability of printing parts in both concentric and isotropic fill types. The Mark Two was used to print specimen for tensile testing using Markforged Nylon filament reinforced with Markforged Carbon Fiber filament in continuous pathways. Various Carbon Fiber orientations and layer proximities were tested and their effects on Tensile Strength and Modulus of Elasticity were examined. A Volume Average Stiffness (VAS) model was also used to predict the elastic properties of these 3d-printed specimen. Tensile Testing of the 3d-printed specimen showed that material properties were directly related to the number of carbon fiber strands loaded in tension within the part, and that the increase in these material properties was linear. Average Ultimate Tensile Strengths of 33.0 MPa, 121.3 MPa, 161.3 MPa, and 300.6 MPa were observed for 3d-printed specimen with carbon fiber volume fractions of 0%, 13.02%, 19.53%, and 39.05% respectively. Average Elastic Moduli of these specimen were 0.75 GPa, 9.5 GPa, 12.6 GPa, and 26.5 GPa respectively. The VAS model increases in accuracy as the amount of fiber reinforcement increases, resulting in differences of 61.26%, 7.34%, 3.30% and 3.60% predicted strength for the same volume fractions, respectively.

3.2 Introduction

The addition of Continuous Carbon fibers into the printed part increases both its Ultimate Tensile Strength as well as the Tensile Modulus. However, these tensile properties are quite inconsistent due to the complicated nature of including continuous carbon fibers within an FDM printed part.

Markforged developed a commercially available semi-industrial grade 3d printer with the capability to automatically and repeatably reinforce Nylon FDM printed parts with a variety of continuous fibers, including glass, Kevlar fibers, and carbon fiber. The first iteration of this printer, the Mark One, was capable of printing these Nylon FDM parts with concentric rings of fibers for reinforcement [32]. The objective of this printer is to produce parts that are stronger than standard FDM parts, reliably with consistent results.

The second iteration of this printer, The Mark Two by MarkForged is similar to the Mark One 3D printer in that it reinforces FDM printed components with continuous glass, Kevlar, and carbon fibers. Both printers have two extruders and utilize the Composite Filament Fabrication (CFF) technology. While the Mark One is only capable of embedding concentric rings of carbon fiber along the outside geometry of the component, the Mark Two allows for concentric placement of fibers as well as isotropic placement of fibers. Both Concentric and Isotropic Fiber fill patterns can be used simultaneously or independent of each other, yielding much more flexibility for the designer [32].

Previous work has been done by Melenka et al to evaluate the tensile properties of continuous fiber reinforced 3D printed components produced using the MarkOne 3D printer [32]. This study performed conventional tensile tests and compared the experimental results with analytical results from a Volume Average Stiffness Model.

However, this study only evaluated components with concentric Kevlar fibers in limited quantities. In order to better understand strength characterizes of parts made with these continuous fiber reinforcement, more work must be done to understand the role of isotropic fibers.

The goal of this study is to further investigate the mechanical properties of continuous fiber reinforced 3D printed parts, specifically using isotropic fill patterns. The first step to this investigation is to perform conventional tensile tests on components printed with a variety of fiber fill patterns. The second step is to refine the Volume Average Stiffness (VAS) model presented by Melenka et al to yield more accurate results of elastic constants [32]. The refinement of this VAS model will provide designers and engineers with an accurate method to determine the tensile properties of a variety of different parts printed on the Mark One and Mark Two 3D printers.

3.3 Experimental Procedures

3.3.1 Mechanical Testing

The specimen used for mechanical testing were printed with a Mark Two 3D printer (Mark Two, MarkForged, Somerville, MA). The geometry of the specimen was defined by ASTM D638-10 (ASTM D638-10, Standard Test Method for Tensile Properties of Plastics) as a Type I geometry [39]. This geometry and its dimensions are shown in Figure 3-1. The specimen was modeled with SolidWorks Computer Aided Design (CAD) software (SolidWorks 2016, Dassault Systemes, Waltham, MA USA). The specimen was then exported as a Standard Tessellation Language (STL) file and uploaded into the MarkForged 3D printer slicing software (Eiger 1.2, MarkForged, Somerville, MA USA). Eiger is the required proprietary slicing software to generate files for the MarkTwo as Eiger

not only determine deposition of the nylon polymer, but also controls the placement of the fibers. For this study, all specimen were printed with MarkForged Nylon (Nylon, MarkForged, Somerville, MA USA and MarkForged Carbon Fiber (Carbon Fiber, MarkForged, Somerville, MA USA) Filaments.

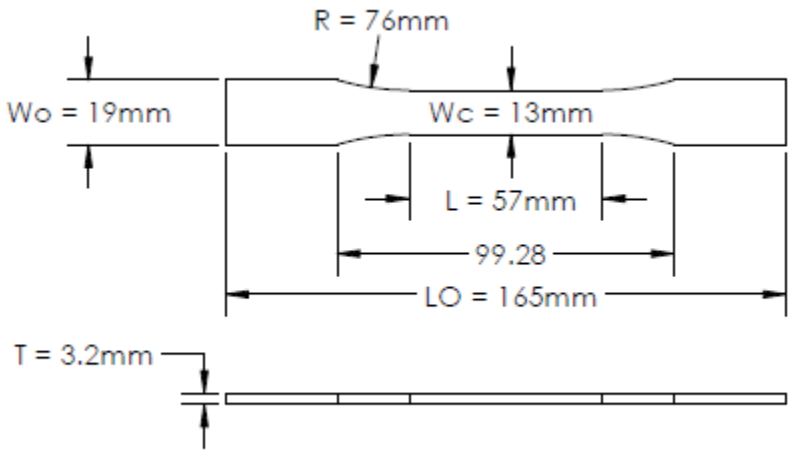

Figure 3-1: Test specimen dimensions as defined by ASTM D638-10

Though Kevlar, Glass, and HSHT Glass fibers were also available, Carbon Fiber was chosen as the material to reinforce the specimen due to its high strength properties. The settings chosen in Eiger to print the parts are outlined in Table 3-1. Isotropic fiber fill types with varying numbers of fiber layers, fiber orientations, and fiber proximities were used in this study. Use of Isotropic Fiber fill allows the designer to choose the orientation of the isotropic fibers, so samples with fiber orientations of 0 degrees (longitudinal), 45 degrees alternating, and 90 degrees (transverse) were studied. Samples with Isotropic Fill with purely longitudinal fibers contained 11 strands of longitudinal fiber through the test section per layer. The number of fiber layers, their proximity to neighboring layers, and the orientation of the isotropic fiber fill were all varied to create a wide variety of sample types and strengths. Figure 3-2 shows a variety of possible fiber fill type combinations

possible. Type A depicts a 0 degree (longitudinal) isotropic fill type, Type B depicts a 4 ring concentric fill type, Type C depicts a combination of 4 ring concentric and 0 degree longitudinal isotropic fill type, Type D depicts a 45 degree isotropic fill type, and Type E depicts a 90 degree (transverse) isotropic fill type. Note that for this study, only Types A, D, and E were examined, and no samples with concentric fiber fills were studied.

Table 3-1: Print Parameters for Test Specimen

Print Parameters	
Layer Height (mm)	0.125
Infill Pattern	Rectangular Fill
Infill Percentage(%)	100
Infill Orientation (degrees)	45
Number of Walls	2
Number of Floor Layers	4
Number of Roof Layers	4
Total Number of Layers	26

Figure 3-2: Fill type combinations within a single layer of the print. Types A, D, and E were examined in this study

Various fiber layer proximities were also studied, as shown in Figure 3-3. From the figure, parts with Layer Proximities of 1 and 2 are shown. A 1 layer proximity part implies that each layer of fiber is surrounded on top and bottom by nylon, such that each Fiber Grouping or fiber cluster contains only 1 layer of carbon fiber. A 2 layer proximity part implies that each group or cluster of fibers has two consecutive layers of carbon fiber before a nylon layer will appear. In this study, up to 6 layer proximity parts were printed. Layer proximity does not imply how many total layers of carbon fiber can exist in the part, but the total number of layers in the part will be an integer multiple of the layer proximity. For

example, a 6 layer proximity part could be a 6 layer part with 1 group of 6 fiber layers, it could also be a 12 layer part with 2 groups of 6 fiber layers, or it could also be an 18 layer part with 3 groups of 6 fiber layers.

Figure 3-3: Example of Layer Proximities. Each specimen above has 4 total layers of CF Filament. Layer Proximity 1 has 4 groups of fibers each with 1 layer per group, while Layer Proximity 2 has 2 groups of fibers each with 2 layers per group. The amount of fibers per cluster, or group of fibers denotes the Layer Proximity Number.

3.3.2 Dimensional Measurement of Samples

All samples were measured before tensile testing and the measurements were recorded for use in the Elastic analysis. The width of the test area (Wc) and the thickness of the part (T), shown in Figure 3-1, were measured with a caliper (Mitutoyo 500-196-30). These measurements are used to calculate stress over the actual cross sectional area and can be used to evaluate the dimensional accuracy of the Mark Two 3D printer showing potential differences between fiber placement methods.

3.3.3 Testing Parameters

The 3D printed test specimen were evaluated for their tensile properties using an MTS machine (MTS 858, MTS, Eden Prairie, MN USA), shown in Figure 3-4. During the tests, strain was measured with a 20mm gauge length extensometer (MTS 634.31F-24, Eden Prairie, MN USA). The samples were loaded in tension at a rate of 5 mm/min according to ASTM D638-10 [14] and load and extensometer data was recorded at 25 Hz.

The data recorded by the MTS Machine was saved as a csv file and analyzed with MATLAB (MATLAB 2017a, The MathWorks, Inc., Natick, MA USA). A sample of the MATLAB script used to analyze the stress-strain data is shown in Appendix A.

Figure 3-4: Mechanical testing of 3D printed specimen using an MTS 858 universal Testing Machine

3.3.4 Digital and Laser Microscopy

In order to gain a better understanding of the materials and internal structure of 3D printed parts, test specimen were examined with both digital and laser microscopy. Cross sections of the specimen of interest were placed in the LECO mounting press (PR-32, LECO, Saint Joseph, MI USA) where 1” diameter molded samples were formed with buehler phenolic powder. These molded samples are cured with heat and pressure inside the mounting press.

The molded samples were then polished with a Digiprep Specimen Mover (DIGIPREP 250, Qualitest North America, Ft. Lauderdale, FL USA) using a 7-step polishing process. First, the molded samples were ground with 240 grit SiC paper, followed by 320 grit SiC paper until plane. Next, the molded samples were ground with 600 grit SiC paper for 1 minute per step, followed by 1200 grit SiC paper for 1 minute per step. The sample was then polished for 3 minutes per step using a 6 µm DIAMAT diamond polishing solution on a TEXPAN polishing pad with DIALUBE Purple extender as a lubricant. This was followed by secondary polishing step for 2 minutes per step using a 1 µm DIAMAT diamond polishing solution on an ATLANTIS polishing pad with DIALUBE Purple extender as a lubricant. Finally, the molded sample was polished for 1 minute per step with a 0.05 µm Nanometer Alumina polishing solution on a NAPPAD polishing pad. Steps 3 through 7 were each repeated a total of 3 times before moving on to the next step. The entire polishing process is shown in Table 3-2. The molded samples were then imaged with either a Keyence Digital Microscope (VHX-6000, Keyence Corporation, Elmwood Park, NJ USA) or a Keyence Laser Scanning Microscope (VK-9700, Keyence Corporation, Elmwood Park, NJ USA) depending on the level of magnification needed.

Table 3-2: Molded specimen polishing procedure

Step	Abrasive/Surface	Table Speed (RPM)	Spindle Speed (RPM)	Time
1	240 grit SiC paper	100 CCW	100 CCW	Until Plane
2	320 grit SiC paper	100 CW	100 CW	Until Plane
3	600 grit SiC paper	150 CCW	150 CCW	1 min
4	1200 grit SiC paper	150 CW	150 CW	1 min
5	6 µm DIAMAT diamond on TEXPAN polishing pad	150 CCW	150 CCW	3 min
6	1 µm DIAMAT diamond on ATLANTIS polishing pad	200 CW	200 CW	2 min

7	0.05 µm Nanometer Alumina on NAPPAD polishing pad	200 CCW	200 CCW	1 min

3.3.5 Image J Analysis and Elastic Constants

ImageJ [40] an open-source image analysis software was used to determine the volume fraction of carbon fiber yarns within a 3D printed cross section of carbon fiber filament as well as the void density of nylon in a 3D printed cross section. Image thresholding in ImageJ was used to determine the carbon fiber yarn volume fraction from five laser microscope images of various zoom levels selected for their overall qualities as a representative sample of printed carbon fiber layers.

The following steps were taken to perform a volume fraction analysis in Image J. First, the image was opened in Image J and cropped to remove any scale bars or unwanted areas of interest. Next, the image was converted to 8-bit grayscale. Then the threshold of the image was adjusted to select the areas of interest within the image (i.e.: voids in a nylon print area or carbon fiber strands in a carbon fiber print area). Once the threshold has been adjusted, a new black and white image is created which isolates the areas of interest from the rest of the image. Lastly, the area of the black and white portions of the image are analyzed with the analyze particles feature. The result is a total area of the desired region, as well as a breakdown of the individual areas and count of these individual areas.

As mentioned above, Image J was used to determine the volume fraction of carbon fiber yarns in a printed carbon fiber layer as well as the void density of printed Nylon. For the determination of carbon fiber yarn volume fraction, 5 laser microscope images of various zoom levels were selected for their overall qualities as a representative sample of printed carbon fiber layers. The percent of carbon fiber yarns in each image was found,

with an average of 28.007% carbon fiber yarn, and a standard deviation of 8.15%. Figure 3-5 below shows a laser microscope image of a printed layer of carbon fiber at 1000x zoom, while Figure 3-6 shows the threshold created in Image J for this image. The volume fraction of carbon fiber yarns for this particular image was found to be 29.552%. Additional Continuous Fiber Microscope images can be seen in Appendix I.

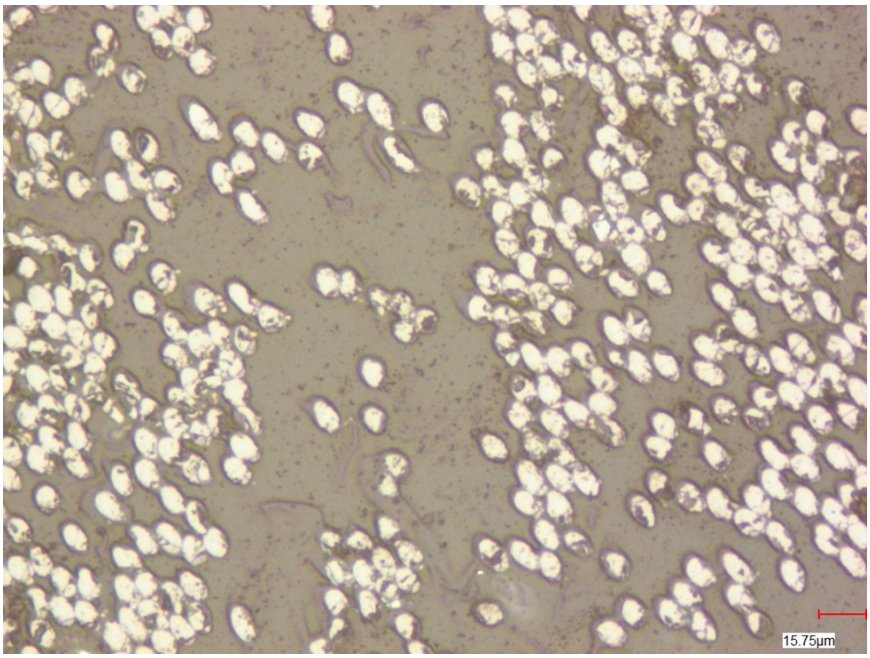

Figure 3-5: Laser microscope image of 3D printed carbon fiber printed filament cross section at 1000x zoom

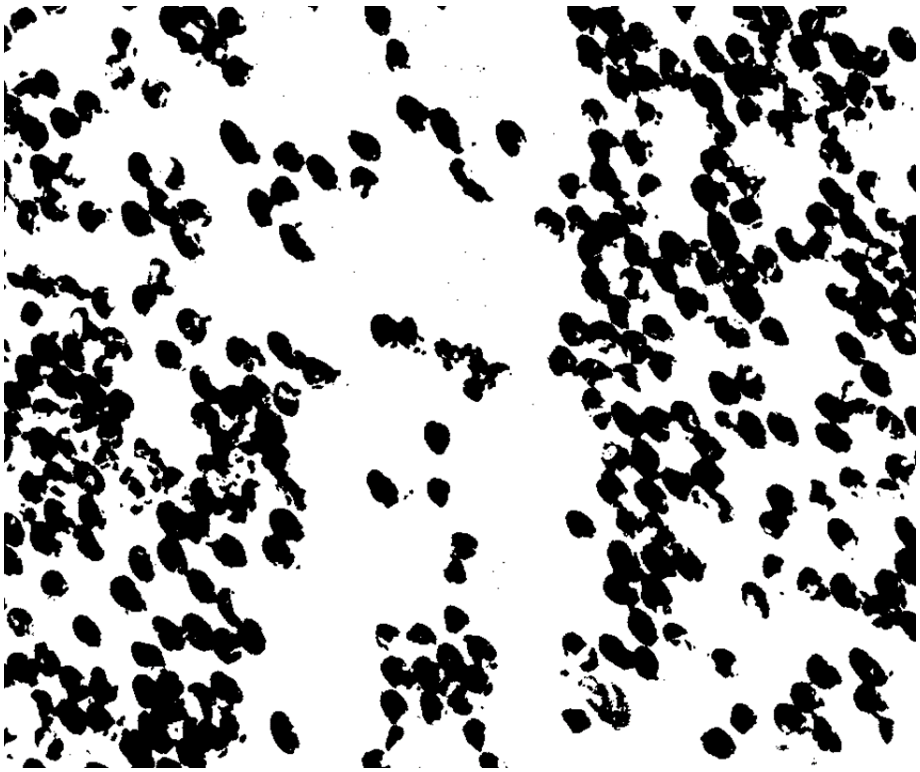

Figure 3-6: Image J cropped threshold image of 3D printed carbon fiber printed filament cross section at 1000x zoom. The volume fraction of CF yarns in this particular image was found to be 29.552%.

The void density of nylon was found in a similar manner. The average void density was found to be 0.973%. This value for void density will be used in a later section pertaining to stiffness modeling, and will be denoted as rho. A cross section of a nylon printed part is shown in Figure 3-7.

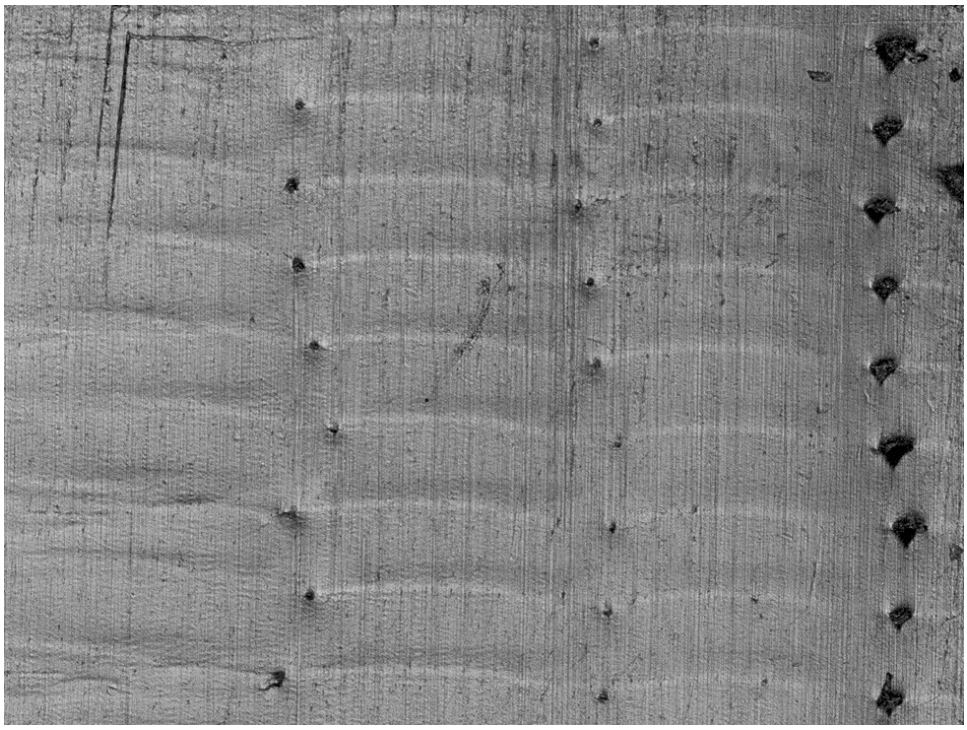

Figure 3-7: Laser microscope image of 3D printed Nylon at 200x zoom

The elastic properties of nylon were obtained from the study performed by Melenka et al, and are summarized in Table 3-3 [32]. The properties for Carbon fiber required a bit more effort to obtain and apply to the Markforged carbon fiber filament. First, the approximate diameter of the carbon fiber yarns was determined with the laser microscope by measuring the diameter of several individual yarns (see Figure 3-5). The average diameter of yarns in the Markforged carbon fiber filament were found to be 7.2 μm, and typical carbon fiber yarn properties from [47] were obtained. These properties are shown in Table 3-4. Note that the longitudinal elastic modulus listed in the table has been multiplied by the carbon fiber yarn density of 28.007%. This is to correct for the fact that the estimated carbon fiber filament volume in the composite includes both carbon fiber yarns and a binding agent, of which, only the carbon fiber yarns are providing any

noticeable tensile strength to the composite part. Multiplying the elastic modulus by the yarn density allows this property to be applied to the entire volume of carbon fiber filament.

Table 3-3: Assumed material properties of Nylon filament [32]

Material Property	Value
Elastic Modulus - E (GPa)	0.75
Shear Modulus - G (GPa)	0.28
Poisson's Ratio - ν	0.35

Table 3-4: Assumed material properties of carbon fiber yarn in filament

Material Property	Value
Axial Elastic Modulus - Ef1 (GPa)	64.7
Transverse Elastic Modulus - Ef2 (GPa)	22.4
Axial Shear Modulus - Gf12 (GPa)	22.1
Transverse Shear Modulus - Gf23 (GPa)	8.3
Axial Poisson's Ratio - $\nu 12$	0.3
Transverse Poisson's Ratio - $\nu 23$	0.35

3.3.6 Internal Microstructure

Figure 3-8 shows the cross-sectional breakdown of the tensile composite specimen by its different materials. From the figure, it can be seen that 3 unique regions exist within the composite specimen. These regions include: Solid regions within the part, in which nylon is printed at ±45 degrees from the longitudinal axis, alternating layer by layer; Shell regions, in which a nylon border is printed around the perimeter of the part layer by layer, and are printed in parallel to the longitudinal axis; and carbon fiber regions, in which carbon fiber filament is printed in an isotropic fill pattern parallel to the longitudinal axis of the part.

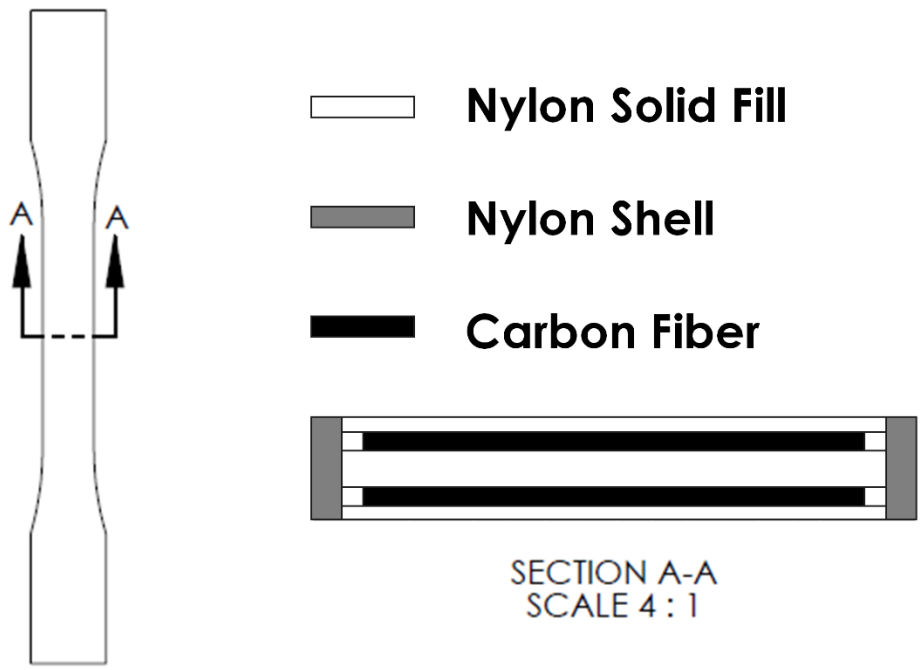

Figure 3-8: Schematic of the internal structure of a typical carbon fiber reinforced 3D printed specimen used in this study. Left: Top view of the printed specimen. Right: Cross section of the specimen. Solid Nylon regions are white, shell regions are gray, and carbon fiber regions are black

Measurements of the various dimensions needed to determine these volumes were obtained from microscope images of the geometry as well as information from Eiger. These dimensions are shown in Table 3-5. Note that for the number of floor and roof layers, 4 layers were used by default in Eiger, but this value was changed to 1 roof and 2 floor layer for 24 layer carbon fiber specimen.

Table 3-5: Internal microstructure dimensions

Dimension Variable	Value
Length - L (mm)	57
Width - W (mm)	13
Height - H (mm)	3.25
Layer Height - H_layer (mm)	0.125
Width of Shell - W_shell (mm)	0.39
Number of Shells - N_shell	4
Width of Fiber Strand - W_strand (mm)	1
Number of Fiber Strands Wide - N_strand	11
Number of Fiber Layers - N_fiber	0 - 24
Number of Floor Layers - N_floor	1, 4
Number of Roof Layers - N_roof	1, 4
Orientation of Solid Fill - Alpha (degrees)	45

With these dimensions, the following equations were used to determine the volume fraction of each of the three fill types.

The total volume of the tensile area in the sample is found with:

$$V_{total} = HWL \tag{1}$$

The Volume of both Shell regions is given by:

$$V_{shell} = N_{shell} W_{shell} HL \tag{2}$$

The volume of the Floor Solid Region is given by:

$$V_{floor} = (W - W_{shell}) N_{floor} H_{layer} L \tag{3}$$

Similarly, the volume of the Roof Solid Region is given by:

$$V_{roof} = (W - W_{shell}) N_{roof} H_{layer} L \tag{4}$$

The volume of Carbon Fiber Filament Regions is given by:

$$V_{fiber} = (W_{strand} N_{strand}) N_{fiber} H_{layer} L \tag{5}$$

Since the width of 11 fibers in a layer plus the width of both shells is less than the overall width of the part, Eiger places a small amount of nylon on either side of the carbon fiber

on each carbon fiber layer to fill in the gaps. The volume of this nylon infill in the fiber layers is given by:

$$V_{fiber\ layer\ infill} = \left(W - W_{shell} - (W_{strand}N_{strand})\right)N_{fiber}H_{layer}L \quad (6)$$

The volume of the Solid Infill layers between the Carbon Fiber layers, not including roof and floor layers, is found with:

$$V_{infill} = (W - W_{shell})L\left(H - \left(H_{layer}\left(2 * N_{floor} + N_{fiber}\right)\right)\right) \quad (7)$$

If done correctly, the following equation should be equivalent to V_{total}, and can be done as a check:

$$V_{sum} = V_{shell} + V_{floor} + V_{roof} + V_{fiber} + V_{fiber\ layer\ infill} + V_{infill} \quad (8)$$

The volume fraction of each of the three regions will then be found. The volume fraction of the Solid Region is given by:

$$Vf_{solid} = \frac{(V_{roof}+V_{floor}+V_{infill}+V_{fiber\ layer\ infill})}{V_{total}} \quad (9)$$

The volume fraction of the Carbon Fiber Region is given by:

$$Vf_{fiber} = V_{fiber}/V_{total} \quad (10)$$

And lastly, the volume fraction of the Shell Region is given by:

$$Vf_{shell} = V_{shell}/V_{total} \quad (11)$$

3.3.7 Volume Average Stiffness Model

The volume average stiffness method was be used to model the elastic properties of these specimen with varying numbers of carbon fiber layers. Calculations were completed using a MATLAB script (MATLAB 2017a, The MathWorks, Inc., Natick, MA). The method developed by Rodriguez et al for FDM printed parts will be used [4]. This method has three steps. First, micromechanical models are used to determine the

micromechanical properties of each unique region within the part to create compliance matrices. Next, a transformation matrix is applied to the Solid fill region so the properties can be used on the same coordinate system as the other regions. Lastly, the compliance matrices are averaged based on their volume fractions, and a global composite matrix is formed, which can be used to determine the overall mechanical properties of the composite.

In the model proposed by Rodriguez et al, FDM printed parts are treated as plastic/void composites, thus, the variable ρ_1 is introduced to represent the void density, or the ratio of void area to total area in a given cross section of the part. The mechanical properties of nylon and carbon fiber filament shown in Tables 3-3 and 3-4 were used to determine the micromechanical properties of the regions with equations (12) – (18) below. For nylon, 0.01 was used for ρ_1. This value represents the void density of Nylon which was discussed above. For the carbon fiber filament printed sections, the region was assumed to have no voids, but a carbon fiber yarn density of 0.28007 was applied to the elastic modulus to better represent the strength of the region as a whole.

A compliance matrix for each region of the composite can be created based on the following form shown in Equation (12).

$$[S] = \begin{bmatrix} \frac{1}{E_1} & -\frac{\nu_{21}}{E_2} & -\frac{\nu_{31}}{E_3} & 0 & 0 & 0 \\ -\frac{\nu_{12}}{E_1} & \frac{1}{E_2} & -\frac{\nu_{32}}{E_3} & 0 & 0 & 0 \\ -\frac{\nu_{13}}{E_1} & -\frac{\nu_{23}}{E_2} & \frac{1}{E_3} & 0 & 0 & 0 \\ 0 & 0 & 0 & \frac{1}{G_{23}} & 0 & 0 \\ 0 & 0 & 0 & 0 & \frac{1}{G_{13}} & 0 \\ 0 & 0 & 0 & 0 & 0 & \frac{1}{G_{12}} \end{bmatrix} \tag{12}$$

To populate the compliance matrix above, the following properties in equations (13) – (18) are found for each region.

$$E_1 = (1 - \rho_1)E \tag{13}$$

$$E_2 = E_3 = \left(1 - \rho_1^{1/2}\right)E \tag{14}$$

$$G_{12} = G_{13} = G * \frac{(1-\rho_1)\left(1-\rho_1^{1/2}\right)}{(1-\rho_1)+\left(1-\rho_1^{1/2}\right)} \tag{15}$$

$$G_{23} = (1 - \rho^{1/2})G \tag{16}$$

$$\nu_{12} = \nu_{13} = (1 - \rho_1)\nu \tag{17}$$

$$\nu_{23} = \nu_{21} = \nu_{31} = \nu_{32} = \left(1 - \rho_1^{1/2}\right)\nu \tag{18}$$

The compliance matrix for the Solid Region must be transformed with a rotation matrix since the nylon in this region is not printed longitudinally with the axis of tension. This is done with as follows:

$$[S_{rotated}] = [T]^T[S'_{rotated}][T] \tag{19}$$

Where the rotation matrix $[T]$ is defined as:

$$[T] = \begin{bmatrix} c^2 & s^2 & 0 & 0 & 0 & 2cs \\ s^2 & c^2 & 0 & 0 & 0 & -2cs \\ 0 & 0 & 1 & 0 & 0 & 0 \\ 0 & 0 & 0 & c & s & 0 \\ 0 & 0 & 0 & -s & -c & 0 \\ -cs & cs & 0 & 0 & 0 & c^2 - s^2 \end{bmatrix}$$

And

$c = \cos(\alpha)$

$s = \sin(\alpha)$

After the compliance matrices have been created and rotated as needed, they are inverted, multiplied by their corresponding volume fractions, and summed to create the global matrix. For the infill region of the composite, the layers exist in equal parts of -45 and 45 degree infills. This is shown in Equation (20) below.

$$[C^G] = Vf_{shell}[S_{shell}]^{-1} + 0.5Vf_{solid}\left[S_{solid,-\alpha}\right]^{-1} + 0.5Vf_{solid}\left[S_{solid,\alpha}\right]^{-1} + Vf_{fiber}\left[S_{fiber}\right]^{-1} \quad (20)$$

Last, the global matrix is inverted once again as shown in (20), and the mechanical properties of the composite are found as shown in (21).

$$S^G = [C^G]^{-1} \quad (21)$$

$$E_x = \frac{1}{S_{11}^G} \qquad E_y = \frac{1}{S_{22}^G} \qquad E_z = \frac{1}{S_{33}^G}$$

$$G_{xy} = \frac{1}{S_{66}^G} \qquad G_{yz} = \frac{1}{S_{44}^G} \qquad G_{xz} = \frac{1}{S_{55}^G} \quad (22)$$

$$\nu_{xy} = -\frac{S_{12}^G}{S_{11}^G} \qquad \nu_{zx} = -\frac{S_{13}^G}{S_{33}^G} \qquad \nu_{yz} = -\frac{S_{23}^G}{S_{22}^G}$$

3.4 Results and Discussion

3.4.1 Fiber Volume Fraction and Void Density Measurement

The percent of carbon fiber yarns in each image was found, with an average of 28.007% carbon fiber yarn, and a standard deviation of 8.15%. Figure 3-5 shows a laser microscope image of a printed layer of carbon fiber at 1000x zoom, while Figure 3-6 shows the threshold created in Image J for this image. The volume fraction of carbon fiber yarns for this particular image was found to be 29.552%. The void density of nylon was found in a similar manner. The average void density was found to be 0.973%. A cross section of a nylon printed part is shown in Figure 3-7.

3.4.2 Dimensional Measurement of Samples

The width and thickness of the printed tensile specimen were measured at the test section in order to calculate the cross sectional area for use with the mechanical testing results. These measured dimensions were compared with the nominal dimensions of the ASTM Type I tensile specimen as shown in Figure 3-1. The measured dimensions were

the width of the tensile area (WC) and the thickness of the part (T), of which, nominal dimensions were 13 mm and 3.2 mm respectively. The results of these measurements and their comparisons with the nominal dimensions are shown in Tables 3-6 and 3-7.

Table 3-6: Comparison of specimen width vs. nominal width of CAD part

		Width (WC): 13 mm nominal	
# CF Layers	Average (mm)	Standard Deviation	% Error
0	12.93	0.01	-0.54
2	12.90	0.06	-0.77
4	12.93	0.10	-0.57
6	12.89	0.06	-0.87
12	12.9	0.13	-0.74

Table 3-7: Comparison of specimen thickness vs. nominal thickness of CAD part

		Thickness (T): 3.2 mm nominal	
# CF Layers	Average (mm)	Standard Deviation	% Error
0	3.35	0.02	4.53
2	3.35	0.06	4.69
4	3.39	0.05	5.87
6	3.39	0.03	5.82
12	3.39	0.04	6.02

It can be seen that the printed specimen did vary from the nominal dimensions of the CAD part. For the width dimension (WC), the printed parts had average widths less than the nominal dimension, while for the thickness dimension (T), the printed parts had average thicknesses greater than the nominal dimension. The results of the thickness measurements are consistent with the dimensional results published by Melenka et al, but the width measurements are not [32]. This may be due to the fact that the reinforcement material used in the Melenka study was Kevlar, which uses a 0.1 mm layer height when

printing parts. This study used carbon fiber as the reinforcement material, which uses a layer height of 0.125 mm. It is observed from Tables 3-6 and 3-7 that the dimensions of these specimen printed with the Markforged Mark Two typically vary +0.2mm to -0.1 mm when printing with continuous carbon fiber.

3.4.3 Mechanical Testing

Many different tensile specimen variables were tested in this study, including the orientation of carbon fibers, the type of carbon fiber infill type, the proximity of carbon fiber layers among each other, and the total amount of carbon fiber layers used in each. These different variable types each had different effects on the mechanical properties of the tensile specimen, so the results will be divided into four distinct sections to discuss the effects of these variables independently.

The Ultimate Tensile Strength, Elastic Modulus, and % Strain at failure were all determined from the stress-strain curves of the test data. Figure 3-9 shows the stress strain curves for all the specimen tested in this study, separated into subplots based on their carbon fiber filament volume fractions. Note that the control specimen subplot is on a different scale than the rest of the subplots. Since Nylon has a relatively low Modulus of Elasticity when compared to carbon fiber, the control specimen were able to experience strain values far greater than the carbon fiber loaded specimen, causing them to stretch many times more than any of the composite samples. Figure 3-10 combines all of the subplots shown in Figure 3-9 into one plot to give the reader another perspective of the stress strain data.

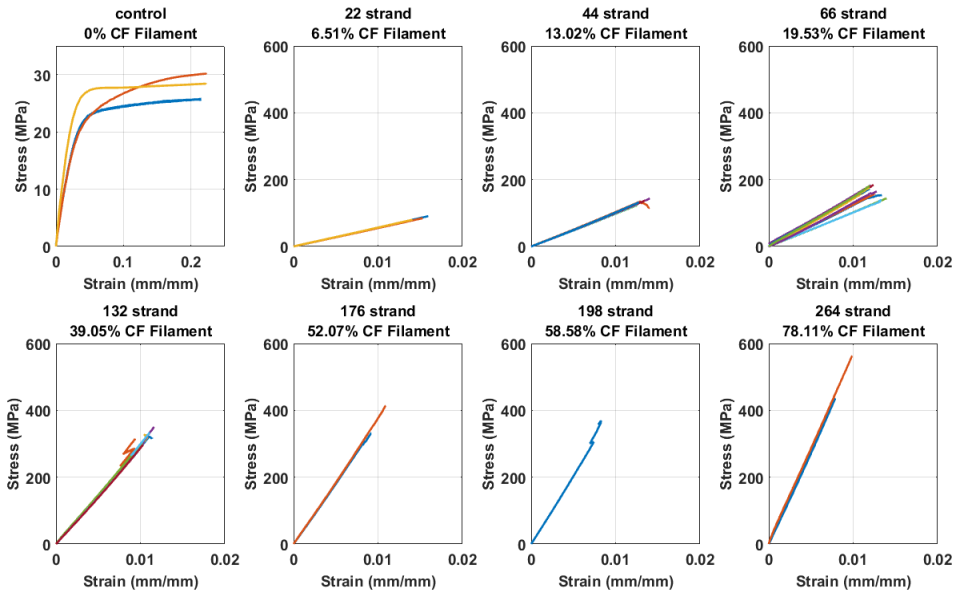

Figure 3-9: Stress Strain Curves of Various CF loaded specimen. Note that the control specimen subplot is on a different scale than the rest of the subplots, as the control specimen sustained strain values far greater than the carbon fiber loaded specimen.

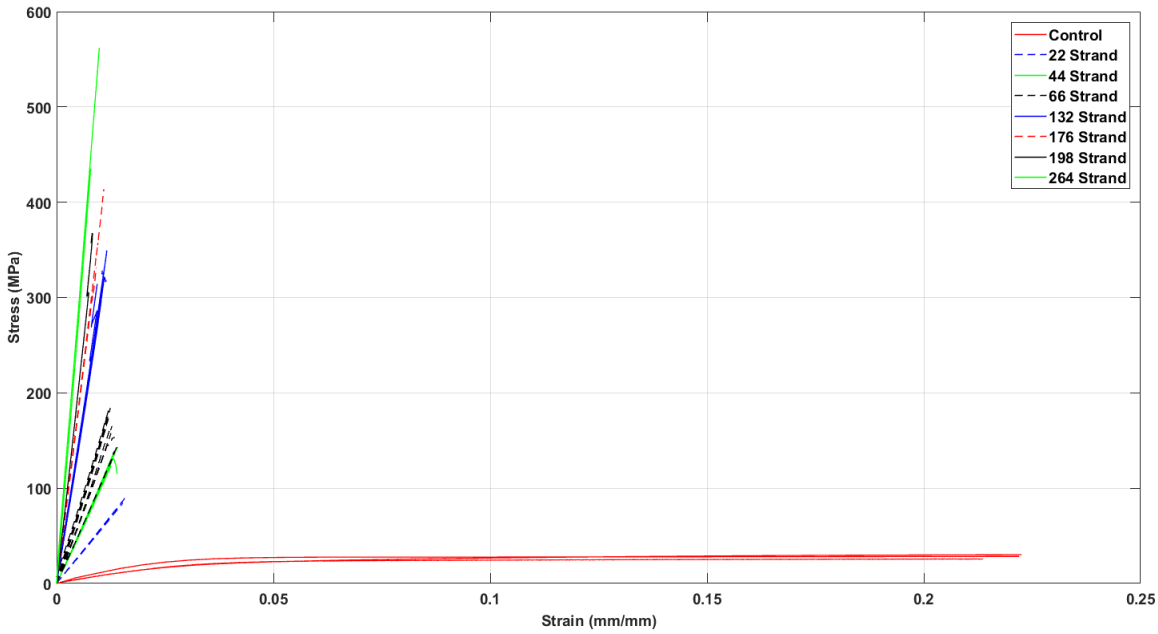

Figure 3-10: Stress Strain Curves of Various CF loaded specimen, shown on one plot. Control specimen are shown across the bottom of the plot, showing their high strain, low UTS properties.

3.4.3.1 Non-axial Fiber Loadings

For this portion of the study, three types of specimen were printed with continuous carbon fibers that were laid into the part in directions not parallel with the axis of tension of the specimen. Examples of these parts can be seen in Figure 3-2. Of the three specimen, two were type D, and one was type E. One of the type D specimen consisted of 45 degree fiber loading where each layer of carbon fiber was the same direction as the last, while the other type D specimen had alternating directions of carbon fiber (e.g. 45 degrees, -45 degrees, 45 degrees, -45 degrees). Each off angle specimen consisted of 4 layers of carbon fiber. The mechanical properties of these specimen will be compared with the control samples which were composed of only nylon filament with no carbon fiber filament because these specimen performed very similar to the control samples, as the fibers weren't loaded longitudinally.

Table 3-8 shows the printing parameters of these specimen and the results of the specimen being analyzed in this section, and Figure 3-11 shows the stress strain curves of each specimen. From the table, the alternating 45 degree specimen provided the most notable strength increase, followed by the 45 degree specimen. It is observed that the 90 degree specimen had the lowest ultimate tensile strength and elastic modulus of the three isotropic off angle fiber specimen. These specimen provided a small increase in ultimate tensile strength over the control samples, but provide an improvement in elastic modulus.

Table 3-8: Control and Off Angle CF Specimen Results

Specimen Name	Description	Number of Fiber layers	Ultimate Tensile Strength (MPa)	Modulus of Elasticity (GPa)	Elongation at Break (%)
Control 1	Pure Nylon Sample	0	30.25	0.551	-
Control 2	Pure Nylon Sample	0	28.49	0.204	-
4A	Type D: 45 Degree fibers	4	41.43	2.367	21.03
4B	Type D: 45 Degree fibers, alternating	4	50.12	2.597	21.25
4C	Type E: 90 Degree fibers	4	36.46	2.189	20.83

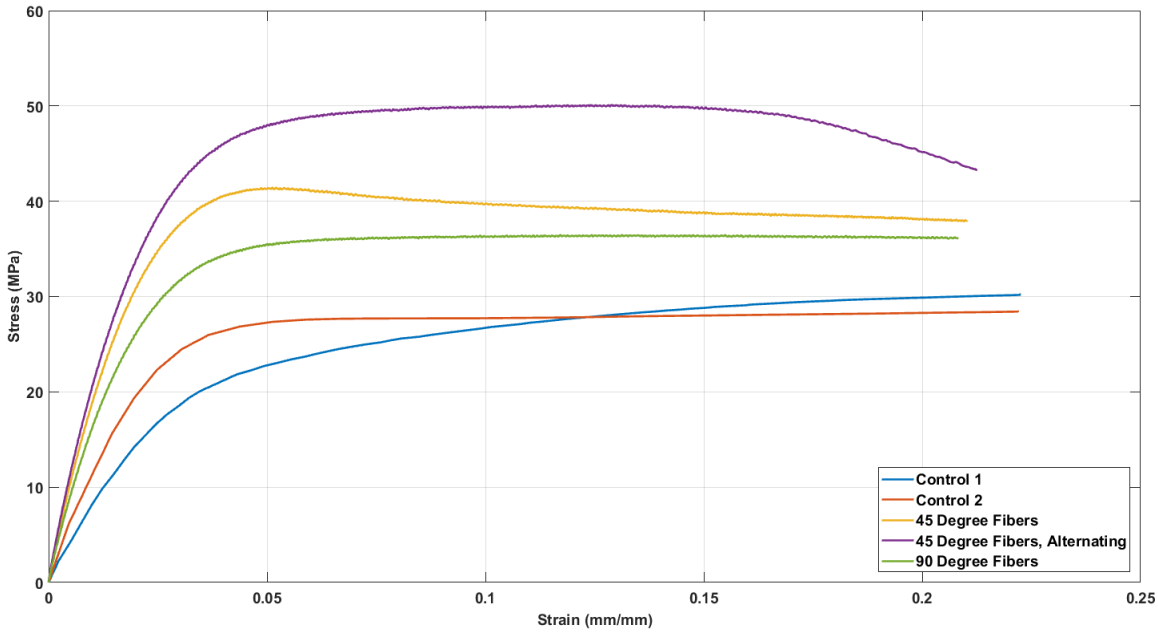

Figure 3-11: Control and Off Angle Fiber Stress Strain Curve

It is seen that non-axial fiber loadings provide some improvements in Ultimate Tensile Strength and Elastic Modulus, but at nearly 2.5 times more expensive per part, use of fiber in this orientation is likely not beneficial for pure axial loading, but can be put to

use in more optimal loadings to perform better for the same amount of fiber, or produce the same results with much less fiber, as will be seen in the next few sections.

3.4.3.2 Effects of Fiber Layer Proximity

Parts with varying layer proximities were printed and analyzed. In this study, layer proximity is defined as the number of consecutive CF layers in a group or cluster. Figures 3-12 and 3-13 show the effects of layer proximity on the Ultimate Tensile Strength and Elastic Modulus of 6 and 12 layer parts. Although there were not enough samples tested in this category to statistically conclude there are no differences in samples due to layer proximity, there does not seem to be any significant differences due to layer proximity.

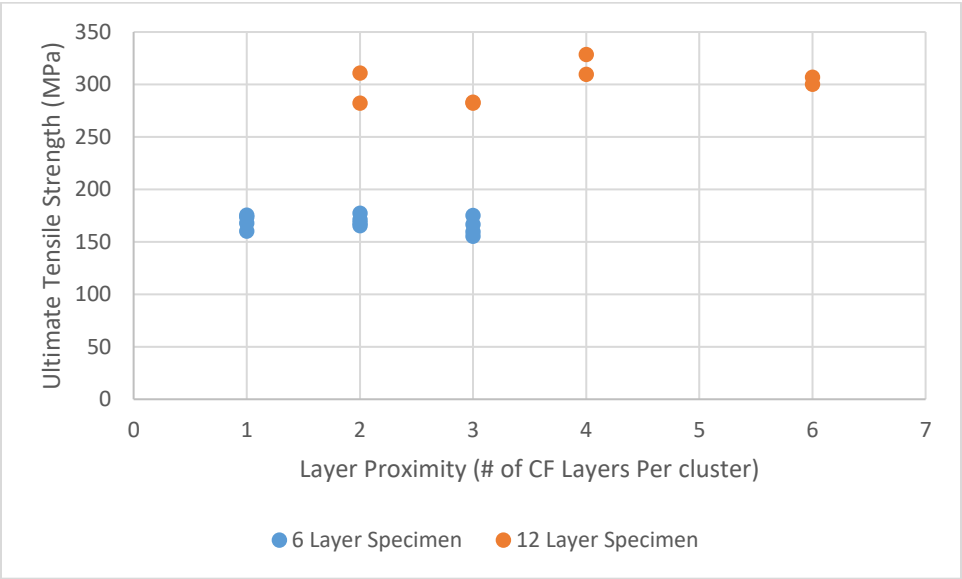

Figure 3-12: Effects of Layer Proximity on UTS

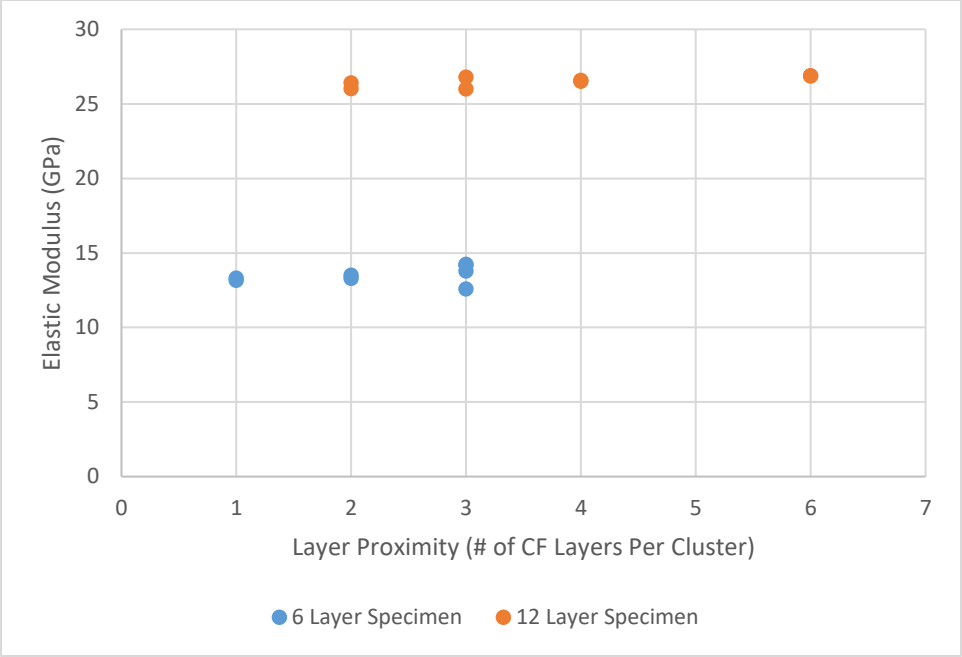

Figure 3-13: Effects of Layer Proximity on Elastic Modulus

3.4.3.3 Effects of Number of Carbon Fiber Strands Loaded in Tension

While the variables above were shown to have little influence on the overall strength of the part, the variable to be examined in this section played a great role in the overall strength of the tensile specimen. On specimen Type A shown in Figure 3-2, 11 fiber deposition paths (shown in blue) can be counted across the narrow region of the test specimen. Each blue line represents one pass of the fiber extruder. With 11 tool paths in a single layer of carbon fiber, it follows that a specimen with 4 layers of carbon fiber will have 44 total tool paths of carbon fiber placed in the part. This will be referred to as a 44 strand specimen in this section. For an isotropic carbon fiber fill type, trends between CF layer count and CF strand count will be the same. However, another equally important classification of these specimen is by the volume fraction of CF filament that makes up the total volume of the specimen.

From Figure 3-14, it can be seen that an increase in Carbon Fiber Filament Volume Fraction leads to an increase in Ultimate Tensile Strength and an increase in Elastic Modulus, and in both cases, the trend is quite linear, with coefficients of determination of 0.9473 for the UTS trend line, and 0.9932 for the Elastic Modulus trend line. With UTS and Modulus of Elasticity treated as functions of Carbon Fiber Filament volume fraction, the following equations of the trend lines are found, as shown in equations 23 and 24. In these equations, Carbon fiber Filament Fraction is a percentage in decimal form, UTS is in MPa, and Modulus of Elasticity is in GPa.

$$UTS = 5.7886(Carbon\ Fiber\ Filament\ Fraction) + 50.441 \quad (23)$$

$$Modulus = 0.6545(Carbon\ Fiber\ Filament\ Fraction) + 0.5313 \quad (24)$$

These equations can be used to determine the strength and modulus of part with a given carbon fiber filament fraction loaded in tension, or they can be rearranged to determine how much carbon fiber should be used for a given UTS of Modulus.

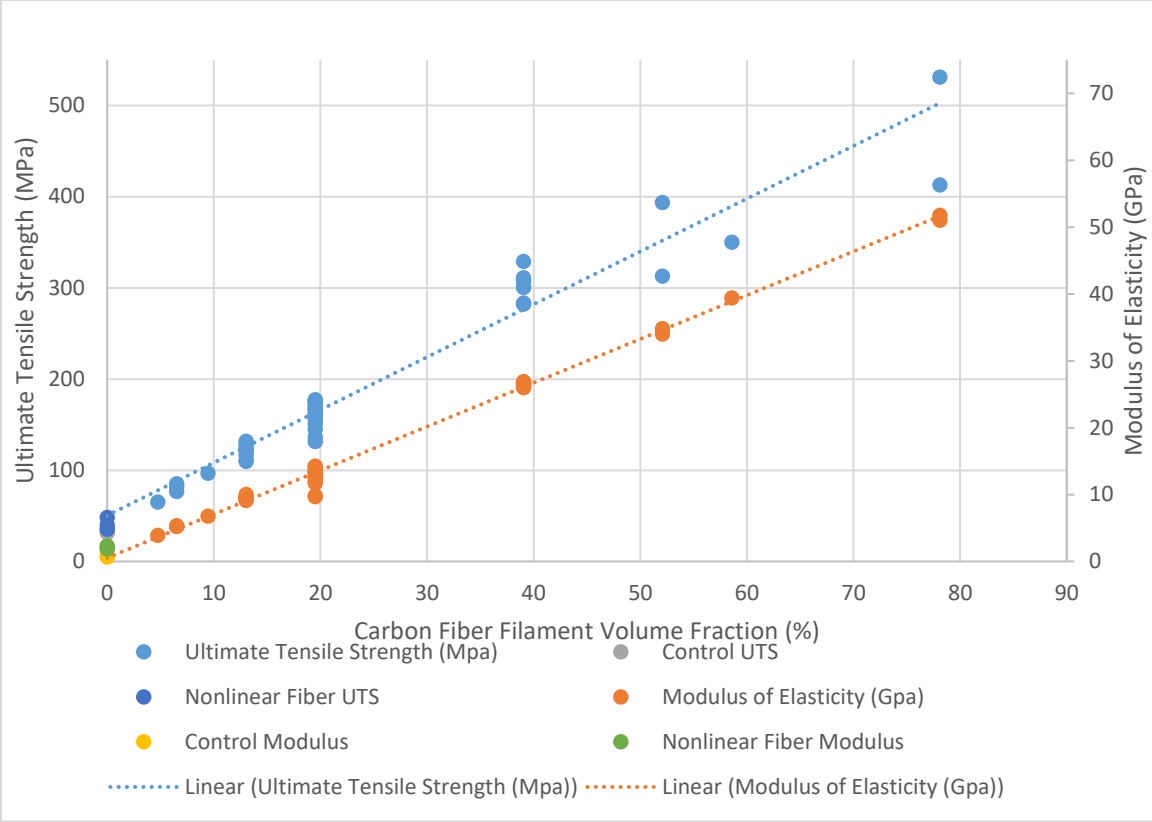

Figure 3-14: Plot of Carbon Fiber Volume Fraction vs. UTS and Elastic Modulus for All Specimen

Figure 3-15 goes on to plot the same UTS and Elastic Modulus data vs. the cost of each sample, and the results are very similar to the results from Figure 3-14 (cost values are due to material usage only according to current MarkForged list prices [48]).

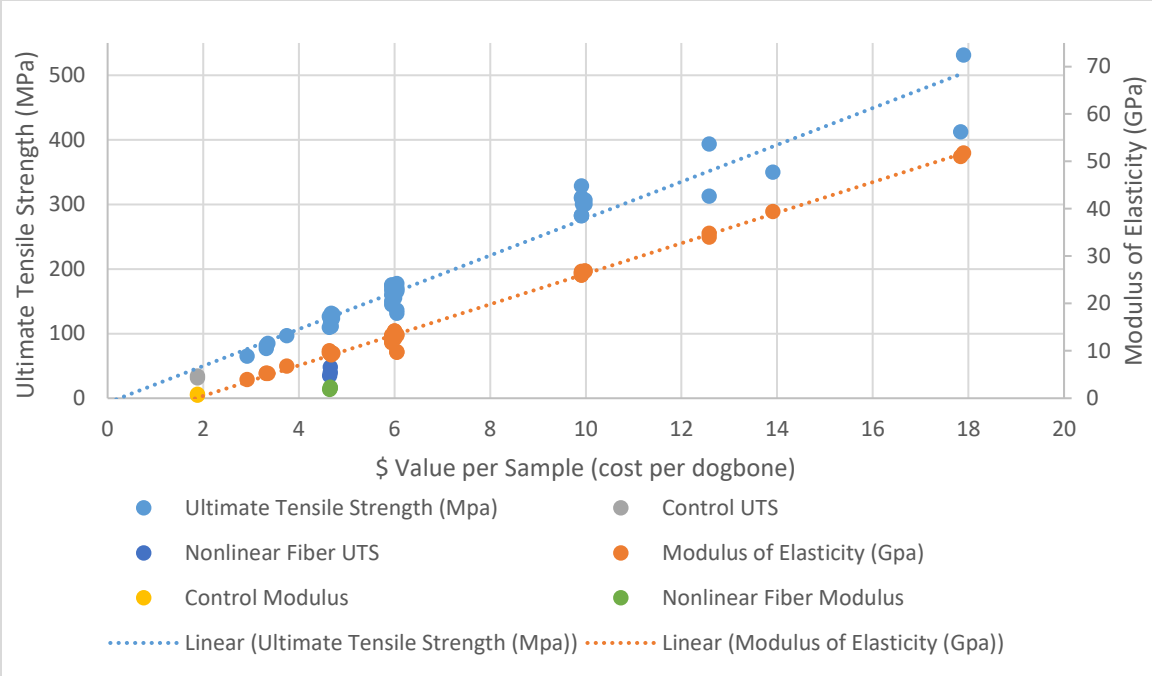

Figure 3-15: Plot of $ Value per Sample vs. UTS and Elastic Modulus for All Specimen

3.4.4 Volume Average Stiffness Modeling

The volume average stiffness method was used to predict the elastic modulus of the tensile specimen which contained purely longitudinal fibers. The method was written as a MATLAB script, which allowed for the model to be calculated with many different fiber layers, and the results were easily compared with experimental results.

Tables 3-1 and 3-5 were used to determine important geometry characteristics of the part within the model, and Figure 3-8 was used as a visual aid when developing the model. Tables 3-3 and 3-4 were used for the material properties in the model.

Figure 3-16 shows the results of the model on a plot as a function of carbon fiber filament volume fraction. The blue line on the plot shows the results of the model, the red circles show the experimental data gathered in this study, and the red line shows the linear

trend line of the experimental data. From the model, the slope of the trend line of the experimental data was compared with the model results, with a percent error of 1.33%.

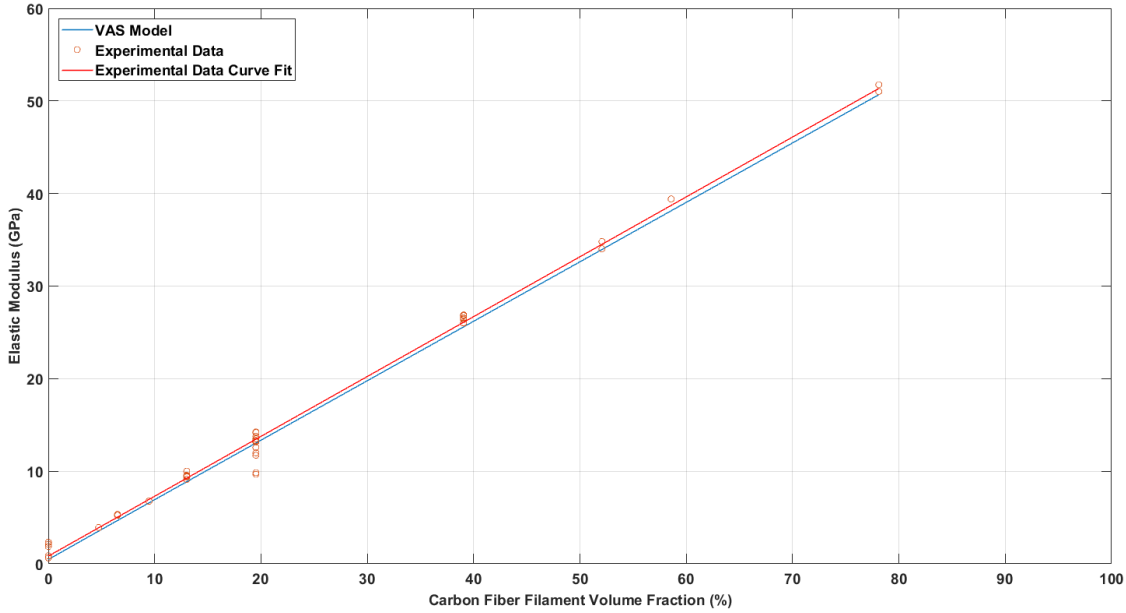

Figure 3-16: Results of Volume Average Stiffness Model with Experimental Data

Table 3-9 shows the results of the model compared with experimental data at select Carbon Fiber Filament Volume Fraction values. It can be seen from the table that the model has a smaller percent error as the amount of carbon fiber in the specimen increases. This implies that the model is a good predictor of elastic modulus for carbon fiber tensile specimen, but it struggles with predicting the elastic modulus of pure nylon parts and parts with lower volume fractions of fibers.

Table 3-9: Results of VAS Model Compared to Experimental Data

CF Filament Volume Fraction (Number of Fiber Layers)	VAS Model Predicted Modulus	Experimental Data Average Modulus	Percent Error
0% (0 Fiber Layers)	0.47	0.75	61.26
13.02% (4 Fiber Layers)	8.85	9.50	7.34
19.53% (6 Fiber Layers)	13.04	12.61	3.30
39.05% (12 Fiber Layers)	25.59	26.51	3.60

3.5 Conclusions

The tensile properties of carbon fiber reinforced composites printed on the MarkForged Mark Two were determined and studied. Mechanical tensile tests were performed on a variety of tensile specimen with varying combinations of fiber layers, fiber layer proximities, and fiber orientations. As a rule of thumb, it was observed that an increase in fibers loaded longitudinally resulted in a linear increase in Ultimate Tensile Strength and Elastic Modulus. Fibers embedded in other directions provided little to no increase in Ultimate Tensile Strength or Tensile Modulus.

The dimensional accuracy of the Mark Two was also studied, and was found to yield tensile specimen whose dimensions varied approximately +0.2mm to -0.1 mm when loaded with continuous carbon fibers. These results were consistent with other reports using the Mark One.

A volume average stiffness method was also employed which predicted the elastic modulus of longitudinally loaded tensile specimen and compared the results to experimental data. The model was shown to become more accurate when predicting properties for parts with more carbon fiber, and less accurate when predicting properties for pure nylon specimen. This model will provide designers and engineers with a basis to

predict the expected mechanical properties of 3d printed continuous carbon fiber parts. More work with this model is required to fully characterize the mechanical properties of these parts in directions other than the longitudinal direction.

CHAPTER 4 - IMPACT STRENGTH OF CARBON FIBER SPECIMEN

4.1 Abstract

3D printed carbon fiber reinforced impact specimen were printed with a Markforged Mark Two 3D printer. Both short/discontinuous and long continuous carbon fiber specimen were printed. Short fiber specimen were printed with Markforged Onyx, while continuous fiber specimen were printed with Markforged Nylon and Carbon Fiber filaments. The impact resistance of these specimen were quantified and compared. Dimensional accuracy of the printer as well as mass estimates of the Markforged slicer, Eiger, were also evaluated. For the Continuous fiber specimen, effects of part orientation, number of carbon fiber layers, and carbon fiber layer proximity were studied. For short fiber specimen, layer height and material infill raster angles were studied. A peak impact resistance of 687 J/m was observed for the continuous fiber specimen with 12 carbon fiber layers, while a maximum impact resistance of 93.9 J/m was observed for the Onyx specimen. Dimensions for continuous fiber specimen had standard deviations of 0.09 mm and 0.14 mm for width and thickness, respectively, with percent errors of 0.2% and 4.99% respectively. Dimensions for Onyx specimen had standard deviations of 0.03 mm and 0.09 mm for width and thickness, with percent errors of 1.46% and 4.56% respectively. Eiger mass estimates were over-predicted by approximately 13% for all specimen, though the mass estimates for pure nylon control specimen were only high by 6.73%.

4.2 Introduction

Impact testing subjects material to a quick blow by a swinging pendulum. This impact measures the energy absorption of the material, which is an indicator of material toughness [14]. Specimen conforming to ASTM D256-10 contain a v-shaped notch, which

provides a stress concentrator on the material. The notch tests the materials resistance to crack propagation.

A study done by Roberson et al [15] sought to study the effects of 3D printed impact specimen which had v-notches either printed with the part or machined after printing. This study also studied the effects of printing the specimen in different orientations on the build plate. For the case of ABS, it was found that part orientation made a significant difference in Impact Resistance, while printed vs. milled v-notch specimen showed statistically insignificant differences in Impact Resistance. Further studies have been performed to analyze the impact resistance of various materials 3D printed with FDM printing methods [14, 16, 17] and these studies all concluded that part orientation of the specimen during printing was an important factor due to the inherent anisotropic nature of FDM printed specimen. The studies concluded that specimen printed with 0° raster angles yielded higher impact resistances than parts printed with other infill directions. The anisotropy of FDM parts may be due to polymer molecules aligning themselves with the direction of flow while being extruding in the fused deposition modelling process [18]. Another source of anisotropy may be due to the formation of pores within the print, and weak interlayer bonding of the material [19].

Composite materials suffer a serious limitation due to the negative effects from localized impact loadings [20]. Failure modes due to impact loading include splitting, delamination, intralaminar matrix cracking, longitudinal matrix splitting, fiber/matrix debonding, fiber pull-out, and fiber fracture [21-25]. Interlaminar shear deformations and flexure are the main energy absorbing mechanisms in composite materials subject to impact loading [26].

Carbon fibers are commonly used as a mechanical reinforcement of materials in composites manufacturing due to their high specific modulus, strength, stiffness, and low density [27]. Strength properties of carbon fiber composites largely rely on the mechanical properties of the carbon fiber, as well as fiber/matrix adhesion.

Further studies have been done to analyze the impact resistance of carbon fiber composites. A study performed by Ozkan et al studied the effects of carbon fiber sizing on impact resistance of carbon fiber composites [27]. It was concluded that the sizing material type used had no effect on impact resistance, but impact resistance was found to decrease with an increase in Carbon Fibers within the composite. It is generally said that the addition of fibers into a ductile polymer matrix makes the material brittle which decreases impact resistance [28-31].

This chapter will focus on the Impact Resistance of 3D printed carbon fiber composites printed with a commercially available desktop 3D printer, the Mark Two by Markforged. Impact specimen will be printed with either continuous Carbon Fiber and Nylon or Markforged Onyx filaments.

4.3 Experimental Procedures

4.3.1 Design of Specimen

The Mark Two by Markforged (Mark Two, Markforged, Somerville, MA USA) was used to print the Impact specimen analyzed in this study. The specimen were modeled with SolidWorks Computer Aided Design (CAD) Software (Solidworks 2016, Dassault Systemes, Waltham, MA USA). The geometry of the specimen was defined by ASTM D256-10 (ASTM D256-10, Standard Test Methods for Determining the Izod Pendulum

Impact Resistance of Plastics) [49]. This geometry and the dimensions specified by ASTM are shown in Figure 4-1.

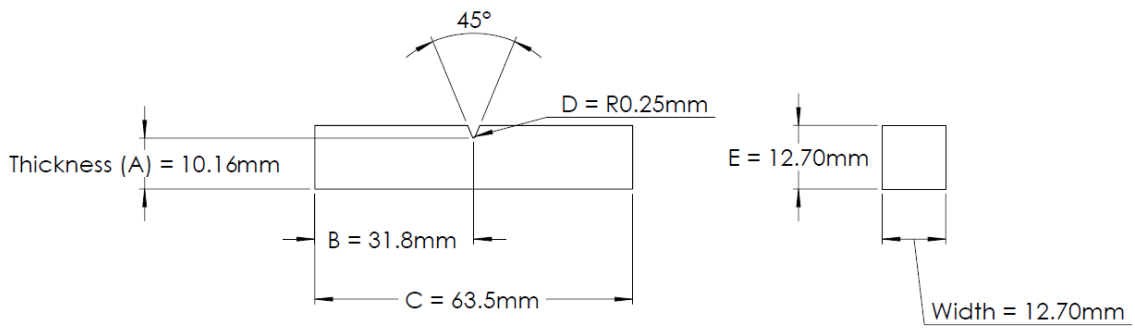

Figure 4-1: Test specimen dimensions as defined by ASTM D256-10

The CAD model was exported as a Standard Tessellation Language (STL) file and uploaded into Eiger, which is a Markforged proprietary slicer software (Eiger 1.6, Markforged, Somerville, MA USA). Eiger 1.6 was used at the time of printing these specimen. Eiger is required to determine both the deposition of Nylon as well as the placement of continuous fibers within the part. In this study, two different types of CF composites were analyzed, both of which were composed of Markforged materials. The first batch of specimen were printed with Markforged Nylon (Nylon, Markforged, Somerville, MA USA) and reinforced with Markforged Carbon Fiber Filament (Carbon Fiber, Markforged, Somerville, MA USA). The second batch of specimen were printed with Markforged Onyx (Carbon Fiber, Markforged, Somerville, MA USA), which is Nylon with chopped carbon fibers included in the same filament.

For the continuous fiber reinforced specimen, Carbon fiber was chosen because Carbon fiber composite parts may be made to take advantage of the properties of CF composites, but may sometimes experience impact loading, making this information

extremely valuable, even though Carbon fiber is reported as the weakest of the fiber reinforcements for Impact Resistance [33]. The standard settings applied to all Continuous Filament Fabrication (CFF) specimen in Eiger are shown in Table 4-1.

Table 4-1: Print Parameters for CFF Specimen

CFF Specimen Print Parameters	
Layer Height (mm)	0.125
Infill Pattern	Rectangular Fill
Infill Percentage (%)	100
Infill Orientation (degrees)	±45, alternating
Number of Walls	2
Number of Floor Layers	4
Number of Roof Layers	4
Total Number of Layers	102
Brim Support	Yes

Brim support was used for these specimen when printing to alleviate the tendency of the specimen to warp during the printing process. An example of brim support is shown in Figure 4-2. The top image in the figure shows the brim as it appears during printing, and the bottom of the figure shows the brim after it has been removed from the part. Brims are a perimeter around the base of the part 4 layers high. The 1st layer of the brim makes direct contact with the main part perimeter, while successive brim layers have a small gap between themselves and the part. This gap on layers 2 through 4 allows the brim to be easily peeled off after the print is complete, but the bond on the first layer provides additional support to prevent part warpage and enhance adhesion to the build plate during printing.

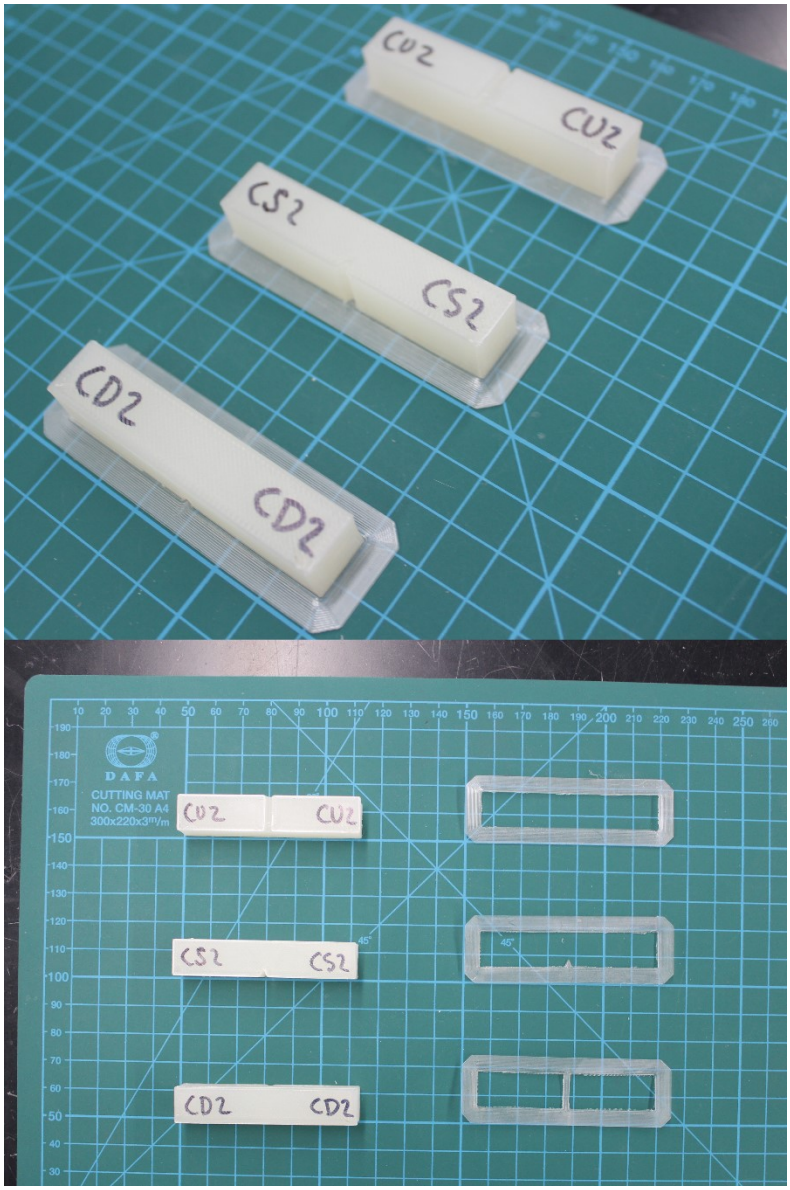

Figure 4-2: Brim Support Representation. Top: View of specimen with Brim attached. Bottom: View of specimen after removal of Brim support

For CFF specimen, Isotropic fiber fill was used with varying numbers of fiber layers and fiber proximities. Use of isotropic fiber in Eiger allows the designer to choose a specific layer or layers to apply isotropic fiber too, and choose a direction that these fibers will be embedded, and Eiger will place this continuous fiber in a zig zag pattern across the

entirety of the layer. In this study, a fiber direction of 0° was used, as shown in Figure 4-3, unless otherwise noted. Other fiber directions used were 45°, ±45° alternating, and 90°.

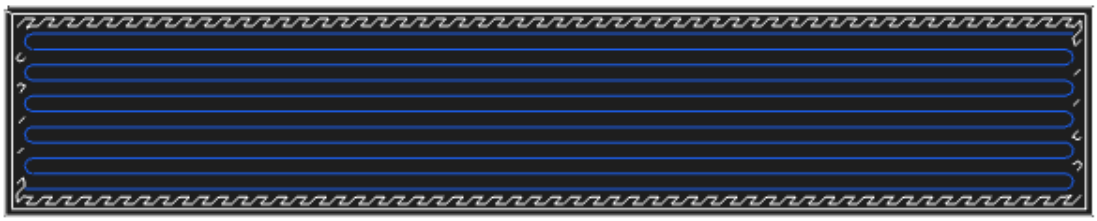

Figure 4-3: Isotropic Fiber Infill within a single layer of a CFF Specimen, 0°. Other fiber directions used were 45°, 45° alternating, and 90°.

Figure 4-4 shows a variety of part orientations with respect to the build plate, which would be the XY plane on the figure. D implies a part orientation with the notch down on the build plate. U implies a part orientation with the notch up away from the build plate. S implies a part orientation with the notch printed on the side of the part, and T implies a part that was printed vertically in a tower fashion. CFF parts were only printed in U and S part orientations, while nylon control specimen were printed in all four orientations.

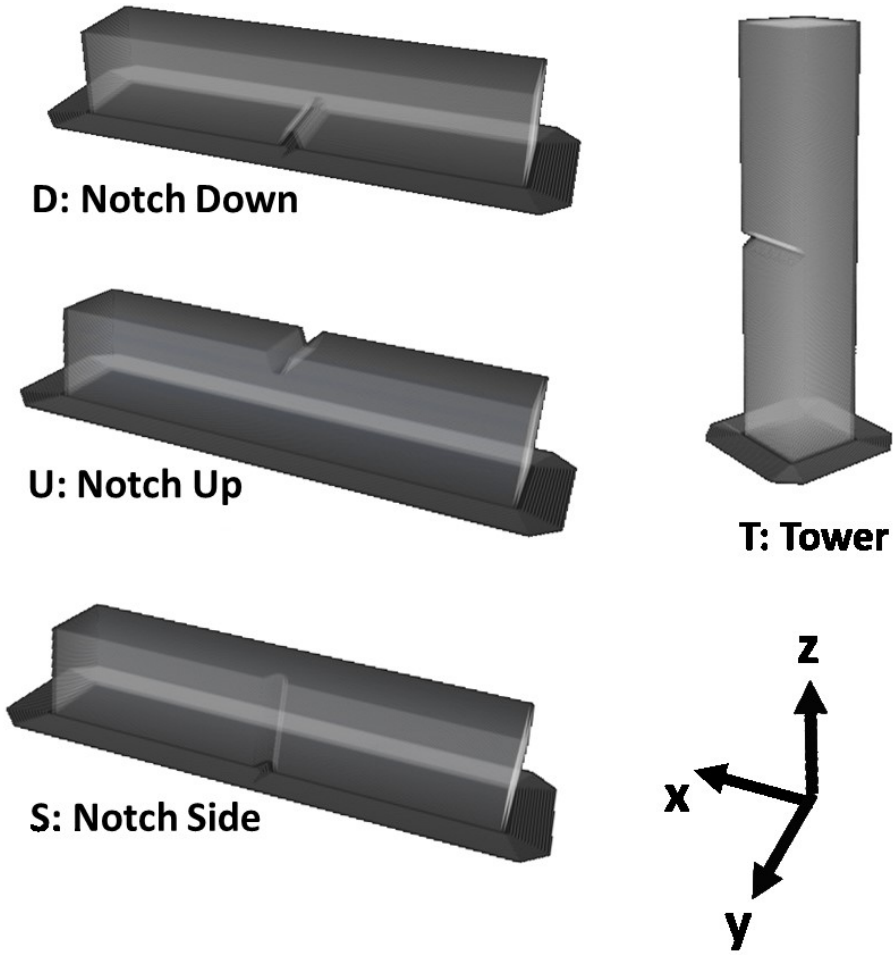

Figure 4-4: Example of Part Orientations. CFF parts were printed in U and S orientations while Nylon control parts were printed in all four orientations.

While only a single fiber direction was used, the number of fiber layers and the proximity of fiber layers was altered for various specimen. Specimen were printed with 4, 8, 16, 20, or 24 carbon fiber layers, as well as control samples which consisted of no fiber layers, only nylon. Of the various specimen with different fiber layers, they were also printed with differing fiber layer proximities as shown in Figure 4-5.

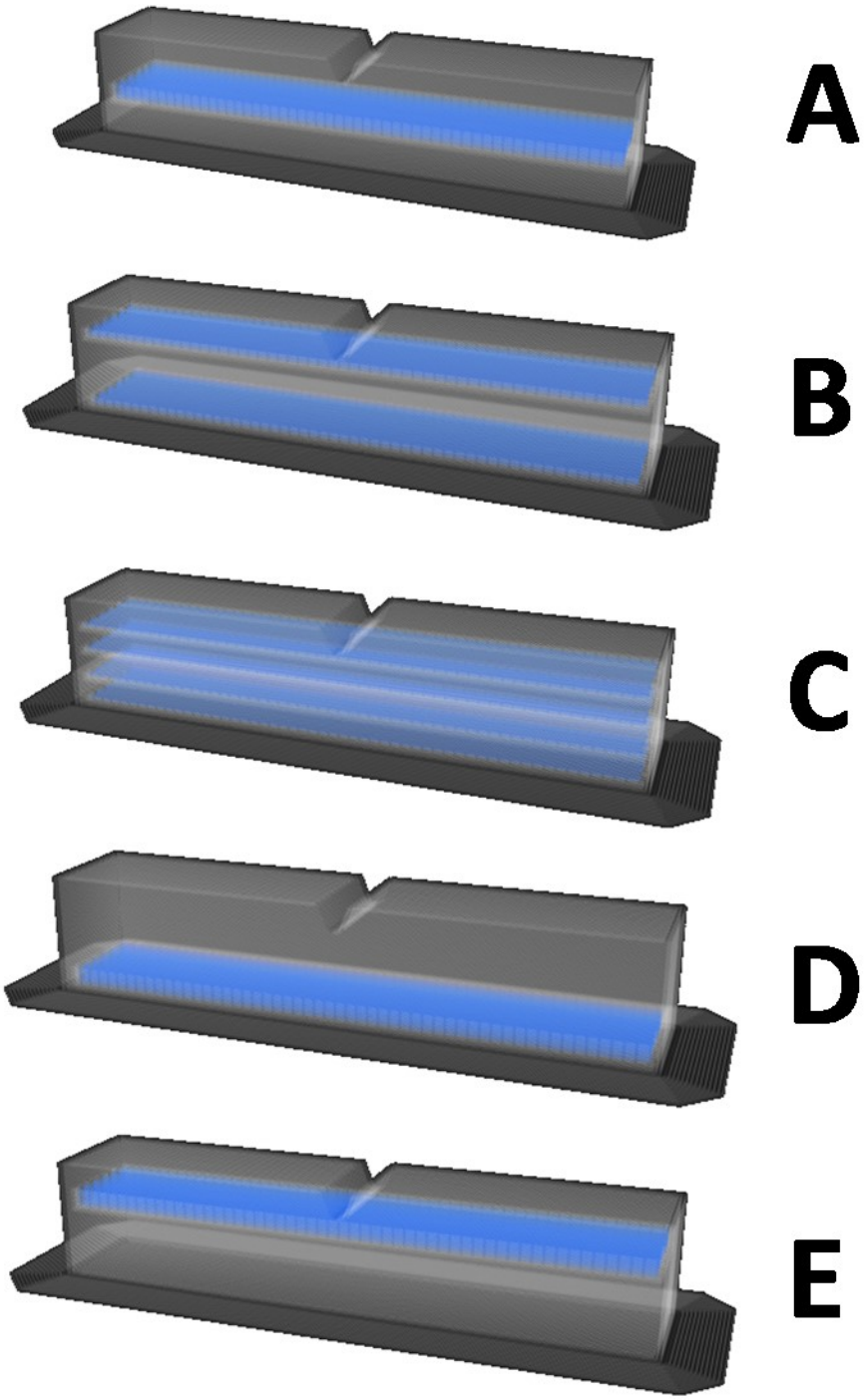

Figure 4-5: Example of Layer Proximities. Each specimen in this figure has 16 carbon fiber layers distributed in different groupings.

In Figure 4-5, 16 carbon fiber layers are shown for each sample specimen. These fiber proximities can be applied to any multiple of 4 fiber layers. Fiber grouping A denotes a specimen with all fiber layers contained in 1 cluster in the center of the part. Fiber grouping B denotes a specimen with the fiber layers equally distributed between the bottom and top layers of the part. Fiber grouping C denotes a specimen with the fiber layers equally distributed between 4 clusters, and evenly spaced throughout the part. Fiber grouping D denotes a specimen which contains all fiber layers at the bottom of the part, and Fiber grouping E denotes specimen which contain all fiber layers at the top of the part.

Because CFF parts were printed in both U and S part orientations, fiber layer placement varied due to the notch bisecting the upper layers in U part orientated parts. For the fiber to provide any functionality, the fiber layers in U oriented parts had to occur entirely below the beginning of the notch. This is shown in Figure 4-6. In the figure, red signifies layers which are bisected by the notch in the part, blue signifies floor or ceiling layers, black signifies carbon fiber filament, and white signifies nylon infill. Each column in the figure represents a cross section through all layers of that particular specimen (Cross section in the XZ plane as shown in Figure 4-4). This figure demonstrates the difference in fiber layer placement between comparable fiber layer proximity groupings in a Notch Up vs. a Notch Side specimen. Note that regardless of notch orientation, carbon fiber layers are evenly distributed within the free space of full layers, and layers fully bisected by a notch are not included in this free space.

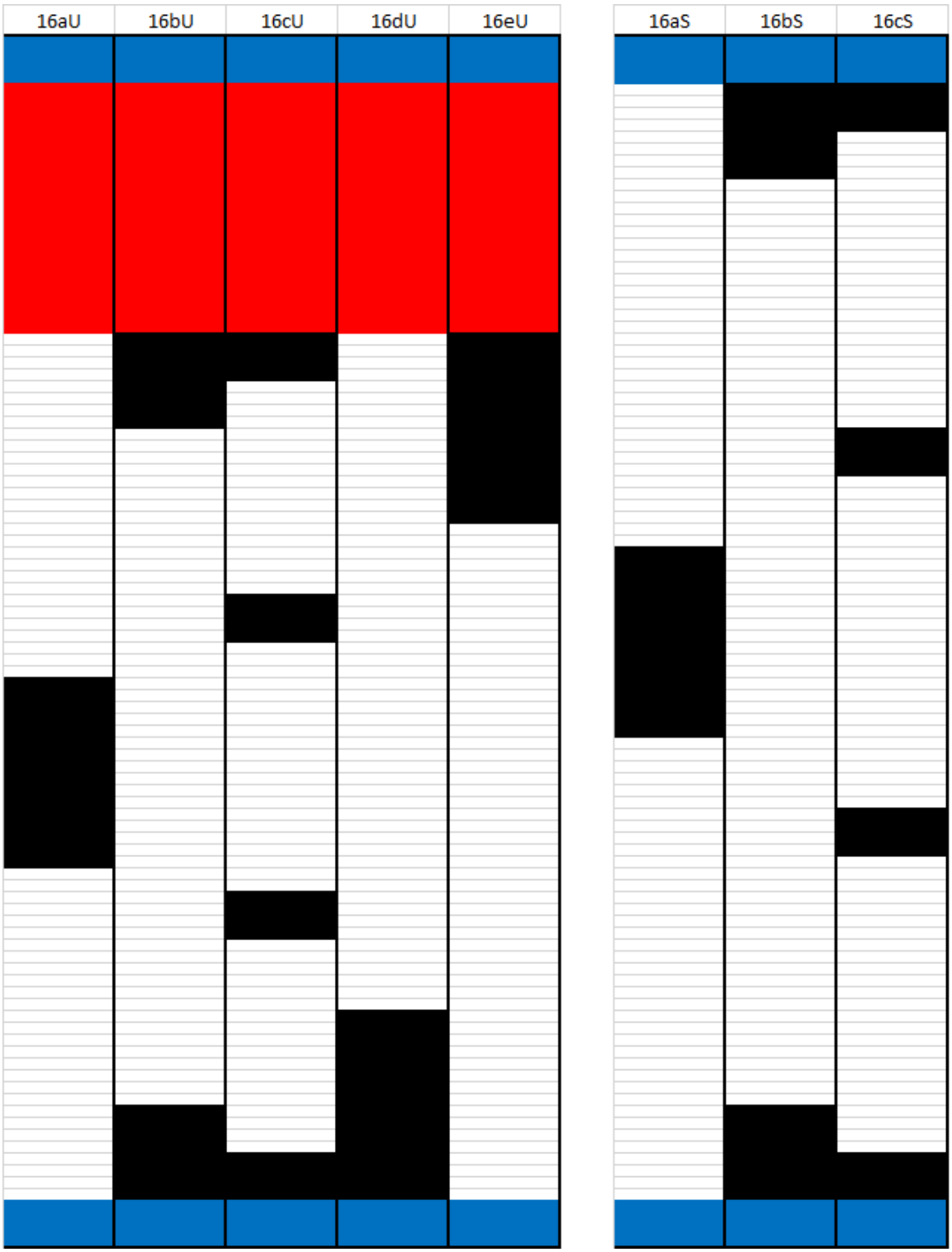

Figure 4-6: Demonstration of Carbon Fiber layer placement in Notch Up vs. Notch Side specimen. Blue is floor/ceiling layers, black is CF layers, white is nylon infill layers, and red is layers completely bisected by the notch in the part.

The second batch of specimen were printed with Onyx. The settings applied in Eiger for these specimen are shown in Table 4-2. Brim support was also used for these specimen to prevent part warping. Refer to Figure 4-2 to see an example of brim support used on a part. Layer height and infill direction were altered for these specimen. Eiger allows the user to choose between 0.1 mm, 0.125 mm, and 0.2 mm layer heights for Onyx. For this study, layer heights of 0.1 mm and 0.2 mm were studied.

Table 4-2: Print Parameters for Onyx Specimen

Onyx Specimen Print Parameters	
Layer Height (mm)	0.1 0.2
Infill Pattern	Rectangular Fill
Infill Percentage (%)	100
Infill Orientation (degrees)	±45, alternating 0/90, alternating
Number of Walls	2
Number of Floor Layers	4
Number of Roof Layers	4
Total Number of Layers	127 (0.1mm layer height) 63 (0.2mm layer height)
Brim Support	Yes

Infill placement in Eiger is fixed at alternating layers of 45°. Thus, each layer has infill rotates by 90°. The specimen can be rotated on the build plate to yield infill in directions other than alternating 45°, while still keeping the notch position fixed. For this study, specimen were printed with both the default infill setting of alternating ±45° (Type **A**), as well as specimen with alternating 0°/90° infill (Type **B**). All Onyx specimen were printed with a part orientation of **U** as shown in Figure 4-4.

4.3.2 Dimensional Measurement of Samples

All impact specimen were measured and weighed before impact testing. Dimensional measurements were performed with a Mitutoyo Caliper (Mitutoyo 500-196-30). Measurements of the part width and thickness were recorded, as shown in Figure 4-1, in order to calculate the cross sectional area of the specimen within the notch region. These measurements will be compared to nominal dimensions to analyze the dimensional accuracy of the Mark Two.

Mass Measurements were taken with a US Solid Lab Scale (USS-DBS5, US Solid). These measurements were taken to analyze the accuracy of the mass estimates given by Eiger.

4.3.3 Mechanical Testing Parameters

These impact specimen were tested on an Izod Pendulum Impact Apparatus as shown in Figure 4-7. Angles of the pendulum before and after striking the specimen were recorded with the use of a custom Arduino and Rotary Encoder. The rotary encoder allows for more precise angle measurements than the traditional needle scale on the apparatus, and the Arduino interprets the rotary encoder data and captures the maximum return angle of the pendulum. Specimen were tested according to Test Method A in ASTM D256-10. Test Method A defines the position of the specimen in the test fixture, which can be seen in Figure 4-7. The specimen is to be oriented such that the pendulum strikes the specimen on the same face as the notch.

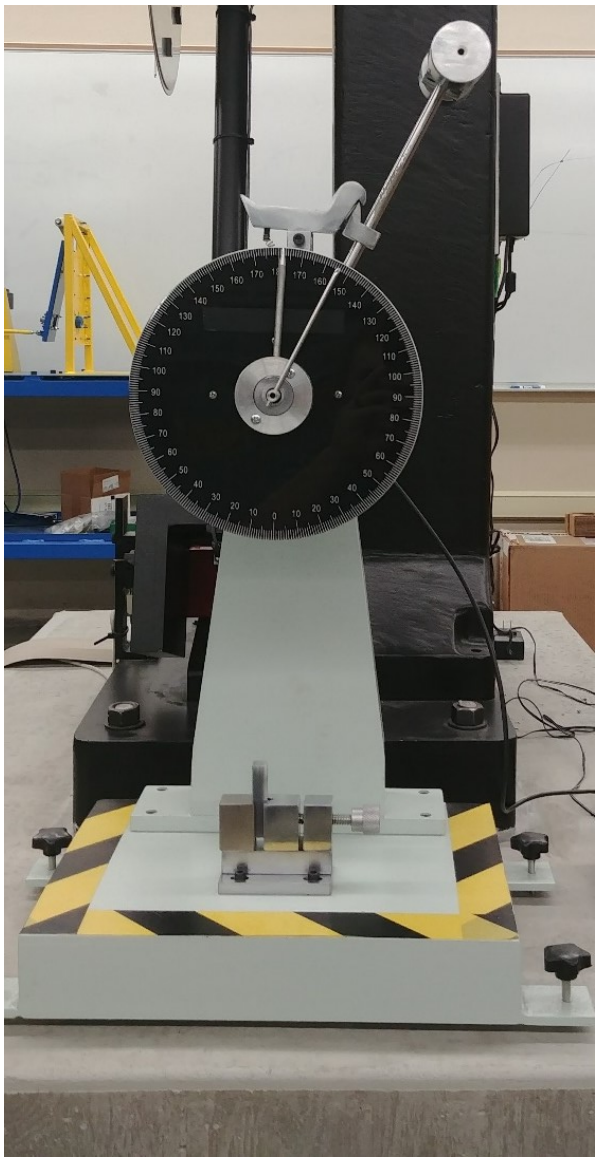

Figure 4-7: Izod Pendulum Impact Apparatus

The impact apparatus works on the principal of potential energy in the pendulum. The pendulum is set to a fixed position, then released which allows it to swing through the specimen. The maximum angle the pendulum reaches after impacting the specimen is recorded. With this information, impact break energy can be obtained. A diagram of the test apparatus is shown in Figure 4-8.

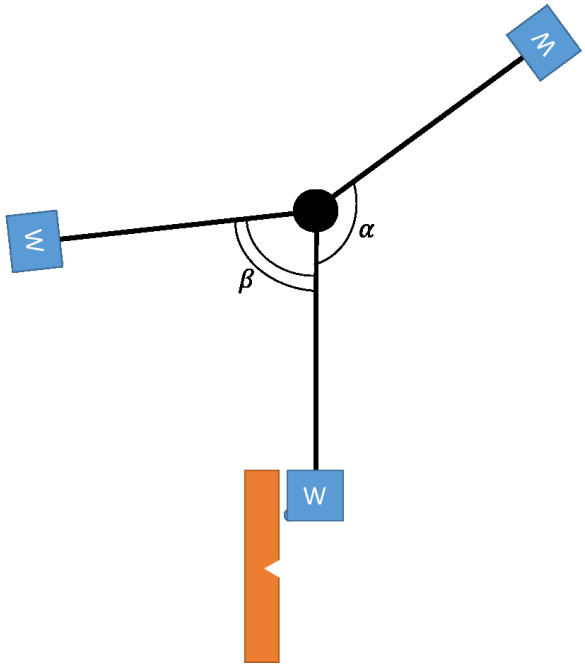

Figure 4-8: Diagram of Impact Apparatus with Pendulum angles shown. Note: Not to scale. Diagram for angle demonstration only.

To determine impact break energy from pendulum angles, the potential energy equation is used. In its general form, the potential energy equation is shown in Equation 1.

$$PE = mgh \tag{1}$$

For a pendulum which follows a circular pattern, its height is found based on the angle of the pendulum arm (α) and the pendulum arm length (L). This is shown in Equation 2.

$$PE_{pendulum} = mgL\cos(\alpha) \tag{2}$$

Neglecting friction losses in the apparatus, the impact break energy of the specimen can be found by determining how much potential energy the pendulum lost. In other words, the difference of the potential energy of the pendulum at its release point and at its highest return point is how much energy was absorbed by the specimen. Finding these two potential

energies and rearranging the equation gives the basic impact break energy of the specimen, as shown in Equation 2.

$$Impact\ Energy = mgL\cos(\beta - \alpha) \quad (3)$$

Equation 3 results in the impact break energy absorbed by the specimen, in Joules, neglecting any friction losses in the apparatus. The friction loss in the test apparatus is determined by allowing the pendulum to free swing and recording the beginning angle and return angle of the pendulum, as shown in Figure 4-8. These angles measured during a free swing capture all friction, air resistance, and other losses in the test apparatus. The angles of the free swing can then be used in Equation 3 to determine the friction loss, in Joules. To include friction losses when calculating the impact break energy of a specimen, Equation 4 is used, where the friction loss calculated with Equation 3 is used in to the friction loss term, and angles recorded while impacting a specimen are substituted for α and β.

$$Impact\ Energy\ with\ Friction = mgL\cos(\beta - \alpha) - Friction\ loss \quad (4)$$

Impact Resistance is defined as Impact energy per unit length of thickness, in meters. Thus the unit J/m is found by calculating the Impact Energy of the specimen and dividing it by the parts thickness in meters.

4.4 Results and Discussion

4.4.1 Dimensional Measurement of Samples

The width and thickness of each part was measured before impact testing. These dimensions are shown in Figure 4-1. These measurements were used to calculate Impact Resistance and Impact Strength, which rely on part thickness and cross sectional area, respectively. Tables 4-3 and 4-4 show the results of dimensional analysis. The

measurements were compared to the nominal dimensions for Width and Thickness of 12.70mm and 10.16mm, respectively. From Table 4-3, it can be seen that the width of the CFF specimen from batch 1 were slightly larger than the nominal dimension, on average. Control specimen and specimen with 6 and 24 layers of carbon fiber averaged smaller widths than nominal, while the rest of the specimen averaged larger than nominal. The overall standard deviation of width measurements was 0.09 mm, with an average error of 0.20%.

Table 4-3: Width Data for CFF Specimen

Width: 12.70 mm Nominal			
# of CF Layers	Average Width (mm)	Standard Deviation (mm)	% Error
0	12.68	0.15	-0.19
2	12.71	0.05	0.04
4	12.75	0.09	0.42
6	12.65	0.04	-0.39
8	12.71	0.06	0.10
12	12.73	0.06	0.24
16	12.77	0.07	0.51
20	12.71	0.08	0.04
24	12.67	0.06	-0.23
All CFF Specimen	12.73	0.09	0.20

From Table 4-4, thickness measurements are shown for the same group of specimen. The thickness measurement averaged higher than nominal for all specimen groups, with an overall average thickness of 10.67, with a 4.99% error from nominal. Standard deviation of all thickness measurements was 0.14mm. It is also interesting to note that the control specimen (0 CF Layer) had the highest standard deviations of all specimen groupings observed.

Table 4-4: Thickness Data for CFF Specimen

Thickness: 10.16 mm Nominal			
# of CF Layers	Average Thickness (mm)	Standard Deviation (mm)	% Error
0	10.58	0.21	4.17
2	10.71	0.04	5.41
4	10.67	0.11	5.01
6	10.69	0.03	5.22
8	10.70	0.14	5.31
12	10.78	0.18	6.05
16	10.68	0.14	5.13
20	10.73	0.02	5.56
24	10.52	0.04	3.54
All CFF Specimen	10.67	0.14	4.99

Tables 4-5 and 4-6 show width and thickness measurement averages for Onyx specimen from batch 2. From Table 4-5, it can be seen that all specimen were wider than nominal, and 0.2 mm layer height specimen were wider than 0.1 mm layer height specimen. The overall error of the width of the specimen was 1.46%. From Table 4-6, it can be seen that the thickness measurements were all larger than nominal as well. 0.2 mm layer height specimen also had larger thickness measurements than 0.1 mm layer height specimen. The overall error of the thickness of these specimen was 4.56%.

Table 4-5: Onyx Width Analysis

		Width: 12.70 mm Nominal		
Name	Description	Average Width (mm)	Standard Deviation (mm)	% Error
1A	0.1 mm layer height, Alternating 45° infill	12.81	0.03	0.89
1B	0.1 mm layer height, Alternating 0°/90° infill	12.80	0.02	0.79
2A	0.2 mm layer height, Alternating 45° infill	12.99	0.01	2.30
2B	0.2 mm layer height, Alternating 0°/90° infill	12.94	0.04	1.85
All Onyx Specimen		12.89	0.03	1.46

Table 4-6: Onyx Thickness Analysis

		Thickness: 10.16 mm Nominal		
Name	Description	Average Thickness (mm)	Standard Deviation (mm)	% Error
1A	0.1 mm layer height, Alternating 45° infill	10.62	0.07	4.48
1B	0.1 mm layer height, Alternating 0°/90° infill	10.49	0.09	3.20
2A	0.2 mm layer height, Alternating 45° infill	10.73	0.09	5.63
2B	0.2 mm layer height, Alternating 0°/90° infill	10.66	0.11	4.92
All Onyx Specimen		10.62	0.09	4.56

From the standard deviation of width and thickness data for Onyx specimen, it can be gathered that the thickness measurement was less consistent than the width measurement. A similar pattern is observed for the CFF specimen, based on standard deviation. The CFF specimen were closer to nominal in width than the Onyx specimen were, with errors of 0.20% and 1.46% for the CFF and Onyx specimen, respectively. Thickness measurements among the two specimen batches were very similar.

4.4.2 Mass Measurement of Samples

Specimen were weighed with their brim support (see Figure 4-2) before impact testing to compare the actual weight of each specimen with the estimate given by Eiger. Table 4-7 shows average mass data for CFF specimen. Mass estimates in Eiger are given in grams with 0.0Xg precision. Eiger mass estimates had an error in the range of -6.73% to -14.37% with a clear upward trend in error being shown with an increase in carbon fiber filament. All CFF specimen were lighter than Eiger estimated they should be. Control specimen with no carbon fiber had the lowest percent error of all specimen in batch 1.

Table 4-7: CFF Mass Analysis

# of CF Layers	Eiger Mass Estimate (g)	Average Mass Measured (g)	% Error
0	12.22	11.3927	-6.73
2	13.27	11.4308	-13.86
4	13.28	11.4615	-13.66
6	13.35	11.5428	-13.54
8	13.41	11.5733	-13.69
12	13.48	11.6896	-13.28
16	13.58	11.6995	-13.85
20	13.64	11.8189	-13.35
24	13.73	11.7568	-14.37

Table 4-8 shows average mass data for the Onyx specimen. Eiger mass estimates had an error between -11.75% and -13.18%, with the 0.1 mm layer height specimen having a larger percent error than the 0.2 mm layer height specimen. Overall, the Onyx specimen mass estimates had percent errors, as well as average masses that were very similar to the CFF specimen.

Table 4-8: Onyx Mass Analysis

Name	Description	Eiger Mass Estimate (g)	Average Mass Measured (g)	% Error
1A	0.1 mm layer height, Alternating 45° infill	13.31	11.56	-13.18
1B	0.1 mm layer height, Alternating 0°/90° infill	13.04	11.34	-13.06
2A	0.2 mm layer height, Alternating 45° infill	12.80	11.28	-11.86
2B	0.2 mm layer height, Alternating 0°/90° infill	12.53	11.06	-11.75

4.4.3 Mechanical Testing of CFF Specimen

For the CFF portion of this study, many different test variables were analyzed, including the orientation of carbon fibers, the proximity of the fiber layers, the amount of fiber layers, and the orientation of the specimen during printing. These variables each had different effects on the impact strength of the specimen groups, and different trends can be seen for the different variable types. The results will be broken up into distinct sections and discussed.

All data gathered for the CFF portion of this study is shown in Figure 4-9. Specimen are plotted with their number of carbon fiber layers vs. the Impact Resistance that specimen was able to achieve. A single "*" represents a single specimen failure, while a red "x" represents a specimen which did not break during impact.

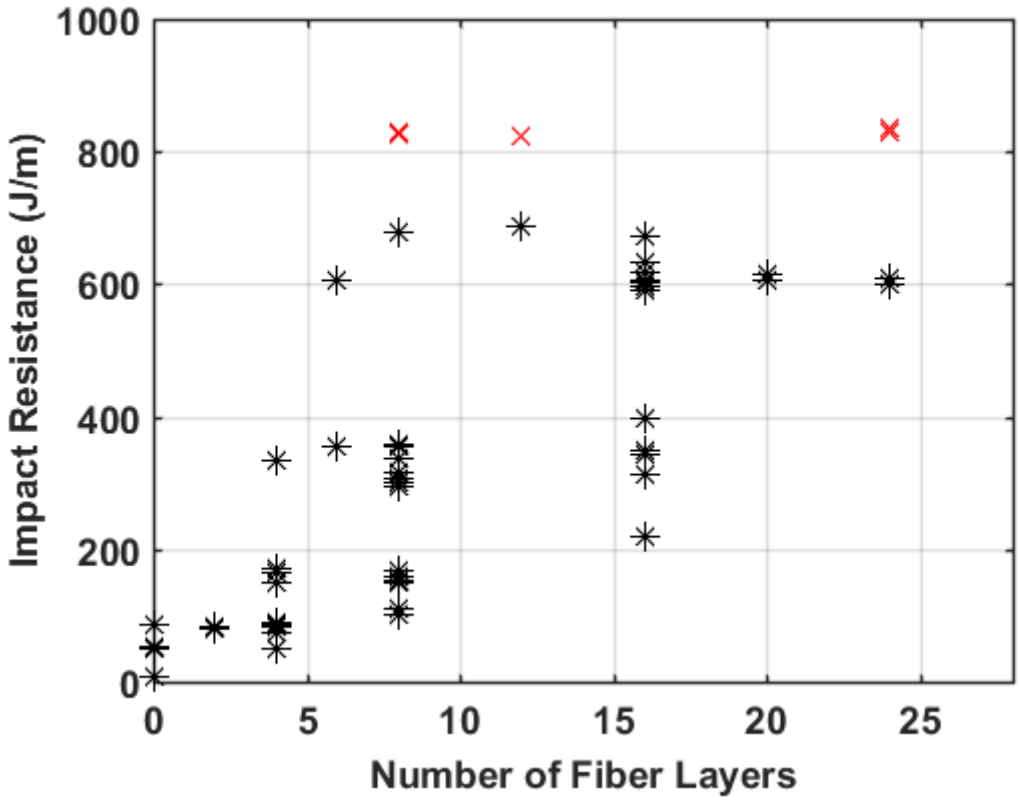

Figure 4-9: Representation of All data gathered for CFF Study, sorted by number of Fiber Layers. Red X's show specimen which did not break upon impact.

4.4.4 Mechanical Testing of Control Specimen

Control specimen consisted of pure nylon parts printed without any carbon fiber filament. They were printed in four part orientations; Notch Up **(U)**, Notch on Side **(S)**, Notch Down **(D)**, and Tower **(T)**. See Figure 4-4 for a representation of the different part orientations. The orientation of the specimen during printing did have a significant effect on Impact Resistance, as shown in Table 4-9.

Table 4-9: CFF Control Specimen Impact Resistance Data

Name	Description	Average Impact Resistance (J/m)	Standard Deviation (J/m)
CU	Control, Notch Up	50.831	1.514
CS	Control, Notch on Side	67.143	26.279
CD	Control, Notch Down	50.474	1.731
CT	Control, Tower	7.363	0.600

From Table 4-9, it is shown that CS specimen had the highest impact resistance of the control specimen, while CT specimen had the lowest impact resistance. CU and CD specimen had impact resistances in between CS and CT, and performed very similarly to each other, likely due to their similarity of the build direction relative to the notch placement. The Tower parts (T) performed the worst overall due to the shearing effect between layers which takes place when a load is applied in a direction parallel to the build plate.

4.4.5 Mechanical Testing of Off Angle CFF Specimen

Although the main focus of the CFF Specimen study was on finding the optimal placement of carbon fibers to increase impact strength, some tests were performed to analyze the effects of carbon fiber loaded in directions other than 0°. Three off angle specimen were printed, 90° fiber fill, 45° fiber fill, and alternating ±45° fiber fill. These fiber fill directions were labeled as **X**, **Y**, and **Z**, respectively, and were each printed with 4 total layers of fiber. The position of these fiber layers within the part is the same as fiber layer position of B type specimen (shown in Figure 4-5), with the only difference between these off angle specimen and a B specimen being the direction of the fiber fill. The results of these off angle specimen were then compared with the results of the standard 4 layer impact specimen printed with 0° fiber fills.

Table 4-10 shows the results of the off angle specimen and compares them with 0° fiber fill specimen with 4 layers of fiber. From the table, it is seen that the 90° fiber fill specimen had the lowest impact resistance, and was similar to the 4D specimen which consisted of 4 layers of fiber at the bottom of the part. These specimen also had a similar impact resistance to the nylon control specimen printed with a notch up part orientation. Off angle specimen with 45° and alternating ±45° fiber fills had higher impact resistances than the 90° fiber filled specimen, but were still weaker than the more effective A, B, C, and E fiber loaded specimen. More on these types of fiber loaded specimen will be discussed in the next section. It is clear that fiber loaded in off angles provide little to no improvement over the control sample for impact resistance.

Table 4-10: Comparison of Off Angle Fiber Specimen with 0° Fiber Fill Specimen

Name	Description	Average Impact Resistance (J/m)
4A	4 Layer, 1 Fiber Group, 0° fibers	138.019
4B	4 Layer, 2 Fiber Groups, 0° fibers	133.357
4C	4 Layer, 4 Fiber Groups, 0° fibers	108.256
4D	4 Layer, 1 Fiber Group Bottom, 0° fibers	49.826
4E	4 Layer, 1 Fiber Group Top, 0° fibers	224.643
4X	4 Layer, Fiber Group X, 90° fibers	50.196
4Y	4 Layer, Fiber Group Y, 45° fibers	83.137
4Z	4 Layer, Fiber Group Z, 45° fibers, alternating	74.227

4.4.6 Mechanical Testing of Carbon CFF with Varying Fiber Layers and Proximities

While part orientation of CFF Specimen had some effect on impact resistance, fiber layer proximity and the number of fiber layers had the greatest overall influence on the impact resistance of the specimen. Figure 4-10 depicts all CFF data sorted into subplots

based on fiber layer proximities A through E, with each subplot showing data broken down between Notch Up and Notch Side Specimen.

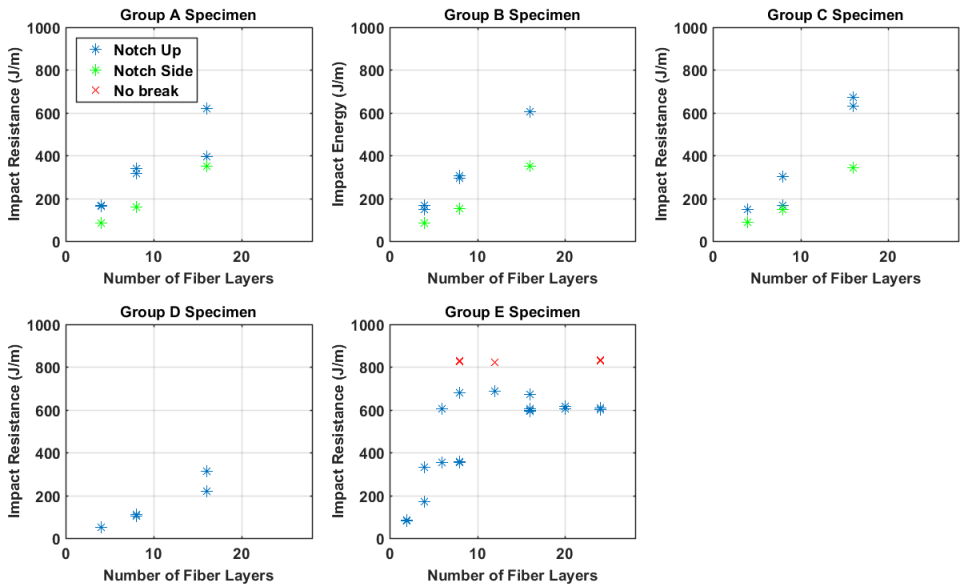

Figure 4-10: Subplot of various Fiber Layer Proximities for Notch up and Notch Side CFF Specimen

The first major distinction to be noticed from the results presented in Figure 4-10 is the discrepancy between Notch Up and Notch Side specimen. For CFF parts, the Notch Up orientation performed better than the Notch Side Orientation, while the opposite was true for the control specimen, where the Notch Side orientation performed better. This is likely explained by the positioning of the CFF layers relative to the notch, as shown in Figure 4-11.

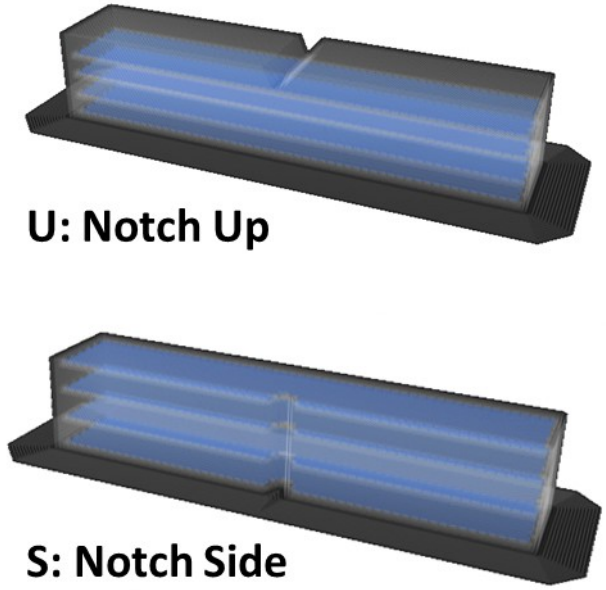

Figure 4-11: Comparison of fiber layers relative to notch for Notch Up and Notch Side CFF Specimen

While a 16 layer Type B specimen for both Notch Up and Notch Side orientations contains 16 layers of carbon fiber distributed amongst 4 equal clusters, the position of these clusters relative to the notch is different. Specimen printed in the Notch Up orientation contain fiber layers that are parallel to the impact strike face, while specimen printed in the Notch Side orientation contain fiber layers that are perpendicular to the impact strike face, which is a sub-optimal fiber direction for Impact Resistance. This data is summarized in Table 4-11.

Table 4-11: Comparison of Notch Up vs. Notch Side CFF Specimen Results

Name	Description	Average Impact Resistance (J/m)
CU	Control, All fiber groups, Notch Up	50.831
4U	4 Layer, All fiber groups, Notch Up	132.948
8U	8 Layer, All fiber groups, Notch Up	346.216
16U	16 Layer, All fiber groups, Notch Up	538.536
CS	Control, All fiber groups, Notch Side	67.143
4S	4 Layer, All fiber groups, Notch Side	86.255
8S	8 Layer, All fiber groups, Notch Side	153.235
16S	16 Layer, All fiber groups, Notch Side	347.005

The second major distinction noticed from the results in Figure 4-10 is the difference between the Group A-D results vs Group E results. Groups A-D saw a positive linear correlation between the number of fiber layers and Impact Resistance for both Notch Up and Notch Side specimen. Group E specimen on the other hand had more of a hyperbolic trend. Group E specimen also reached a peak Impact Resistance at approximately 8 layers of carbon fiber, compared to group A-D specimen with 8 layers of CF which saw Impact Resistances that were half of Group E specimen. Figure 4-12 shows all Notch Up CFF specimen based on their fiber layer proximities.

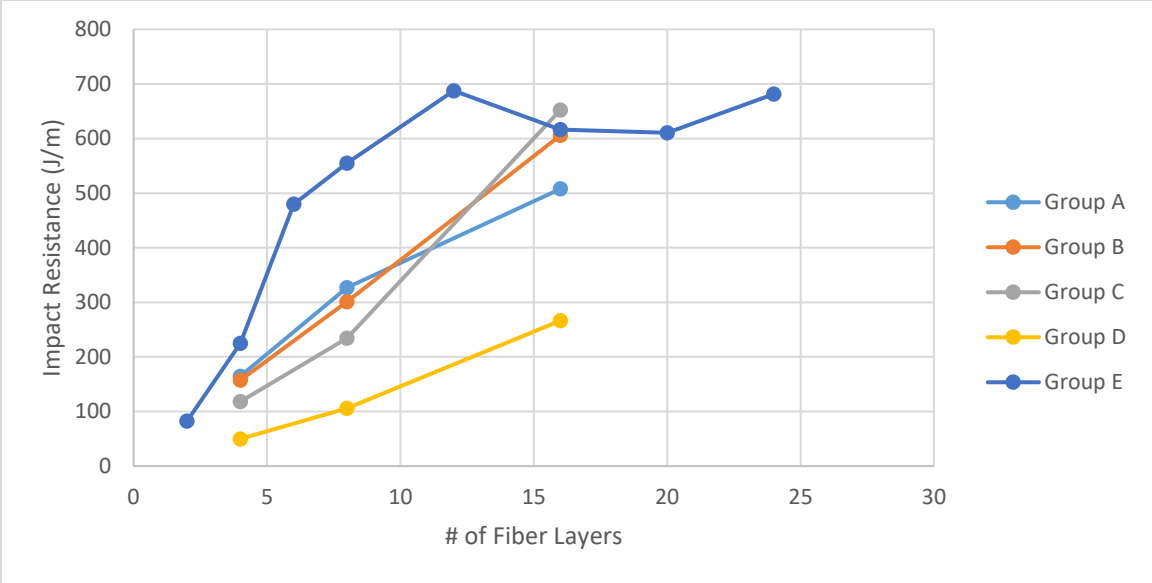

Figure 4-12: Comparison of Different Fiber Proximities for Notch Up CFF Specimen

This figure shows the differences between the different fiber proximities, and the trend that each group follows as the number of fiber layers is increased. From the figure, it can be seen that Group E specimen reach a maximum Impact Resistance with fewer carbon fiber layers than Groups A-D. Groups A, B, and C all follow a similar pattern of linearity, though Group B experiences the highest Impact Resistance of the 16 layer specimen.

It is also clear from Figure 4-12 that Group D specimen had the lowest impact resistance overall, and that fibers placed on the bottom of the specimen relative the notch provide the least amount of reinforcement. This difference in Impact Resistance due to fiber layer proximity and placement is likely explained by the failure mode of these specimen, as shown in Figure 4-13.

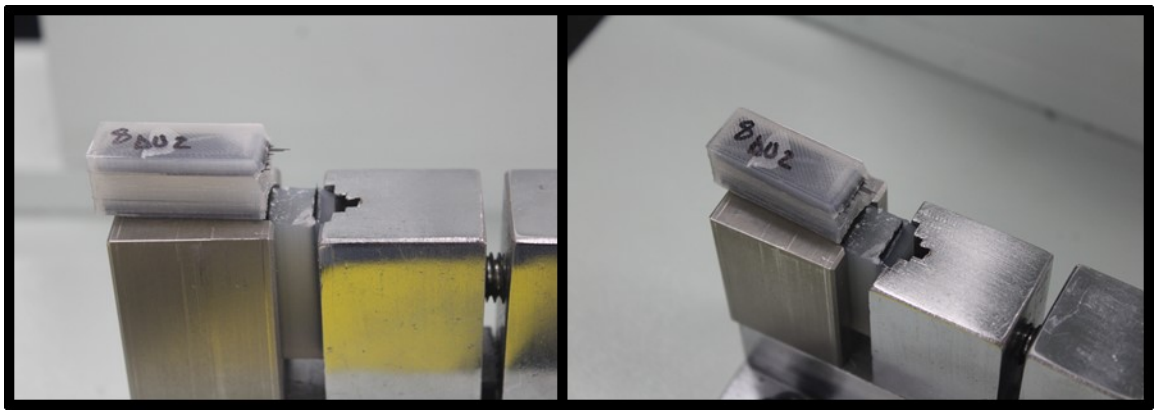

Figure 4-13: Common failure mode of CFF Specimen

From the figure, a common failure mode of CFF specimen is shown in two different views. Nearly every CFF specimen failed in a 'Hinge Break' manner, where the specimen folded over on the clamp, but the two halves of the part did not separate. Since Group D specimen contain only fibers on the bottom of the specimen, opposite of the notch, the nylon matrix nearest the notch is able to crack and separate, and allow the specimen to begin failing in a hinge manner before the crack reaches the fiber layers, where the fibers are loaded in more of a bending manner. This results in less overall fiber interaction to the overall impact resistance, and thus, weaker specimen. This phenomenon also likely explains why Group E specimen provided the highest Impact Resistance with the fewest carbon fiber layers, due to the entirety of fiber layers being oriented right next to the notch. Group E specimen had the highest amount of specimen which did not break, and those that did break commonly did so in a complete manner. That is, the two halves of the specimen were completely separated about the notch.

4.4.7 Mechanical Testing of Onyx Specimen

For the Onyx portion of the study, layer height and Onyx infill direction were analyzed. Layer heights of 0.1 mm and 0.2 mm were studied in combination with Onyx

infill directions of alternating 45° (Type **A**) and 0°/90° (Type **B**) infill. All specimen were printed with a Notch Up part orientation (**U**) as shown in Figure 4-4.

4.4.8 Onyx Specimen Results

Table 4-12 shows the average Impact Resistance of each Onyx Impact Specimen grouping, and Figure 4-14 shows the same data in graphical form. From the table and figure, it is shown that alternating ±45° infill (Type **A**) yielded higher Impact Resistances than 0°/90° infill (Type **B**). Furthermore, 0.2 mm layer height specimen had higher impact Resistances than 0.1 mm layer height specimen. A 0.2 mm layer height specimen with Type A infill yielded the highest impact resistances overall. Specimen 1A and 2A share similar traits with CU control specimen. Comparing the results of these Onyx Specimen with the control specimen of the same part orientation shows that Onyx does provide a marginal increase in Impact Resistance over pure nylon specimen.

Table 4-12: Comparison of Onyx Specimen Results

Name	Description	Average Impact Resistance (J/m)	Standard Deviation (J/m)
1A	0.1 mm layer height, Alternating 45° infill	73.197	4.715
1B	0.1 mm layer height, Alternating 0°/90° infill	48.418	4.564
2A	0.2 mm layer height, Alternating 45° infill	93.947	4.966
2B	0.2 mm layer height, Alternating 0°/90° infill	69.507	4.668

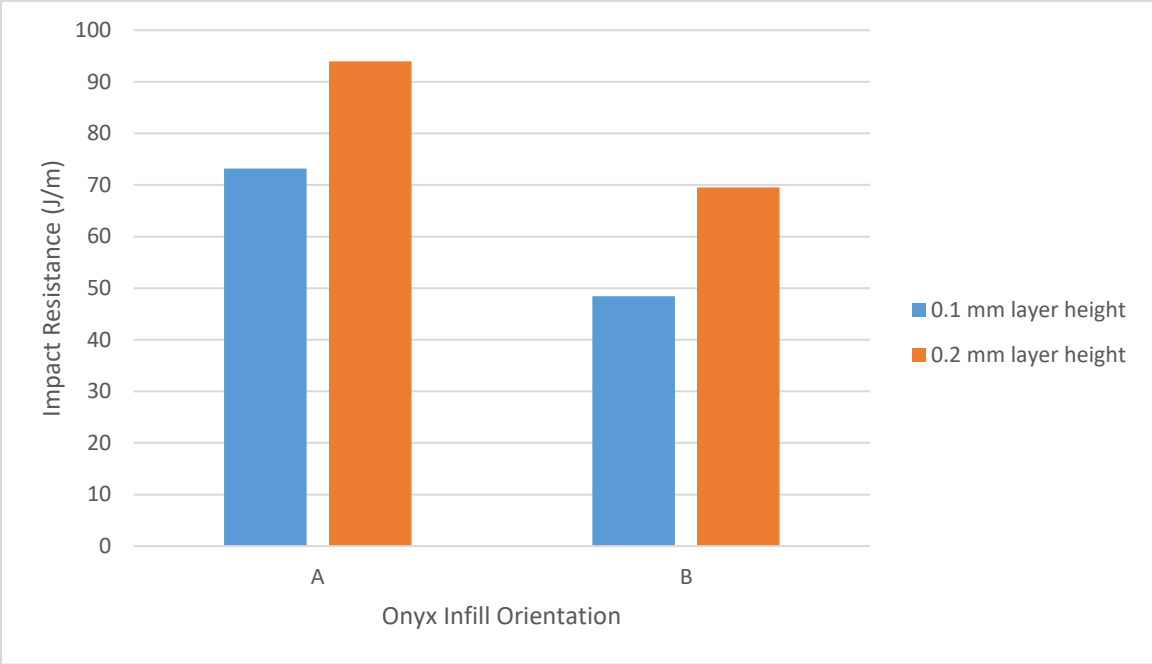

Figure 4-14: Graphical Representation of Onyx Specimen Results

4.5 Conclusions

The impact resistance of both continuous carbon fiber and short fiber specimen 3d printed with a Markforged Mark Two were analyzed. It was shown that these specimen did portray a level of anisotropy and that part orientation during printing as well as the proximity of carbon fiber layers had the greatest effect on impact resistance.

1. For CCF specimen, fiber proximity Groups A, B, and C exhibited a linear trend of increased impact resistance with increased carbon fiber layers. Fiber Proximity

Group D also exhibited this trend, but the overall impact resistances for a given number of carbon fiber layers was much lower.

2. CCF specimen printed with Fiber Proximity Group E exhibited a hyperbolic trend of Carbon Fiber Layers vs. Impact Resistance. This fiber grouping produced the highest impact resistance specimen at 687 J/m, and reached a peak at 12 layers of carbon fiber before leveling off.
3. Nylon control specimen yielded varying impact resistances depending on the part orientation. Control specimen printed with the notch on the side of the part were strongest overall at 67.1 J/m. Specimen printed with the notch up or down on the part yielded impact resistances of 51 J/m and specimen printed in a tower configuration had an impact resistance of 7.3 J/m.
4. CFF specimen printed with off angle carbon fiber loadings performed similarly to control specimen.
5. 0.2 mm layer height Onyx specimen had a higher impact resistance than 0.1 mm layer height specimen, and Onyx specimen printed with raster angles of alternating 45° infill were stronger than those printed with 0°/90° infill. The strongest Onyx specimen was the 0.2 mm layer height 45° infill specimen at 93.9 J/m.
6. Dimensional accuracy of the Mark Two was examined and errors of 0.2% and 4.99% were observed for width and thickness measurements of CFF parts, respectively. Errors of 1.46% 4.56% were observed for Onyx specimen. From this, it is concluded that CFF specimen width dimensions are more consistent than Onyx specimen, while thickness measurements are nearly the same.

7. Eiger mass estimates were consistently heavier than the actual mass measurement of the part. Control specimen mass estimates were heavy by 6.73%, while CFF specimen estimates were heavy by about 14% on average. Onyx mass estimates were heavy by about 13% on average.

The results presented here are useful for designing parts with the possibility of receiving impact loadings. The accuracy of the Mark Two printer can also be used for future designing of parts to understand the dimensions of the final product vs. its designed dimensions.

CHAPTER 5 - COMPARISON OF RESULTS WITH MARKFORGED DATA

Markforged has released a wide variety of Mechanical Properties for their Continuous Fiber and Nylon based materials [33]. The data presented on this sheet released by Markforged is meant to represent the best case scenario of each specific mechanical property. Some of these properties will be compared with experimental data obtained in this thesis, namely the Tensile Strength, Tensile Modulus, Tensile Strain at Break, and Izod Impact Resistance of Carbon CFF, Nylon, and Onyx filaments.

For the sake of comparison with the reported Markforged mechanical properties, experimental data only from the strongest specimen groups were chosen for each material type. For Carbon CFF, specimen with 24 CF layers (78% Carbon CFF Fraction) were chosen for the tensile comparison, and 12 Layer Type E specimen were chosen for the impact comparison. See figure 4-5 in Chapter 4 for an example of Type E impact specimen. For Onyx, rectangular specimen with 100% infill were chosen for the tensile comparison, and Group 2A specimen were chosen for the impact comparison. See table 4-12 in Chapter 4 for a description of a Group 2A specimen. Control specimen data was used for the Nylon comparison, all consisting of specimen with 100% rectangular infill. All tensile testing for both Markforged reported values and the values obtained in this thesis were done in accordance with ASTM D638-10 [39], and all Izod impact testing was done according to ASTM D256-10, following the Type A test method for notched specimen [49]. Table 5-1 shows the comparison of the Carbon CFF results, while table 5-2 shows the comparison of the Nylon and Onyx results.

Table 5-1: Comparison of Thesis Results with Markforged Data: Carbon CFF

	Tensile Strength (MPa)	Tensile Modulus (GPa)	Tensile Strain at Break (%)	Notched Izod Impact Resistance (J/m)
Markforged Reported Value	700	54	1.5	958
Experimental Average (78% CFF Fraction)	531	51.4	0.9	687
Curve Fit Data at 100% CFF Fraction	629	65.9	-	-

From table 5-1, Values reported by Markforged for Carbon CFF Specimen are shown along with experimental data obtained by this thesis. Experimental Data matched well with the Markforged reported values for Tensile Modulus. Experimental data of Impact Resistance was lower than reported by Markforged, meaning the Impact Resistance of Carbon CFF may be overstated by Markforged. Tensile strain at break was less for the experimental data set than was reported by Markforged, meaning these tensile specimen stretched less overall than reported by Markforged. Tensile strength of the experimental data was lower than reported by Markforged. This was theorized to be due to a lower Carbon CFF Fraction within the experimental test specimen than the specimen used by Markforged to come up with their published values, as the maximum CFF Fraction of experimental data studied in this thesis was 78%.

In an attempt to explain the discrepancy between Markforged and experimental data for Tensile Strength, trend lines of the experimental data were used to extrapolate what Tensile Strength and Modulus values could be expected for a part printed with 100% Carbon CFF. Note that a specimen with 100% Carbon CFF is not possible, as Eiger must place at least 1 floor and 1 ceiling layer of nylon. However, as more layers of Carbon CFF are added with only 2 total nylon layers, the fraction of Carbon CFF will approach 100%.

Equations 1 and 2 show lines of fit of experimental data for Carbon CFF specimen. These lines of fit can be seen on the plot of experimental data in figure 3-14.

$$UTS = 5.7886(CFF\ Fraction) + 50.441 \quad (1)$$

$$Modulus = 0.6545(CFF\ Fraction) + 0.5313 \quad (2)$$

Plugging in a theoretical maximum of 100% CFF Fraction into equations 1 and 2 yields the values shown in the bottom row of Table 5-1. From these lines of fit equations, a Tensile Strength of 700 MPa is still not achieved, as reported by Markforged, while a Tensile Modulus exceeds the Markforged reported value. Based on this info, it is likely that Markforged has simply overstated the Tensile Strength of Carbon CFF specimen.

Table 5-2: Comparison of Thesis Results with Markforged Data: Nylon and Onyx Specimen

	Tensile Strength at Break (MPa)	Tensile Modulus (GPa)	Tensile Strain at Break (%)	Notched Izod Impact Resistance (J/m)
Markforged Reported Value - Nylon	54	0.94	260	1015
Experimental Average - Nylon	54.7	0.49	236	67.1
Markforged Reported Value - Onyx	30	1.4	58	334
Experimental Average - Onyx printed with Mark Two (100% Infill Density)	44.8	2.01	50.2	93.9
Experimental Average - Onyx printed with Creator Pro (100% Infill Density)	47.4	3.18	21.2	-

Table 5-2 shows Markforged Reported values for Onyx and Nylon along with experimental data for each. In the case of nylon, all specimen were printed with Rectangular infill at 100% fill density. The Tensile properties reported by Markforged correlate well with the experimental data obtained in this thesis. However, The Impact Resistance reported by Markforged is off by more than an order of magnitude over the experimental data. Both data sets performed Izod impact testing according to ASTM D256-

10, and both followed the Type A test method for notched specimen [49]. The only apparent explanation for this is that the Markforged reported Impact Resistance for Nylon is either a typo of miscalculation.

For Onyx, specimen used for the Markforged Property comparison were printed with Rectangular infill at 100% fill density. Tensile specimen printed with the same part settings on the Flashforge Creator Pro were also included in the comparison. The tensile properties of Onyx reported by Markforged are an underestimate in the case of Tensile Strength and Tensile Modulus, and an overestimate in the case of Elongation at Break, when compared to experimental results. It is also shown that Onyx specimen printed with a creator pro had more favorable tensile properties than specimen printed with the Mark Two, although both experimental data sets correlate fairly well with each other. In the case of Impact Resistance, the Markforged Reported value is more than 3 times greater than experimental data from the Mark Two printer. Like the Nylon Impact Resistance Values, values reported were for the Type A test method of notched impact specimen according to ASTM D256-10 [49]. As with the nylon results, the results of Impact Resistance for Onyx are extremely overstated by Markforged. The only reasonable explanation for this discrepancy is an error or type in the Markforged Properties Data sheet.

CHAPTER 6 - CONCLUSIONS, RECOMMENDATIONS, AND FUTURE WORK

6.1 Conclusions

The work presented in this thesis makes a case for 3D printed Carbon Fiber Composites to be used as functional components in a variety of every day uses. Mechanical Properties shown in this thesis demonstrate that parts can be fabricated to be very robust, and even rival Aluminum in some cases. The key takeaways from each chapter are listed below.

6.2 Short Fiber Composite Tensile Properties

1. Higher infill densities resulted in higher tensile strengths and tensile moduli.
2. Specimen printed with the Creator Pro achieved marginally higher tensile properties than specimen printed with the Mark Two.
3. Specimen printed with the Mark Two were dimensionally more accurate than those printed with the Creator Pro.
4. The Modified Rule of Mixtures Model most accurately predicted the tensile properties of these short fiber composites.

6.3 Continuous Fiber Composite Tensile Properties

1. An increase in continuous fibers loaded longitudinally within the part resulted in a linear increase in tensile strength and tensile modulus.
2. Continuous fibers embedded in directions other than the longitudinal direction provided little to no reinforcement.
3. Tensile specimen printed with the Mark Two saw dimensional variances of +0.2 mm to -0.1mm.

4. A Volume Average Stiffness model was able to accurately predict the tensile modulus of these specimen.

6.4 Short and Continuous Fiber Composite Impact Properties

1. A linear trend was observed of increase Impact Resistance with increased Carbon Fiber layers for Groups A, B, and C, and D
2. Fiber Group E exhibited a hyperbolic trend of Carbon Fiber Layers vs. Impact Resistance which peaked at around 12 layers of Carbon Fiber
3. Continuous Fiber Specimen printed with off angle fibers performed similarly to Nylon control specimen.
4. Onyx specimen with a layer height of 0.2 mm and Raster angles of alternating 45 degree infill had the highest impact resistance of all onyx specimen.

6.5 Future Work

The current work performed in this thesis was limited to Tensile and Impact properties of Carbon fiber composites only, though Markforged also sells Fiber Glass and Kevlar fibers. Further investigation into the effects of these fiber reinforcements on Tensile and Impact Properties would provide an Additive Manufacturing Designer with more material options to choose from.

Work on other mechanical properties such as compression, flexure, and fatigue would also provide much useful info into how these composites would perform under a variety of conditions.

The Volume Average Stiffness Method may also be refined to better account for Continuous Fiber Composites with off angle fiber directions, to understand the tensile properties of these parts in directions other than the longitudinal direction.

REFERENCES

[1] Gibson I, Rosen D, Stucker B. Additive Manufacturing Technologies: 3D printing, Rapid Prototyping, and Direct Digital Manufacturing. New York, NY: Springer, 2015.

[2] Ferreira RTL, Amatte IC, Dutra TA, Bürger D. Experimental characterization and micrography of 3D printed PLA and PLA reinforced with short carbon fibers. Composites Part B: Engineering. 2017;124:88-100.

[3] Stratasys. FDM Thermoplastics. http://wwwstratasyscom/materials/fdm, 2017.

[4] Rodríguez JF, Thomas JP, Renaud JE. Mechanical behavior of acrylonitrile butadiene styrene fused deposition materials modeling. Rapid Prototyping Journal. 2003;9:219-30.

[5] Sood AK, Ohdar RK, Mahapatra SS. Parametric appraisal of mechanical property of fused deposition modelling processed parts. Materials & Design. 2010;31:287-95.

[6] Letcher T, Waytashek M. Material Property Testing of 3D-Printed Specimen in PLA on an Entry-Level 3D Printer. Volume 2A: Advanced Manufacturing2014.

[7] Melenka GW, Eujin Pei D, Schofield JS, Dawson MR, Carey JP. Evaluation of dimensional accuracy and material properties of the MakerBot 3D desktop printer. Rapid Prototyping Journal. 2015;21:618-27.

[8] Ivey M, Melenka GW, Carey JP, Ayranci C. Characterizing short-fiber-reinforced composites produced using additive manufacturing. Advanced Manufacturing: Polymer & Composites Science. 2017;3:81-91.

[9] Tekinalp HL, Kunc V, Velez-Garcia GM, Duty CE, Love LJ, Naskar AK, et al. Highly oriented carbon fiber–polymer composites via additive manufacturing. Composites Science and Technology. 2014;105:144-50.

[10] Li N, Li Y, Liu S. Rapid prototyping of continuous carbon fiber reinforced polylactic acid composites by 3D printing. Journal of Materials Processing Technology. 2016;238:218-25.

[11] Yang C, Tian X, Liu T, Cao Y, Li D. 3D printing for continuous fiber reinforced thermoplastic composites: mechanism and performance. Rapid Prototyping Journal. 2017;23:209-15.

[12] Nakagawa Y, Mori K-i, Maeno T. 3D printing of carbon fibre-reinforced plastic parts. The International Journal of Advanced Manufacturing Technology. 2017;91:2811-7.

[13] Holt JM, Mindlin H, Ho CY. Structural alloys handbook: CINDAS/Purdue University, 1994.

[14] Es-Said OS, Foyos J, Noorani R, Mendelson M, Marloth R, Pregger BA. Effect of Layer Orientation on Mechanical Properties of Rapid Prototyped Samples. Materials and Manufacturing Processes. 2000;15:107-22.

[15] Roberson DA, Torrado Perez AR, Shemelya CM, Rivera A, MacDonald E, Wicker RB. Comparison of stress concentrator fabrication for 3D printed polymeric izod impact test specimens. Additive Manufacturing. 2015;7:1-11.

[16] Vega V, Clements J, Lam T, Abad A, Fritz B, Ula N, et al. The Effect of Layer Orientation on the Mechanical Properties and Microstructure of a Polymer. Journal of Materials Engineering and Performance. 2010;20:978-88.

[17] Ziemian C, Sharma M, Ziemi S. Anisotropic Mechanical Properties of ABS Parts Fabricated by Fused Deposition Modelling. Mechanical Engineering. 2012.

[18] Gentle D. Function and properties factors in process selection. Engineering Plastics. 1988;2:279-88.

[19] Brown AS. Rapid prototyping-Parts without tools. Aerospace America. 1991;29:18-23.

[20] Cantwell WJ, Morton J. The impact resistance of composite materials — a review. Composites. 1991;22:347-62.

[21] Cantwell W, Morton J. Detection of impact damage in CFRP laminates. Composite Structures. 1985;3:241-57.

[22] Elber W. Failure mechanics in low-velocity impacts on thin composite plates. 1983.

[23] Clark G. Modelling of impact damage in composite laminates. Composites. 1989;20:209-14.

[24] Adams DF, Miller AK. An analysis of the impact behavior of hybrid composite materials. Materials Science and Engineering. 1975;19:245-60.

[25] Vedula M, Koczak MJ. Impact Resistance of Cross-Plied Polyphenylene Sulfide Composites. Journal of Thermoplastic Composite Materials. 2016;2:154-63.

[26] Chamis C, Hanson M, Serafini T. Impact Resistance of Unidirectional Fiber Composites. Composite Materials: Testing and Design (Second Conference): ASTM International. p. 324-6.

[27] Ozkan C, Gamze Karsli N, Aytac A, Deniz V. Short carbon fiber reinforced polycarbonate composites: Effects of different sizing materials. Composites Part B: Engineering. 2014;62:230-5.

[28] Karsli NG, Ozkan C, Aytac A, Deniz V. Effects of sizing materials on the properties of carbon fiber-reinforced polyamide 6,6 composites. Polymer Composites. 2013;34:1583-90.

[29] Crosby JM, Drye TR. Fracture Studies of Discontinuous Fiber Reinforced Thermoplastic Composites. Journal of Reinforced Plastics and Composites. 2016;6:162-77.

[30] Joshi M, Maiti SN, Misra A, Mittal RK. Influence of fiber length, fiber orientation, and interfacial adhesion on poly (butylene terephthalate)/polyethylene alloys reinforced with short glass fibers. Polymer Composites. 1994;15:349-58.

[31] Caldeira G, Maia JM, Carneiro OS, Covas JA, Bernardo CA. Production and characterization of innovative carbon fiber-polycarbonate composites. Polymer Composites. 1998;19:147-51.

[32] Melenka GW, Cheung BKO, Schofield JS, Dawson MR, Carey JP. Evaluation and prediction of the tensile properties of continuous fiber-reinforced 3D printed structures. Composite Structures. 2016;153:866-75.

[33] Markforged Mark Two Materials Data Sheet. In: Markforged, editor.2016.

[34] Tucker III CL, Liang E. Stiffness predictions for unidirectional short-fiber composites: Review and evaluation. Composites Science and Technology. 1999;59:655-71.

[35] Parandoush P, Lin D. A review on additive manufacturing of polymer-fiber composites. Composite Structures. 2017;182:36-53.

[36] Patanwala HS, Hong D, Vora SR, Bognet B, Ma AWK. The microstructure and mechanical properties of 3D printed carbon nanotube-polylactic acid composites. Polymer Composites. 2017.

[37] Fliegener S, Luke M, Gumbsch P. 3D microstructure modeling of long fiber reinforced thermoplastics. Composites Science and Technology. 2014;104:136-45.

[38] Graupner N, Beckmann F, Wilde F, Müssig J. Using synchroton radiation-based micro-computer tomography (SR μ-CT) for the measurement of fibre orientations in cellulose fibre-reinforced polylactide (PLA) composites. Journal of Materials Science. 2013;49:450-60.

[39] ASTM D638-10. Standard Test Method for Tensile Properties of Plastics. 2010.

[40] Schneider CA, Rasband WS, Eliceiri KW. NIH Image to ImageJ: 25 years of image analysis. Natural Methods. 2012;9(7):671-5.

[41] Rueden CT, Schindelin J, Hiner MC, DeZonia BE, Walter AE, Arena ET, et al. ImageJ2: ImageJ for the next generation of scientific image data. BMC Bioinformatics. 2017;18:529.

[42] Alger MSM. Polymer Science Dictionary. 2nd Ed. ed: Springer Publishing, 1997.

[43] O'Regan MDF, Akay, Meenan B. A comparison of Young's modulus predictions in fibre-reinforced-polyamide injection mouldings. Composites Science and Technology. 1999;59:419-27.

[44] Coleman JN, Khan U, Blau WJ, Gun'ko YK. Small but strong: A review of the mechanical properties of carbon nanotube–polymer composites. Carbon. 2006;44:1624-52.

[45] Cox HL. The elasticity and strength of paper and other fibrous materials. British Journal of Applied Physics. 1951;3.

[46] Krenchel H. Fibre Reinforcement. Akademisk Forlag: Copenhagen. 1964.

[47] Meddad A, Azaiez J, Ait-Kadi A, Guenette R. Micromechanical Modeling of Tensile Behavior of Short Fiber Composites. Journal of Composite Materials. 2016;36:423-41.

[48] Markforged. Order Materials. https://markforgedcom/order-materials/, 2018.

[49] ASTM D256-10. Standard Test Methods for Determining the Izod Pendulum Impact Resistance of Plastics. 2010.

APPENDICES

Appendix A: MATLAB Code to Generate Stress-Strain Curves from MTS Data

```
clear all
close all
clc

format long

% Data from the MTS machine should be in the following units and order....
% "Time (s)","Extension (mm)","Load (N)","_Strain1 (mm)"

%-------------------------------------------------------------------------
-------------------------------
%   Create a spreadsheet with the following contents:
%   Column A: names of files that include raw data from MTS machine.
%       Include file extension. EX. "a1.txt" without quotes
%   Column B: names to use when saving figures and photos.
%       DO NOT INCLUDE file extension. EX. "a1" without quotes
%   Column C: names to use as Plot titles on top of all Plots
%       This can be anything to be used within title(). EX. "0.1 mm Layer, 25%
infill" without quotes
%   Column D: Width of the specimen, in mm.
%   Colum E: Thickness of the specimen, in mm.
%-------------------------------------------------------------------------
-------------------------------

[null, file] = xlsread('onyx_results.xlsx', 'A2:A49');              %reads File
names from spreadsheet to load data from
[null, fig] = xlsread('onyx_results.xlsx', 'B2:B49');               %reads
names to use when saving figures
[null, plt_title] = xlsread('onyx_results.xlsx', 'C2:C49');         %reads
names to put as title on top of plots
width = xlsread('onyx_results.xlsx','H2:H49')/1000;
thickness = xlsread('onyx_results.xlsx','I2:I49')/1000;

for i = 1:length(file)
%for i = 4
    filename = [file{i,1}{, 2010 #99}{, 2010 #99}];
    filename2 = [fig{i,1}];
    plot_title = [plt_title{i,1}];

    data = load(filename);
    time = data(:,1);
    disp = data(:,2);
```

```
    force = data(:,3);
    extens = data(:,4);

    extens = extens - extens(1);
    extens = smooth(extens,25);

    area = width(i)*thickness(i);
    stress = force/area;        %Pa
    strain = extens/20;         %mm/mm

    range = 5:25;
    [coeff] = polyfit(strain(range),stress(range),1);
    E = coeff(1);

%     deriv = diff_central(strain,stress/1e6);
%     threshold = 25;
%     threshold1 = 50;
%     flag = 0;

    broken(i) = length(strain-1);           %Position at which to stop plotting
data due to break of sample
    final = length(strain);                 %Final data point in strain array
for plotting.

    [stress_max, loc] = max(stress);

    for k = loc:length(strain)
       if stress(k) < 0.95*stress_max       %if stress after max stress dips
below 95% of max stress, set stop point for chart
           broken(i) = k-1;                 %set broken back one step to ensure
all excess data is removed
           break
       end
    end

    for j = 2:length(strain)                %if extensometer is maxed out, set
stop point for chart
        if strain(j) > 0.22
            broken(i) = j;
            break
        end
    end

%     for j = 2:length(strain-10)
%        if stress(j+10) <= stress(j)
%            broken(i) = j;
%            break
%        end
```

```
%     end

%     for j = 2:length(strain-1)
%         check(j) = abs(deriv(j)/deriv(j-1));
%         if (check(j) >= threshold || check(j) <= 1/threshold)
%             flag = 1;
%         end
%         if (check(j) >= threshold || check(j) <= 1/threshold) && flag == 1
%             broken(i) = j;
%             check(j);
%             flag = 0;
%             break
%         else
%             flag = 0;
%         end
%     end

%     for j = 2:length(strain)
%         check(j) = abs(strain(j)/strain(j-1));
%         check1(j) = abs(stress(j)/stress(j-1));
%         if check(j) <= 1/threshold || check(j) <= 1/threshold %||...
%                  %check1(j) >= threshold1 || check1(j) <= 1/threshold1
%             broken(i) = j;
%             break
%         end
%     end

    figure(1)
    %plot(strain,stress/1e6)
    plot(strain(1:broken(i)),stress(1:broken(i))/1e6,'LineWidth',2)
        %strain(broken(i):final),stress(broken(i):final)/1e6,'r')
    axis([0 0.25 0 50])
    hold on
    grid on

    figure(i+1)
    %plot command commented out for sake of publishing code
    %uncomment this command to run code
%
plot(strain(1:broken(i)),stress(1:broken(i))/1e6,'.b',strain(broken(i):final),s
tress(broken(i):final)/1e6,'.r',...
%         strain(1:50),(E*strain(1:50)+coeff(2))/1e6,...
%         [strain(range(1)) strain(range(end))],[stress(range(1)),...
%         stress(range(end))]/1e6,'ko','LineWidth',2)
    grid on
    axis([0 0.25 0 50])
    xlabel('Strain (mm/mm)')
    ylabel('Stress (MPa)')
```

```
    title(plot_title);
    legend('Raw Data', 'Omitted Data', 'Tensile Modulus Polyfit', 'Bounds of
Polyfit','Location','southeast')
    saveas(gcf,filename2,'fig')
    saveas(gcf,filename2,'jpeg')

    paste_in_Excel(i,1) = max(stress)/1e6;
    paste_in_Excel(i,2) = E/1e9;
    paste_in_Excel(i,3) = max(strain)*100;            %output is in MPa, mm/mm,
GPa

end

paste_in_Excel
```

Appendix B: MATLAB Code for Generating Subplots of all Data in a given study

```
clear all
close all
clc

width = 12.85/1000;   %in meters
thickness = 3.42/1000;    %in meters

rect_1 = {'A1'; 'A2'; 'A3'; 'B1'; 'B2'; 'B3'; 'C1'; 'C2'; 'C3'; 'D1'; 'D2';
'D3'};
%rect_1 = {'B1'};
rect_2 = {'E1'; 'E2'; 'E3'; 'F1'; 'F2'; 'F3'; 'G1'; 'G2'; 'G3'; 'H1'; 'H2';
'H3'};
hex_1 = {'I1'; 'I2'; 'I3'; 'J1'; 'J2'; 'J3'};
hex_2 = {'M1'; 'M2'; 'M3'; 'N1'; 'N2'; 'N3'};
tri_1 = {'K1'; 'K2'; 'K3'; 'L1'; 'L2'; 'L3'};       %7c_1 omitted for now
tri_2 = {'O1'; 'O2'; 'O3'; 'P1'; 'P2'; 'P3'};

ending = '.txt';

%0.1 Rect
for i = 1:length(rect_1)
    file = strcat(rect_1,ending);
    fig= rect_1;

    filename = [file{i,1}];
    filename2 = [fig{i,1}];

    plot_title = '0.1mm Layer - Rectangular Infill';

    data = load(filename);
    time = data(:,1);
    disp = data(:,2);
    force = data(:,3);
    extens = data(:,4);

    extens = extens - extens(1);
    extens = smooth(extens,25);

    area = width*thickness;
    stress = force/area;        %Pa
    strain = extens/20;         %mm/mm

    broken(i) = length(strain-1);           %Position at which to stop plotting
```

```
data due to break of sample
    final = length(strain);                 %Final data point in strain array
for plotting.

    [stress_max, loc] = max(stress);

    for k = loc:length(strain)
       if stress(k) < 0.95*stress_max       %if stress after max stress dips
below 95% of max stress, set stop point for chart
           broken(i) = k-1;                 %set broken back one step to ensure
all excess data is removed
           break
       end
    end

    for j = 2:length(strain)                %if extensometer is maxed out, set
stop point for chart
        if strain(j) > 0.22
            broken(i) = j;
            break
        end
    end

    figure(1)
    subplot(2,3,1)
    plot(strain(1:broken(i)),stress(1:broken(i))/1e6,'LineWidth',2)
    axis([0 0.25 0 60])
    hold on
    grid on
    xlabel('Strain (mm/mm)')
    ylabel('Stress (MPa)')
    title(plot_title);
end

%0.2 Rect
for i = 1:length(rect_2)
    file = strcat(rect_2,ending);
    fig= rect_2;

    filename = [file{i,1}];
    filename2 = [fig{i,1}];

    plot_title = '0.2mm Layer - Rectangular Infill';

    data = load(filename);
    time = data(:,1);
    disp = data(:,2);
    force = data(:,3);
```

```
    extens = data(:,4);

    extens = extens - extens(1);
    extens = smooth(extens,25);

    area = width*thickness;
    stress = force/area;        %Pa
    strain = extens/20;         %mm/mm

    broken(i) = length(strain-1);           %Position at which to stop plotting
data due to break of sample
    final = length(strain);                 %Final data point in strain array
for plotting.

    [stress_max, loc] = max(stress);

    for k = loc:length(strain)
       if stress(k) < 0.95*stress_max       %if stress after max stress dips
below 95% of max stress, set stop point for chart
           broken(i) = k-1;                 %set broken back one step to ensure
all excess data is removed
           break
       end
    end

    for j = 2:length(strain)                %if extensometer is maxed out, set
stop point for chart
        if strain(j) > 0.22
            broken(i) = j;
            break
        end
    end

    figure(1)
    subplot(2,3,4)
    plot(strain(1:broken(i)),stress(1:broken(i))/1e6,'LineWidth',2)
    axis([0 0.25 0 60])
    hold on
    grid on
    xlabel('Strain (mm/mm)')
    ylabel('Stress (MPa)')
    title(plot_title);
end

%0.1 Hex
for i = 1:length(hex_1)
    file = strcat(hex_1,ending);
    fig= hex_1;
```

```
    filename = [file{i,1}];
    filename2 = [fig{i,1}];

    plot_title = '0.1mm Layer - Hexagonal Infill';

    data = load(filename);
    time = data(:,1);
    disp = data(:,2);
    force = data(:,3);
    extens = data(:,4);

    extens = extens - extens(1);
    extens = smooth(extens,25);

    area = width*thickness;
    stress = force/area;        %Pa
    strain = extens/20;         %mm/mm

    broken(i) = length(strain-1);           %Position at which to stop plotting
data due to break of sample
    final = length(strain);                 %Final data point in strain array
for plotting.

    [stress_max, loc] = max(stress);

    for k = loc:length(strain)
       if stress(k) < 0.95*stress_max       %if stress after max stress dips
below 95% of max stress, set stop point for chart
           broken(i) = k-1;                 %set broken back one step to ensure
all excess data is removed
           break
       end
    end

    for j = 2:length(strain)                %if extensometer is maxed out, set
stop point for chart
        if strain(j) > 0.22
            broken(i) = j;
            break
        end
    end

    figure(1)
    subplot(2,3,2)
    plot(strain(1:broken(i)),stress(1:broken(i))/1e6,'LineWidth',2)
    axis([0 0.25 0 60])
    hold on
```

```
    grid on
    xlabel('Strain (mm/mm)')
    ylabel('Stress (MPa)')
    title(plot_title);
end

%0.2 Hex
for i = 1:length(hex_2)
    file = strcat(hex_2,ending);
    fig= hex_2;

    filename = [file{i,1}];
    filename2 = [fig{i,1}];

    plot_title = '0.2mm Layer - Hexagonal Infill';

    data = load(filename);
    time = data(:,1);
    disp = data(:,2);
    force = data(:,3);
    extens = data(:,4);

    extens = extens - extens(1);
    extens = smooth(extens,25);

    area = width*thickness;
    stress = force/area;        %Pa
    strain = extens/20;         %mm/mm

    broken(i) = length(strain-1);           %Position at which to stop plotting
data due to break of sample
    final = length(strain);                 %Final data point in strain array
for plotting.

    [stress_max, loc] = max(stress);

    for k = loc:length(strain)
       if stress(k) < 0.95*stress_max       %if stress after max stress dips
below 95% of max stress, set stop point for chart
           broken(i) = k-1;                 %set broken back one step to ensure
all excess data is removed
           break
       end
    end

    for j = 2:length(strain)                %if extensometer is maxed out, set
stop point for chart
        if strain(j) > 0.22
```

```
            broken(i) = j;
            break
        end
    end

    figure(1)
    subplot(2,3,5)
    plot(strain(1:broken(i)),stress(1:broken(i))/1e6,'LineWidth',2)
    axis([0 0.25 0 60])
    hold on
    grid on
    xlabel('Strain (mm/mm)')
    ylabel('Stress (MPa)')
    title(plot_title);
end

%0.1 Tri
for i = 1:length(tri_1)
    file = strcat(tri_1,ending);
    fig= tri_1;

    filename = [file{i,1}];
    filename2 = [fig{i,1}];

    plot_title = '0.1mm Layer - Triangular Infill';

    data = load(filename);
    time = data(:,1);
    disp = data(:,2);
    force = data(:,3);
    extens = data(:,4);

    extens = extens - extens(1);
    extens = smooth(extens,25);

    area = width*thickness;
    stress = force/area;        %Pa
    strain = extens/20;         %mm/mm

    broken(i) = length(strain-1);           %Position at which to stop plotting
data due to break of sample
    final = length(strain);                 %Final data point in strain array
for plotting.

    [stress_max, loc] = max(stress);

    for k = loc:length(strain)
       if stress(k) < 0.95*stress_max       %if stress after max stress dips
```

```
below 95% of max stress, set stop point for chart
            broken(i) = k-1;                %set broken back one step to ensure
all excess data is removed
            break
        end
    end

    for j = 2:length(strain)                %if extensometer is maxed out, set
stop point for chart
        if strain(j) > 0.22
            broken(i) = j;
            break
        end
    end

    figure(1)
    subplot(2,3,3)
    plot(strain(1:broken(i)),stress(1:broken(i))/1e6,'LineWidth',2)
    axis([0 0.25 0 60])
    hold on
    grid on
    xlabel('Strain (mm/mm)')
    ylabel('Stress (MPa)')
    title(plot_title);
end

%0.2 Tri
for i = 1:length(tri_2)
    file = strcat(tri_2,ending);
    fig= tri_2;

    filename = [file{i,1}];
    filename2 = [fig{i,1}];

    plot_title = '0.2mm Layer - Triangular Infill';

    data = load(filename);
    time = data(:,1);
    disp = data(:,2);
    force = data(:,3);
    extens = data(:,4);

    extens = extens - extens(1);
    extens = smooth(extens,25);

    area = width*thickness;
    stress = force/area;        %Pa
    strain = extens/20;         %mm/mm
```

```
    broken(i) = length(strain-1);           %Position at which to stop plotting
data due to break of sample
    final = length(strain);                 %Final data point in strain array
for plotting.

    [stress_max, loc] = max(stress);

    for k = loc:length(strain)
       if stress(k) < 0.95*stress_max       %if stress after max stress dips
below 95% of max stress, set stop point for chart
           broken(i) = k-1;                 %set broken back one step to ensure
all excess data is removed
           break
       end
    end

    for j = 2:length(strain)                %if extensometer is maxed out, set
stop point for chart
        if strain(j) > 0.22
            broken(i) = j;
            break
        end
    end

    figure(1)
    subplot(2,3,6)
    plot(strain(1:broken(i)),stress(1:broken(i))/1e6,'LineWidth',2)
    axis([0 0.25 0 60])
    hold on
    grid on
    xlabel('Strain (mm/mm)')
    ylabel('Stress (MPa)')
    title(plot_title);
end

saveas(gcf,'compiled stress-strain curves onyx','fig')
saveas(gcf,'compiled stress-strain curves onyx','tiffn')
saveas(gcf,'compiled stress-strain curves onyx','pdf')
```

Appendix C: MATLAB Code for Short Fiber Modeling

```
clear all
close all
clc

vf = .09129;                 %average estimate from 10 imageJ image analyses

eta_orientation = 0.5575;   %orientation factor
                            %summation(vfi*cos^4(theta_i) from imageJ
histogram;

l = 108.2;                  %average length from 19 microscope measurements
d = 7.36;                   %average diameter from 13 microscope measurements

Ef = 232;                   %Modulus of Elasticity of fibers, GPa
%Em = 0.75;                  %Modulus of Elasticity of Nylon, assumed, GPa
Em = 0.94;                  %Modulus of Elasticity of Nylon, reported by
Markforged

%Modified Rule of Mixtures Model
Beta = sqrt((3*Em)/(2*Ef*log(vf*100)));
eta_L = 1 - (tanh(Beta*l/d)/(Beta*l/d));

E_composite_mrom = Em*(1-(vf))+eta_L*eta_orientation*Ef*vf

%Halpin-Tsai model
eta_ll = ((Ef/Em)-1)/((Ef/Em)+2*(l/d));
E_composite_halpin = Em*((1+(2*(l/d)*eta_ll*vf))/(1-(eta_ll*vf)))

%Rule of Mixtures Model
E_composite_inverse_ROM = ((vf/Ef)+(1-vf)/Em)^(-1)
E_composite_rom = Em*(1-(vf))+Ef*vf

%ROM comparison
vf = 0:0.01:1;

for i = 1:length(vf)
    E_composite_inverse_ROM(i) = ((vf(i)/Ef)+((1-vf(i))/Em))^(-1);
    E_composite_rom(i) = Em*(1-(vf(i)))+Ef*vf(i);
end

plot(vf,E_composite_inverse_ROM,vf,E_composite_rom)
legend('Inverse ROM','ROM')
```

```
E_composite_mrom =

   2.744104184998643


E_composite_halpin =

   3.467033053422730


E_composite_inverse_ROM =

   1.034012542483001


E_composite_rom =

  22.033467399999999
```

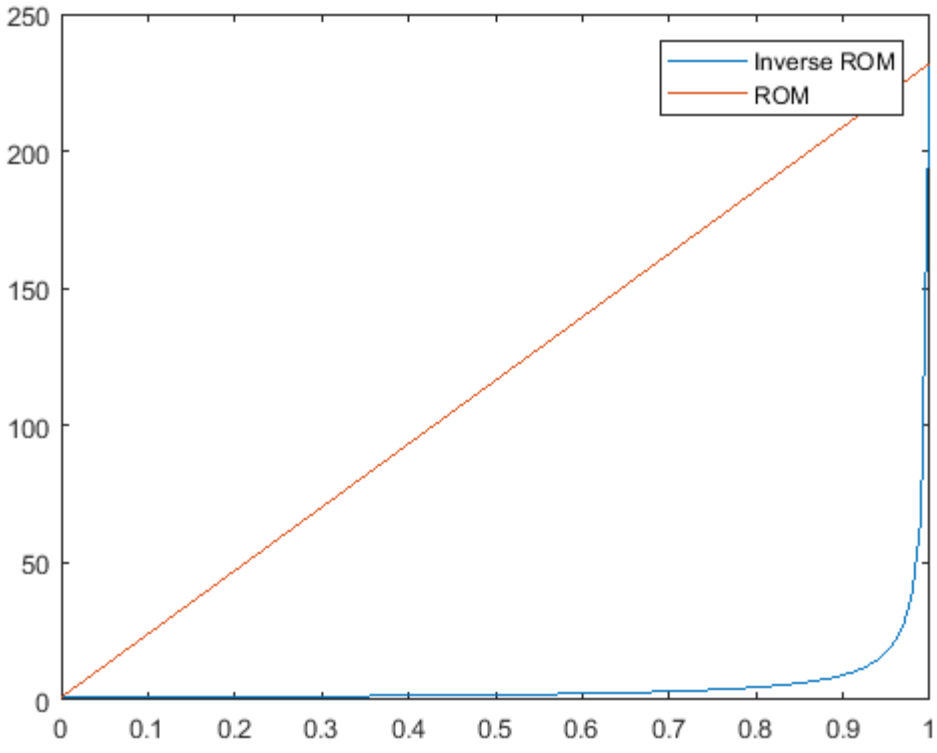

Appendix D: MATLAB Code for Volume Average Stiffness Method

```
clear all
close all
clc

%-------------------------------------------------------------------------
% Reading in Experimental Results
%-------------------------------------------------------------------------
filename = 'experimental_data.xlsx';
data = xlsread(filename);
numCFLayers = data(:,3);
numCFStrands = data(:,4);
materialCost = data(:,5);
Width = data(:,6);
Thickness = data(:,7);
UTS = data(:,8);
Modulus = data(:,9);
Elongation = data(:,10);

clear data

for i=0:24
%-------------------------------------------------------------------------
% Volume of Tensile area
%-------------------------------------------------------------------------

% Variables Below, the sum of (2*numFloor+numFiberLayers) cannot exceed 26,
% but can be less than 26.
if i<= 18
    numFloor = 4;           %Constant across all samples
else
    numFloor = 1;
end
numFiberLayers = i;     %Variable depending on the part.

Wstrand = 1;             %Width of one extruded fiber strand, mm

H = 3.25;                %Height of cross section, mm
W = 13;                 %Width of cross section, mm
L = 57;                 %Length of tensile area, mm

Hlayer = 0.125;         %Height of one printed layer, mm

Wshell = 4*0.39;        %Width of both outer walls, mm
Vshell = Wshell*H*L;    %Volume of outer walls, mm^3
```

```
Vfloor = (W-Wshell)*numFloor*Hlayer*L;  %Volume of floor layers, mm^3
Vroof = Vfloor;

Wfiber = 11*Wstrand;    %Width of Fiber layers, mm
Vfiber = Wfiber*numFiberLayers*Hlayer*L; %Volume of all Carbon Fiber, mm^3

WinfillFiber = W-Wshell-(Wfiber);    %Width of Nylon infill next to CF, mm
VinfillFiber = WinfillFiber*numFiberLayers*Hlayer*L;   %Volume of Infill next
to CF, mm^3

Winfill = W-Wshell;     %Width of standard infill, mm
Vinfill = Winfill*L*(H-(Hlayer*(2*numFloor + numFiberLayers)));   %Volume of
standard infill, mm^3

Vtotal = H*W*L;         %Total Volume of tensile area, mm^3
Vsum = Vshell + Vfloor + Vroof + Vfiber + VinfillFiber + Vinfill;   %the same
as Vtotal, used as a check

Vfinfill = (Vroof+Vfloor+Vinfill+VinfillFiber)/Vtotal;
Vfshell = Vshell/Vtotal;
Vffiber = Vfiber/Vtotal;

Vftotal = Vfinfill+Vfshell+Vffiber;

%-------------------------------------------------------------------------
% Material Properties
%-------------------------------------------------------------------------

% Nylon Properties
% Melenka 2016
% properties for nylon shell volumes
E = 0.75; %GPa
nu = 0.35;
G = E / (2*(1+nu)); %GPa

% Carbon Fiber Properties
% Meddad Et al 2002
% Ef1 = 231; %GPa
% Ef2 = 22.4; %GPa

% Properties for PITCH Fibers
% Ef1 = 65;     %Value that correlates well with experimental data
Ef1 = 64.696;    %Value obtained from average carbon fiber ...
                %density (Image J analysis) times Modulus from Meddad Et al

%Ef2 = 3.08;
Ef2 = 22.4;
```

```
Ef3 = Ef2;
Gf12 = 22.1; %GPa
% Gf12 = 500;
Gf13 = Gf12;
Gf23 = 8.3; %GPa
nuf12 = 0.3;
nuf13 = nuf12;
nuf21 = nuf12*(Ef2/Ef1);
nuf31 = nuf12*(Ef3/Ef1);
nuf23 = 0.35;
nuf32 = nuf23*(Ef3/Ef2);

% % Kevlar Properties
% % Kawabata 1990
% Ef1 = 79.8; %GPa
% Ef2 = 2.59; %GPa
% Ef3 = Ef2;
% Gf12 = 2.1; %GPa
% Gf13 = Gf12;
% Gf23 = 1.5; %GPa
% nuf12 = 0.33;
% nuf13 = nuf12;
% nuf21 = nuf12*(Ef2/Ef1);
% nuf31 = nuf12*(Ef3/Ef1);
% nuf23 = 0.1;
% nuf32 = nuf23*(Ef3/Ef2);

% Micromechanical Properties from Rodriguez et al 2003
% Infill properties for floor, roof, and infill volumes
rho = 0.01; % void density of infill found from Image J analysis of nylon walls
E1 = (1-rho)*E; %GPa
E2 = (1-rho^0.5)*E; %GPa
E3 = E2;
G12 = G*(1-rho)*(1-rho^0.5) / ((1-rho) + (1-rho^0.5)); %GPa
G13 = G12;
G23 = (1- rho^0.5)*G; %GPa
nu12 = (1-rho)*nu;
nu13 = nu12;
nu23 = (1 - rho^0.5)*nu;
nu21 = (1 - rho^0.5)*nu;
nu31 = nu21;
nu32 = nu21;

%-------------------------------------------------------------------------
% Compliance Matrices
%-------------------------------------------------------------------------

Sshell = [1/E -nu/E -nu/E 0 0 0;
```

```
        -nu/E 1/E -nu/E 0 0 0;
        -nu/E -nu/E 1/E 0 0 0;
        0 0 0 1/G 0 0;
        0 0 0 0 1/G 0;
        0 0 0 0 0 1/G];

Sinfill = [1/E1 -nu21/E2 -nu31/E3 0 0 0;
        -nu12/E1 1/E2 -nu32/E3 0 0 0;
        -nu13/E1 -nu23/E2 1/E3 0 0 0;
        0 0 0 1/G23 0 0;
        0 0 0 0 1/G13 0;
        0 0 0 0 0 1/G12];

Scarbon = [1/Ef1 -nuf21/Ef2 -nuf31/Ef3 0 0 0;
        -nuf12/Ef1 1/Ef2 -nuf32/Ef3 0 0 0;
        -nuf13/Ef1 -nuf23/Ef2 1/Ef3 0 0 0;
        0 0 0 1/Gf23 0 0;
        0 0 0 0 1/Gf13 0;
        0 0 0 0 0 1/Gf12];

% Rotation of solid and infill layers
alpha = 45*(pi/180);

SinfillPos = transform_compliance(alpha, Sinfill);
SinfillNeg = transform_compliance(-alpha, Sinfill);

CinfillPos = inv(SinfillPos);
CinfillNeg = inv(SinfillNeg);
Cshell = inv(Sshell);
Ccarbon = inv(Scarbon);

Ctotal = Vfinfill*CinfillPos*0.5 + Vfinfill*CinfillNeg*0.5 + Cshell*Vfshell +
Ccarbon*Vffiber;

Stotal = inv(Ctotal);

Ex = 1/Stotal(1,1);
Ey = 1/Stotal(2,2);
Ez = 1/Stotal(3,3);
Gxy = 1/Stotal(6,6);
Gyz = 1/Stotal(5,5);
Gzx = 1/Stotal(4,4);
vxy = -Stotal(1,2)/Stotal(1,1);

VF(i+1) = Vffiber*100;

i;
```

```
Headings = ['Ex ' 'Ey ' 'Ez ' 'Gxy ' 'Gyz ' 'Gzx ' 'vxy ' 'VF'];
Results = [Ex Ey Ez Gxy Gyz Gzx vxy VF];
Ex_new(i+1) = Ex;
end

VF_exp = volume_fraction(numCFStrands/11);

plot(VF,Ex_new,'LineWidth',1)
xlabel('Carbon Fiber Filament Volume Fraction (%)')
ylabel('Elastic Modulus (GPa)')
axis([0 100 0 60])
grid on
hold on
plot(VF_exp,Modulus,'o','LineWidth',1)

VAS_Fit = polyfit(VF,Ex_new,1);
Experimental_Fit = polyfit(VF_exp,Modulus,1);

y = Experimental_Fit(1)*VF + Experimental_Fit(2);
plot(VF,y,'r','LineWidth',1)
legend('VAS Model', 'Experimental Data', 'Experimental Data Curve Fit',
'location','northwest')

percent_error = abs(y(25)-Ex_new(25))/Ex_new(25)*100
```

```
percent_error =

   1.329406798233518
```

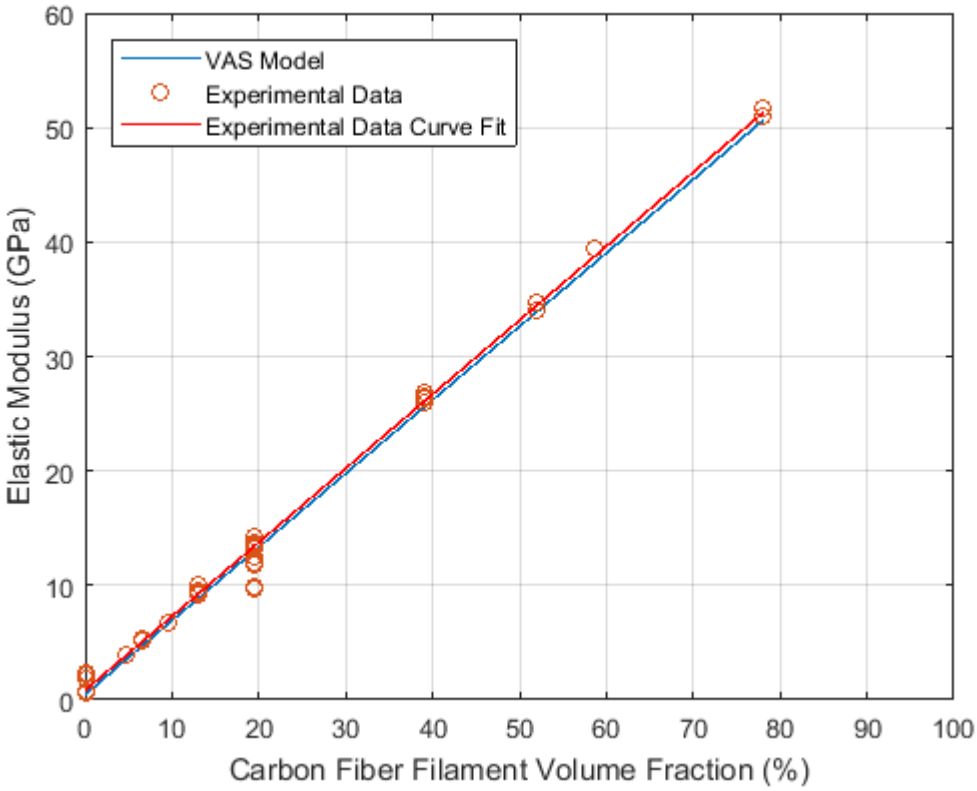
VAS Model
Experimental Data
Experimental Data Curve Fit
Elastic Modulus (GPa)
Carbon Fiber Filament Volume Fraction (%)
0
10
20
30
40
50
60
70
80
90
100

Appendix E: volume_fraction function used in VAS Model

```
function [ Vffiber ] = volume_fraction( numFiberLayers )
if numFiberLayers<= 18
    numFloor = 4;           %Constant across all samples
else
    numFloor = 1;
end

Wstrand = 1;             %Width of one extruded fiber strand, mm

H = 3.25;                %Height of cross section, mm
W = 13;                 %Width of cross section, mm
L = 57;                 %Length of tensile area, mm

Hlayer = 0.125;         %Height of one printed layer, mm


Wshell = 4*0.39;        %Width of both outer walls, mm
Vshell = Wshell*H*L;    %Volume of outer walls, mm^3

Vfloor = (W-Wshell)*numFloor*Hlayer*L;  %Volume of floor layers, mm^3
Vroof = Vfloor;

Wfiber = 11*Wstrand;    %Width of Fiber layers, mm
Vfiber = Wfiber*numFiberLayers*Hlayer*L; %Volume of all Carbon Fiber, mm^3

WinfillFiber = W-Wshell-(Wfiber);    %Width of Nylon infill next to CF, mm
VinfillFiber = WinfillFiber*numFiberLayers*Hlayer*L;   %Volume of Infill next
to CF, mm^3

Winfill = W-Wshell;     %Width of standard infill, mm
Vinfill = Winfill*L*(H-(Hlayer*(2*numFloor + numFiberLayers)));   %Volume of
standard infill, mm^3
Vtotal = H*W*L;         %Total Volume of tensile area, mm^3
Vsum = Vshell + Vfloor + Vroof + Vfiber + VinfillFiber + Vinfill;   %the same
as Vtotal, used as a check

Vfinfill = (Vroof+Vfloor+Vinfill+VinfillFiber)/Vtotal;
Vfshell = Vshell/Vtotal;
Vffiber = Vfiber/Vtotal;
Vffiber = Vffiber*100;

Vftotal = Vfinfill+Vfshell+Vffiber;

end
```

Appendix F: Experimental Data used in VAS Model

Specimen Number	Number of CF Layers	Total Strands of CF in Tension	Ultimate Tensile Strength (Mpa)	Modulus of Elasticity (Gpa)	Elongation at Break (%)
Control 1	0	0	31.52	0.64	22.25
Control 2	0	0	34.39	0.86	22.20
4A1	4	0	39.86	2.11	21.03
4B1	4	0	48.26	2.33	21.25
4C1	4	0	35.13	1.86	20.83
1a	4	44	111.03	9.56	1.14
1b	4	44	131.66	9.12	1.40
1c	2	22	84.94	5.23	1.60
2a	4	16	64.94	3.92	1.64
2b	4	32	96.83	6.77	1.40
3a	4	44	130.20	9.46	1.35
3b	4	44	123.57	9.39	1.27
1A2	4	44	126.45	10.01	1.40
1A3	4	44	109.84	9.58	1.16
1B2	4	44	116.72	9.40	1.25
1B3	4	44	121.27	9.50	1.27
Full Rerun	18	198	349.99	39.41	0.83
5A1	6	66	145.06	11.72	1.34
5A2	6	66	150.60	11.97	1.26
5A5	6	66	173.80	13.32	1.14
5A6	6	66	175.67	13.16	1.21
5B1	6	66	136.24	9.85	1.40
5B2	6	66	131.44	9.67	1.37
5B5	6	66	177.42	13.51	1.24
5B6	6	66	165.54	13.29	1.20
5C1	6	66	155.50	14.23	1.10
5C2	6	66	166.74	14.18	1.19
5C3	6	66	159.72	12.57	1.28
5C4	6	66	175.22	13.79	1.19
6A1	2	22	82.07	5.24	1.53
6A2	2	22	76.86	5.33	1.41
7A1	12	132	306.95	26.87	1.14
7A2	12	132	300.44	26.88	0.94
7B1	12	132	309.72	26.59	1.08

7B2	12	132	328.83	26.51	1.16
7C1	12	132	283.29	26.00	1.08
7C2	12	132	282.44	26.80	1.39
7D1	12	132	311.07	26.03	1.11
7D2	12	132	282.46	26.41	1.03
8A1	16	176	312.86	34.02	0.91
8A2	16	176	393.70	34.81	1.09
New_Full1	24	264	412.66	51.02	0.79
New_Full_Concentric1	24	264	531.12	51.75	0.99

Appendix G: Additional Microscope Images of Short Fiber Specimen

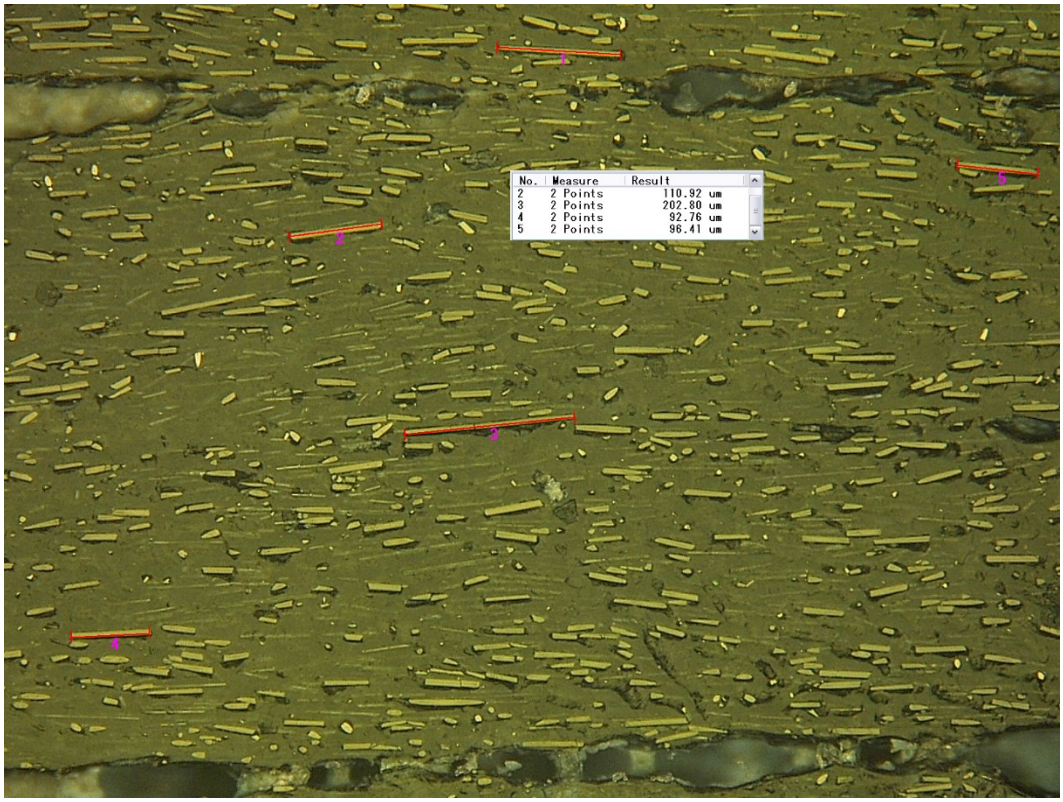

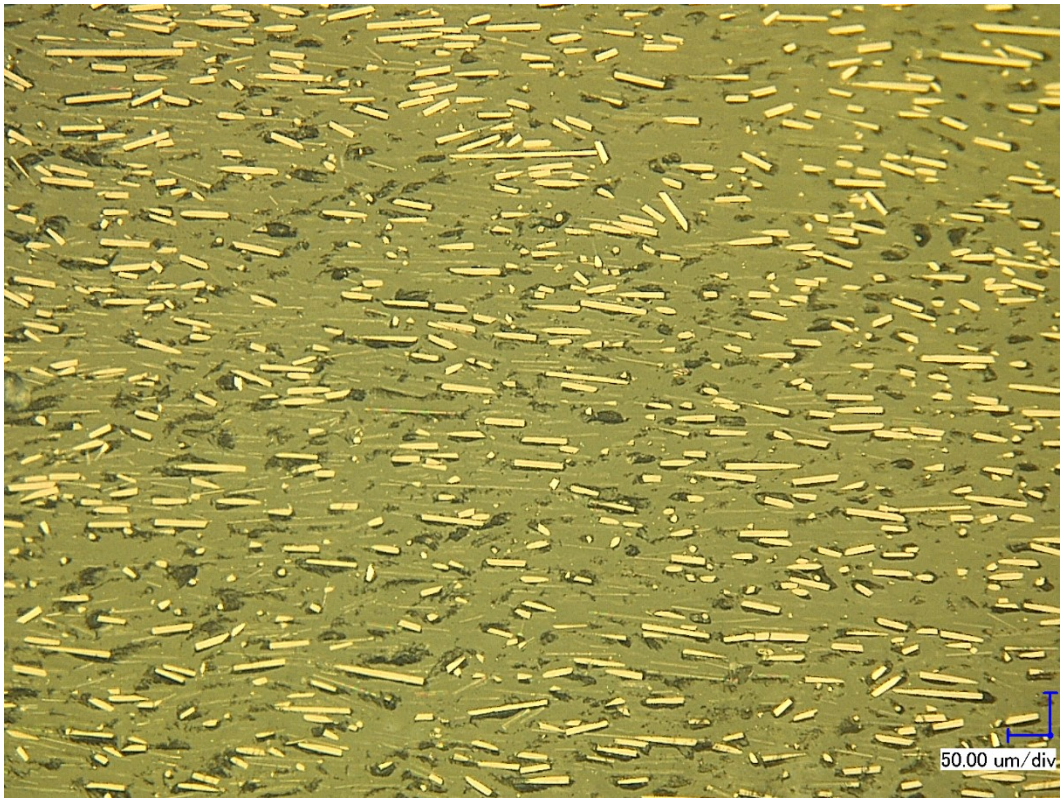

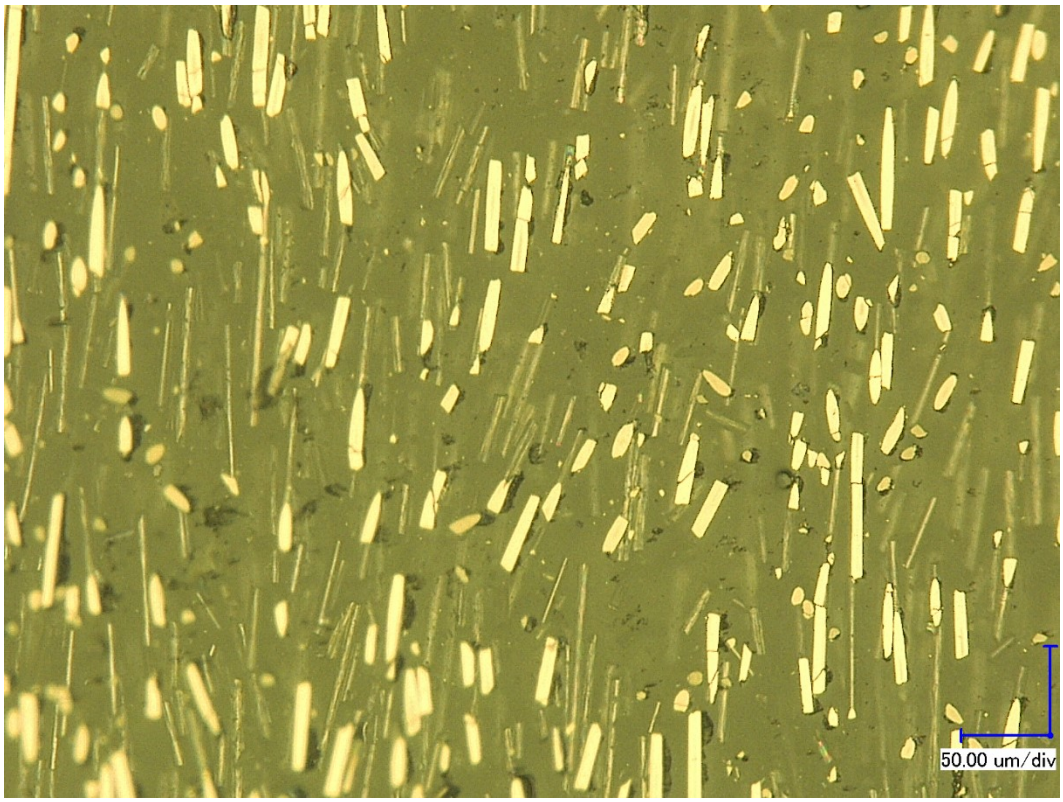
50.00 um/div

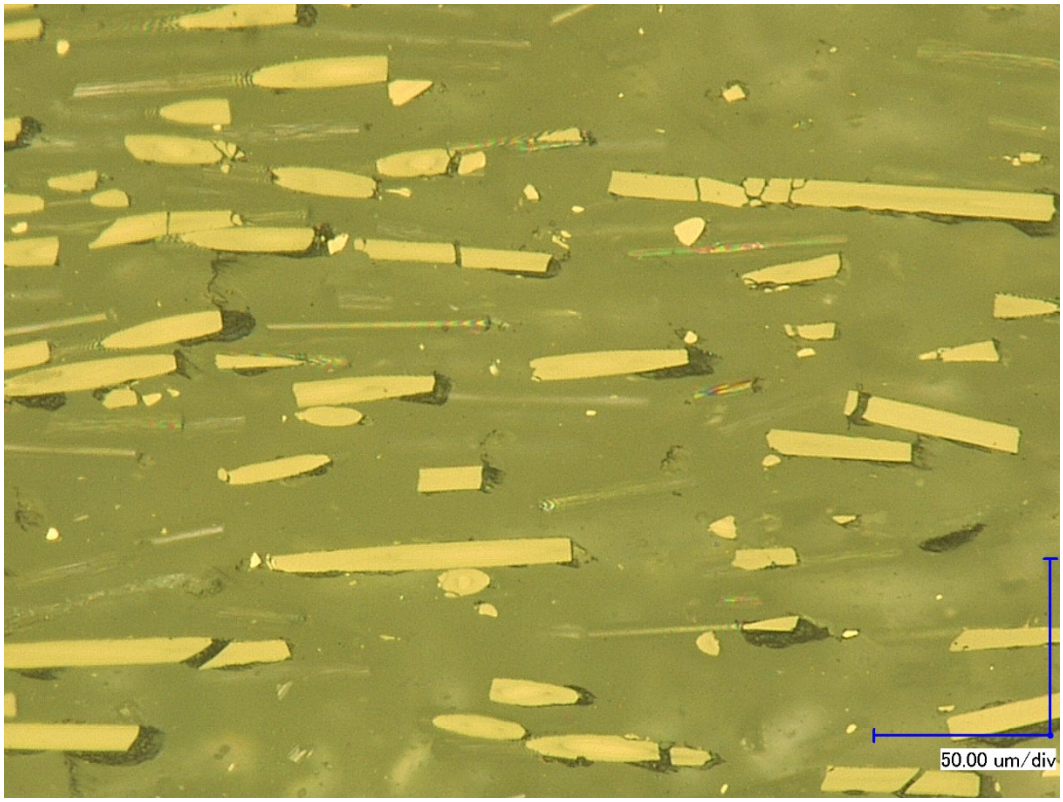
50.00 um/div

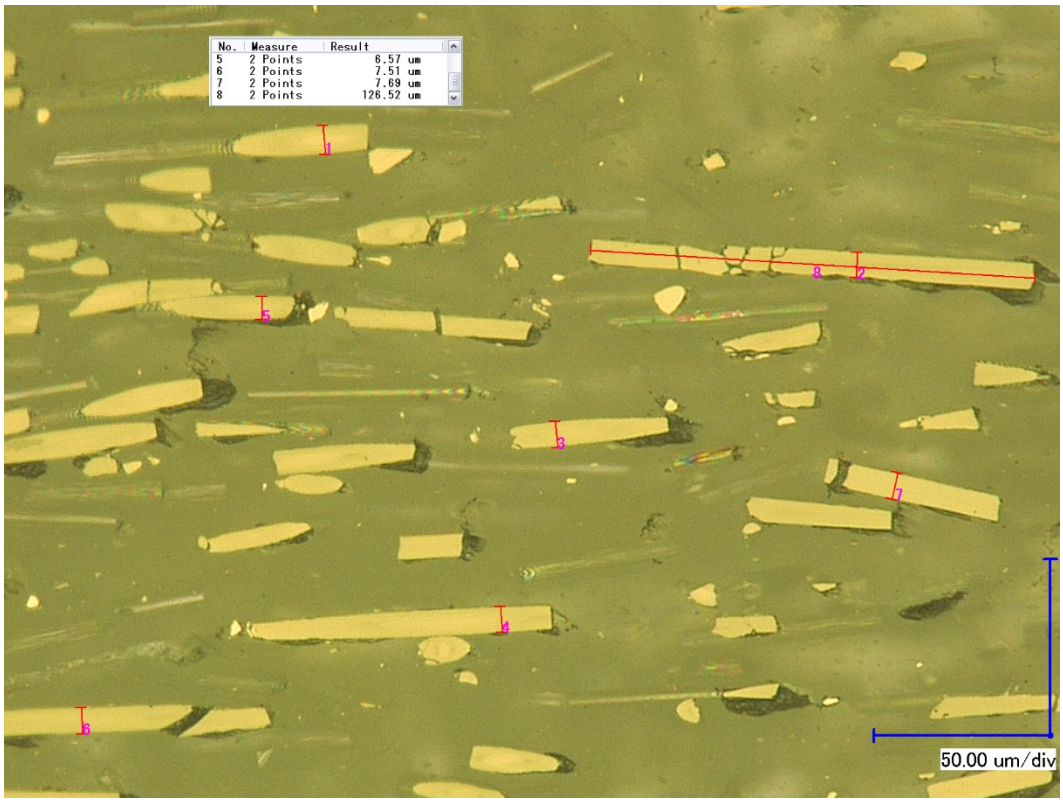
No. Measure Result
5 2 Points 6.57 um
6 2 Points 7.51 um
7 2 Points 7.69 um
8 2 Points 126.52 um
50.00 um/div

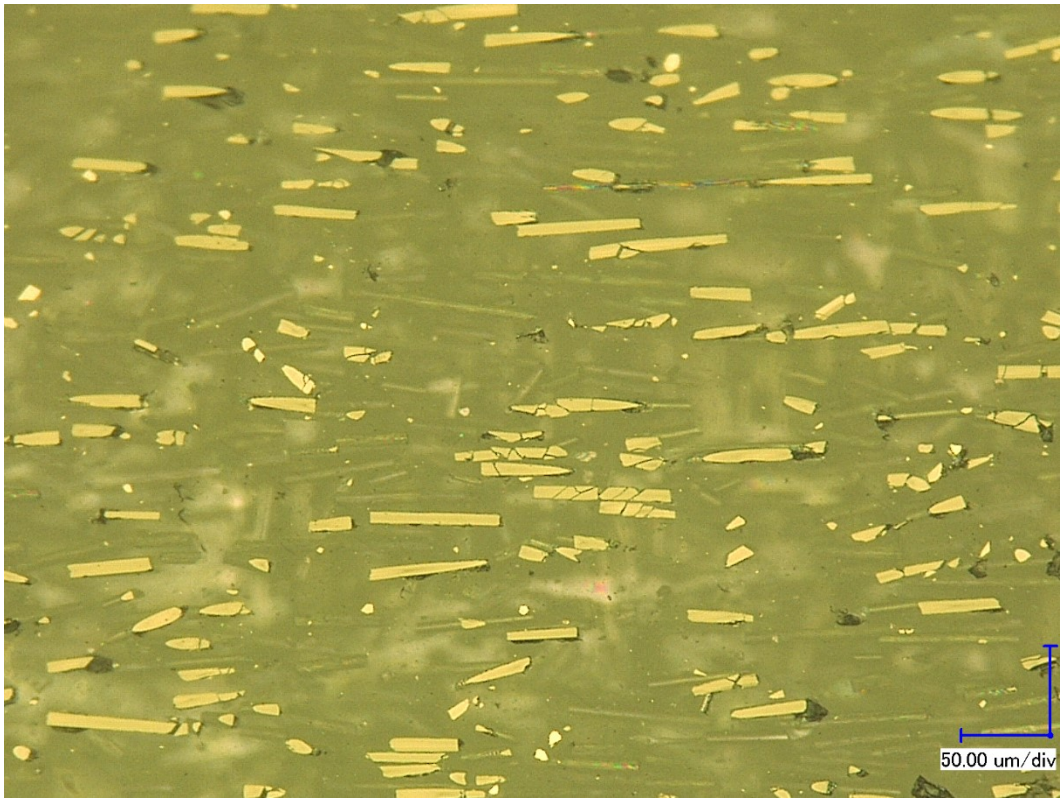
50.00 um/div

Appendix H: Sample Calculation of the Krenchel Orientation Factor

Bin Number	Direction (°)	2c2	cos^4(theta)	vfi*cos
1	-90	0.016181509	0.040308579	0.000652254
2	-88	0.000698097	0.99749549	0.000696349
3	-86	0.001192147	0.021675052	2.58398E-05
4	-84	0.005239837	0.213843313	0.001120504
5	-82	0.004817663	0.813401477	0.003918694
6	-80	0.001744989	0.000148483	2.59101E-07
7	-78	0.000963993	0.541440118	0.000521944
8	-76	0.004503356	0.461750343	0.002079426
9	-74	0.005506131	0.000869474	4.78744E-06
10	-72	0.002727775	0.875298149	0.002387616
11	-70	0.003148976	0.160875766	0.000506594
12	-68	0.000780022	0.037529717	2.9274E-05
13	-66	0.006646458	0.998590569	0.00663709
14	-64	0.002084863	0.023578244	4.91574E-05
15	-62	0.002080524	0.205763754	0.000428096
16	-60	0.008597731	0.822813148	0.007074326
17	-58	0.00323597	0.000201751	6.5286E-07
18	-56	0.001118523	0.529961508	0.000592774
19	-54	0.005350539	0.473006663	0.002530841
20	-52	0.004162575	0.000705752	2.93775E-06
21	-50	0.000404798	0.867057896	0.000350983
22	-48	0.000858649	0.167923562	0.000144187
23	-46	0.021728259	0.034885938	0.000758011
24	-44	0.000740111	0.999373382	0.000739647
25	-42	0.000766873	0.025596241	1.96291E-05
26	-40	0.006447413	0.197852714	0.001275638
27	-38	0.008981921	0.832046201	0.007473373
28	-36	0.001536802	0.000268131	4.12064E-07
29	-34	0.005874516	0.518502981	0.003045954
30	-32	0.026679312	0.484316637	0.012921235
31	-30	0.003213148	0.000566131	1.81906E-06
32	-28	0.00369365	0.858606192	0.003171391
33	-26	0.035644653	0.175146108	0.006243022
34	-24	0.002057746	0.032374024	6.66175E-05
35	-22	0.011622171	0.999843315	0.01162035
36	-20	0.010795619	0.027732564	0.00029939
37	-18	0.069667743	0.190111832	0.013244662
38	-16	0.034550589	0.841093834	0.029060287
39	-14	0.003527565	0.00034958	1.23317E-06

40	-12	0.015185485	0.507071461	0.007700126
41	-10	0.047476162	0.495673773	0.023532688
42	-8	0.043533882	0.00044818	1.9511E-05
43	-6	0.008480367	0.849949355	0.007207882
44	-4	0.004869328	0.182542548	0.00088886
45	-2	0	0.029990685	0
46	1.27E-13	0.267213725	1	0.267213725
47	2	0.003101804	0.029990685	9.30252E-05
48	4	0.007856447	0.182542548	0.001434136
49	6	0.027436534	0.849949355	0.023319664
50	8	0.027471	0.00044818	1.2312E-05
51	10	0.00832628	0.495673773	0.004127119
52	12	0.002112798	0.507071461	0.00107134
53	14	0.018306282	0.00034958	6.39952E-06
54	16	0.033902916	0.841093834	0.028515534
55	18	0.00728521	0.190111832	0.001385005
56	20	0.007459219	0.027732564	0.000206863
57	22	0.001332909	0.999843315	0.0013327
58	24	0.019084666	0.032374024	0.000617847
59	26	0.002727643	0.175146108	0.000477736
60	28	0.002644567	0.858606192	0.002270642
61	30	0.01539686	0.000566131	8.71664E-06
62	32	0.004089439	0.484316637	0.001980583
63	34	0.001333484	0.518502981	0.000691415
64	36	0.006093373	0.000268131	1.63382E-06
65	38	0.004559603	0.832046201	0.0037938
66	40	0.000577612	0.197852714	0.000114282
67	42	0.000863076	0.025596241	2.20915E-05
68	44	0.016691518	0.999373382	0.016681059
69	46	0.000806784	0.034885938	2.81454E-05
70	48	0.000370598	0.167923562	6.22321E-05
71	50	0.004034077	0.867057896	0.003497778
72	52	0.004870944	0.000705752	3.43768E-06
73	54	0.000927712	0.473006663	0.000438814
74	56	0.003107183	0.529961508	0.001646687
75	58	0.008324509	0.000201751	1.67948E-06
76	60	0.001664282	0.822813148	0.001369393
77	62	0.001649694	0.205763754	0.000339447
78	64	0.007444366	0.023578244	0.000175525
79	66	0.000649531	0.998590569	0.000648616
80	68	0.003022425	0.037529717	0.000113431
81	70	0.002948625	0.160875766	0.000474362
82	72	0.005566805	0.875298149	0.004872614

83	74	0.00471876	0.000869474	4.10284E-06
84	76	0.000967335	0.461750343	0.000446667
85	78	0.001682101	0.541440118	0.000910757
86	80	0.005032358	0.000148483	7.47218E-07
87	82	0.005174824	0.813401477	0.004209209
88	84	0.001365426	0.213843313	0.000291987
89	86	0.000686255	0.021675052	1.48746E-05
90	88	0	0.99749549	0
			SUM	0.533974464
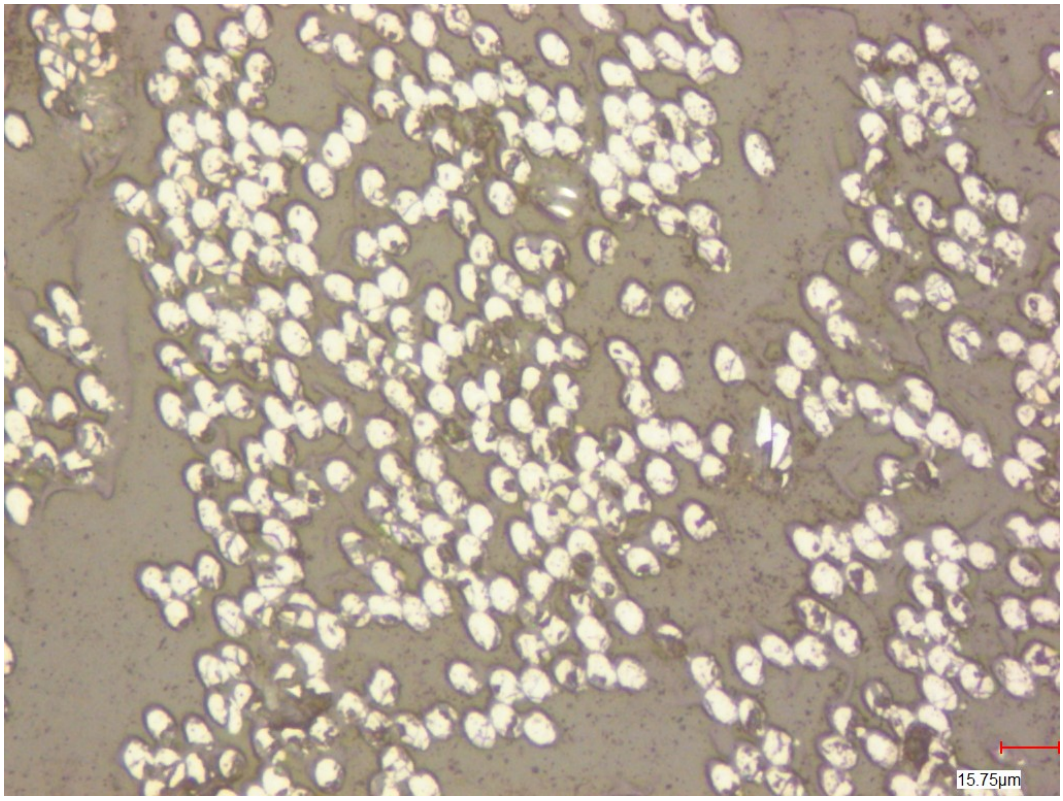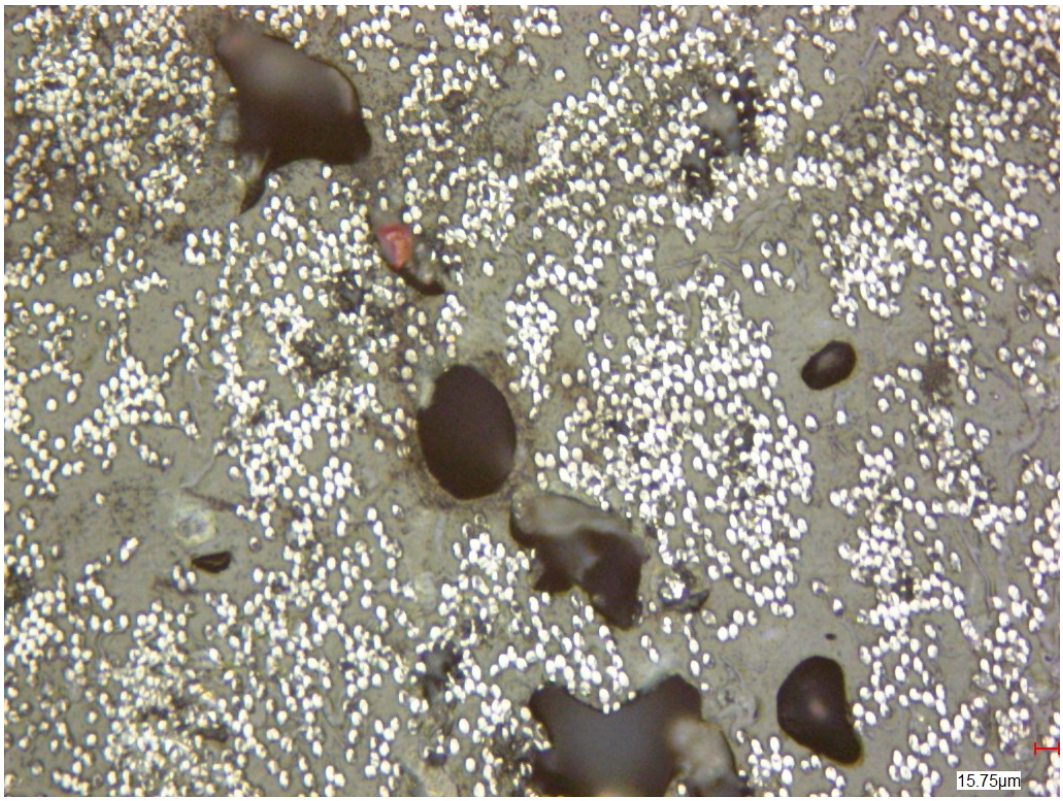
Appendix I: Additional Microscope Images of CCF Specimen